



HAL
open science

Elaboration of TiO₂ nanoparticle-based organic-inorganic hybrids: modification and study of the organic component

Ana Paola Diazgomez Trevino

► To cite this version:

Ana Paola Diazgomez Trevino. Elaboration of TiO₂ nanoparticle-based organic-inorganic hybrids: modification and study of the organic component. Chemical and Process Engineering. Université Paris-Nord - Paris XIII, 2019. English. NNT: 2019PA131080 . tel-03228914

HAL Id: tel-03228914

<https://theses.hal.science/tel-03228914v1>

Submitted on 18 May 2021

HAL is a multi-disciplinary open access archive for the deposit and dissemination of scientific research documents, whether they are published or not. The documents may come from teaching and research institutions in France or abroad, or from public or private research centers.

L'archive ouverte pluridisciplinaire **HAL**, est destinée au dépôt et à la diffusion de documents scientifiques de niveau recherche, publiés ou non, émanant des établissements d'enseignement et de recherche français ou étrangers, des laboratoires publics ou privés.

Université Paris XIII, Sorbonne Paris Cité

École Doctorale Galilée

THESE

Pour obtenir le grade de

Docteur de l'Université Paris XIII

**Élaboration de matériaux hybrides organiques-inorganiques à
base de nanoparticules de TiO₂ : Modification et étude de la
composante organique**

*Elaboration of TiO₂ nanoparticle-based organic-inorganic hybrids:
Modification and study of the organic component*

Présentée par :

Ana Paola DIAZGOMEZ TREVINO

Thèse de doctorat de Génie des Procédés

Dirigée par Andrei Kanaev et Mamadou TRAORE

Présentée et soutenue publiquement le 09 Décembre 2019

Devant un jury composé de :

Anatole KHODAN

Senior Researcher, IPCE RAS, Russie

Alexis EVSTRATOV

Research Professor, HD Chem., IMT Mines Ales

Laurence ROZES

Professeur, UPMC, Paris

Rabah AZOUANI

Professeur de l'EBI, Cergy

Mamadou TRAORE

Maître de Conférences, HDR, LSPM

Andrei KANAEV

Directeur de Recherche CNRS, LSPM

Rapporteur

Rapporteur

Examineur

Examineur

Directeur de thèse

Directeur de thèse

Dedication

To my beloved husband, for give me the courage to start this adventure and a life together.

To my mother that its an example of a strong women in my life.

To my grand parents that was my fisrt teachers and friends

To my son....

Acknowledgements

This work was possible thanks to “Consejo Nacional de Ciencia y Tecnología” (CONACyT) with the scholarship 381463.

Contents

General Introduction	7
Chapter 1 : Bibliography	13
1.1 What is an Organic-Inorganic Hybrid?	15
1.2 History	15
1.2.1 Materials.....	16
1.2.2 Organic derivative of inorganic solids:	17
1.2.3 Classification.....	18
1.2.4 Properties	19
1.2.5 Technology driven exploration of hybrid materials	19
1.3 Strategies for the synthesis of Hybrid Materials	19
1.3.1 In situ approach.....	20
1.3.2 Building block approach	24
1.4 State-of-art techniques for the synthesis of hybrid materials	27
1.4.1 Sol-Gel process	27
1.4.2 Polymerization and Co-Polymerization	33
1.5 Hybrid Materials based on TiO ₂	40
1.5.1 Kameneva synthesis route	40
1.5.2 Gorbovyi synthesis route.....	43
1.5.3 Light induced darkening of pHEMA-TiO ₂ gel based hybrids.....	46
1.6 Conclusions.....	49
Chapter 2 : Experimental Techniques.....	51
2.1 Glove-box	53
2.2 Sol-Gel reactor	53
2.3 Dynamic Light Scattering (DLS).....	55
2.4 Transmission Electron Microscopy (TEM), Scanning electron microscopy (SEM)	56

2.5 RAMAN spectroscopy	58
2.6 Thermal Gravimetric Analysis and Differential Scanning Calorimetry (TGA-DSC).....	59
2.7 Gas Chromatography - Mass Spectrometry	60
2.8 Fourier Transformed Infra-red Spectroscopy.....	61
2.9 TGA-DSC coupled to GC-MS and FTIR	62
2.10 Conclusions.....	67
Chapter 3 : Material Synthesis	69
3.1 Chemicals and their characteristics	71
3.2 Purification processes.....	76
3.2.1 Distillation of monomers.....	76
3.2.2 AIBN recrystallization	77
3.3 TiO ₂ nanoparticles synthesis	78
3.4 Solvent Exchange.....	79
3.5 Radical Thermal Polymerization	81
3.6 Conclusions.....	82
Chapter 4 : TiO₂ hybrids with HEMA organic component	85
4.1 Solvent exchange on HEMA-TiO ₂ hybrids.....	87
4.1.1 Thermogravimetric study of solvent extraction.....	87
4.1.2 TGA-DSC / GC-MS / FTIR analysis of solvent	91
4.1.3 TGA-DSC/GC-MS/FTIR analysis of colloid	99
4.2 Influence of NP on HEMA polymerization studied by coupled TGA- DSC/GC-MS/FTIR.....	110
4.3 Conclusions.....	120
Chapter 5 : TiO₂ hybrids with mixed HEMA-EMA inorganic component.....	122
5.1 Colloid stability.....	124
5.1.1 Polymerization.....	126
5.1.2 TEM micrography	132

5.2 Conclusions.....	136
Chapter 6 : Two-photon polymerization of hybrid solutions	137
6.1 Introduction.....	139
6.2 Experiment.....	141
6.2.1 Materials.....	141
6.2.2 Two photo adsorption direct laser writing.....	141
6.3 Results	142
6.3.1 Monomer with and without a cross-linker.....	142
6.3.2 Hybrid materials	146
6.3.3 Development and characterization	147
6.4 Conclusions.....	148
General conclusions	151
References	155
Index of figures.....	169
Index of tables	173
Publications	174

General Introduction

General Introduction

Nanomaterials offer interesting properties and useful functionalities that can differ substantially from their bulk counterparts. Among a variety of these materials, hybrid nanomaterials compared to single component nanomaterials permit flexibility of properties by varying their composition, morphology and interface. The properties in the hybrid nanomaterials depend on both the chemical nature and the interaction between the components. In case of the negligible interaction, they could be a sum of individual component's properties.

In the 1970s, a new concept «chimie douce», proposed by Livage, 1977, opened up new horizons of synthetic chemistry. Finally, the sol-gel chemistry has become, probably, the central concept of the elaboration of hybrid materials. New precursors and possible reaction paths, based on the sol-gel approach, have become possible to use in synthetic chemistry. Recently, in last 20 years (Gómez-Romero and Sanchez, 2003; Kickelbick, 2006; Merhari, 2009; Sanchez et al., 2010), TiO₂-based materials attract much attention due to their properties and possibilities of practical use in photocatalysis, solar cells, micromachining, painting industry, etc. The TiO₂-based materials can be found in different forms, such as polymorphs of crystalline solid TiO₂ (rutile, anatase, brookite), wet sols and gels, powders with different presence of crystalline and amorphous phases and hybrid materials.

The TiO₂-based hybrid materials are well known for unique photosensitivity and photochromic properties. The observable “darkening” phenomenon is due to relatively simple reduction reaction ($\text{Ti}^{4+} + \tilde{\epsilon} = \text{Ti}^{3+}$), which can take place in hybrid materials while being irradiated with UV light. The efficiency of Ti⁴⁺ reduction, thus darkening characteristics, is defined by the material involved. Kuznetsov A. (PhD thesis, 2006) has shown that quantum yield of the darkening process, defined as the initial (t=0) charge separation efficiency of the process, depends on the inner morphology of the hybrid material: nanoparticle size, size distribution, inter-component connection type, fact of gelation, etc. For his studies, he used hybrid materials produced by the synthesis process, which was presented in details in the PhD thesis by Kameneva O. (2006).

In order to get well-defined TiO₂-based hybrid material and repetitivity of its properties, two approaches can be envisaged:

- The morphology control of the inorganic component, for which the sol-gel process has to be adequately designed and optimised to obtain macroscopic

quantities of size selected nanoparticles. This study has been realized in the PhD work by Pavlo Gorbovyi (2012)

- The control of the organic component, which forms a large contact interface with inorganic single and/or chained and defines structural and electronic properties of the hybrid material. The related studies constitutes the main purpose of this PhD work.

AIM OF THIS THESIS

The work presented herein was carried out at the Laboratoire des Sciences des Procédés et des Matériaux (LSPM, UPR3407 CNRS) under the supervision of Research Director Andrei Kanaev and Assistant Professor Mamadou Traore as a continuation of the series of previous studies related to the synthesis of TiO₂-based nanoparticulate materials. The objective of this work was to provide more details for the better understanding of the polymer – inorganic nanoparticle interaction during the (inorganic) gelation / (organic) polymerization processes with an ultimate goal to improve the overall quality and structural stability of the hybrid materials related to the tolerance to ambient humidity and oxygen. Furthermore, in frame of this work the mixed organic component of HEMA-EMA and HEMA-TEGMA copolymers was proposed and investigated; as a result, the obtained hybrid materials have shown an improved tolerance to water, better photopolymerization and easier handling in the laser one- and two- photon microstructuring.

This manuscript is organized in six chapters. Chapter I introduces the organic-inorganic hybrid materials and provides the state of art of research in the field. In Chapter II, a detailed description of the experimental equipment and apparatus used in the current studies is given. Chapter III described chemicals and methods used to conduct the experiments, as well as purification methods, applied in order to reach the best process performance. Chapters IV and V then constitute the main part of the experimental study carried out in this PhD work, where a thorough analysis of the material composition and modifications was carried out during the hybrid solution formation and organic radical polymerization. More precisely, in Chapter IV by using a complex experimental installation of Thermo Gravimetric Analysis (TGA) coupled to Fourier Transformed Infrared Spectroscopy (FTIR), Gas Chromatography

and Mass Spectroscopy (GC-MS) we were able to reveal fine details of the complex interactions between organic HEMA monomers and size-selected TiO₂ nanoparticles at the solvent exchange and polymerization stages. We have also performed TGA-DSC experiments, which complement the above measurements. Chapter V pursues the studies engaged in Chapter IV by addressing the complex analysis of the hybrid samples with the organic component composed of HEMA-EMA and HEMA-TEGMA copolymers. The availability of the hybrid material for microfabrication via direct laser writing by using two-photon polymerization (2PP) process is described in Chapter VI. The last Chapter of General conclusions and Perspectives concludes the manuscript resuming the main results and open points to be resolved of this study.

Chapter 1 : Bibliography

Chapter 1: Bibliography

1.1 What is an Organic-Inorganic Hybrid?

The definition of organic-inorganic material is not always clear, the IUPAC definition is: “*a hybrid material is composed of an intimate mixture of inorganic, organic materials, or both types of components*” (note: the component usually interpenetrate on scale of less than 1 μ m) (Aleman et al, 2007). However, this definition had disadvantage indeed it's not clear enough and could cover some kinds of inorganic crystalline materials, polymer blend or nanocomposites; a more specific definition could be: “*a hybrid material consist of at least two components-usually an inorganic and organic component-that are molecularly dispersed in the material*” (Kickelbick, 2014) making a difference between the nanocomposites and the hybrid base on structural features. The big differences between these concepts are at the intimate mixture of the components on the molecular scale, this can change many properties compared to those of nanocomposites (Kickelbick, 2007). Thus, conventional hybrid systems, as for instance typical commercial polymers containing mineral charges, or pure molecular systems such as the metal salts of organic anions, or macromolecules containing small inorganic counter-ions of polymer such as (Polyaniline)⁺/ClO₄, should not be included. Exceptions related to these last materials, are the systems based on much bigger counter-ions, as for the instance the polyoxometalates based on Keggin or Wells Dawson structures which could be regarded as metal oxide clusters and which present their own chemical and electrochemical activity (Gomez-Romero, 2001).

1.2 History

Nowadays, hybrid materials have a great potential: the most obvious advantage that they can combine very different properties of organic and inorganic components in one material. It could seem something artificial and modern but, definitely, the hybrid materials are known for a long time. Beautiful example of the material's age is “Maya blue”. It's an extremely old and breath-taking man-made hybrid materials elaborated via soft chemical conditions.

An organic pigment (indigo) and inorganic substrate (clay mineral, also known as palygorskite) are combined together forming a synergic material, where a coloration of organic component and mechanical property (resistance) of the clay have been resulted in astonishing example of, probably, the most ancient material.

Later, on industrial era, hybrid materials were also used in paint industry, where inorganic nano-pigments are suspended in organic mixtures: various surfactants, solvents and etc. But the true burst in hybrid organic – inorganic synthesis happened in the eighties, with the expansion of soft inorganic chemistry processes.

1.2.1 Materials

Through time, the kind of hybrid materials that can be prepared and the synthetic routes to obtain these materials have changed. The evolution of synthesis routes is depicted in this section:

1.2.1.1 Intercalation compounds

This is the first type of organic-inorganic materials resulting from the intra crystalline insertion of organic compounds inside the layers of some lamellar solids. The intercalation compounds could be grouped in:

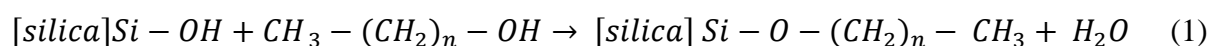
- Intercalation of ionic species: among the typical 2D material acting as host for intercalation of organic compounds, the phyllosilicates are a group of solids belonging to the clay minerals family. These substitutions are characteristics of a large variety of smectite minerals being responsible for frameworks charge deficiency which is compensated by interlamellar cations. Such cations are named exchangeable cations as they can easily be exchanged by treatment of clay with salts solution. [Giesecking, 1939]
- Intercalation of neutral species: the formation of organic-inorganic compounds of neutral molecules in 2D solids was also accomplished of the clay minerals family. The first systems of this sort were reported in 1944-1945. The polarity of the guest molecules plays an important role in their tendency to be inserted between the inorganic layers and the stability of this new class resulting complexes. A large variety of compounds of very different organic functionality are able to intercalated phyllosilicates, like kaolinite, smectites and vermiculites. The Van der Walls forces are especially relevant in the insertion of long chain alkylammonium species in the different 2D solids. [Yariv & Cross, 2002]
- Polymer intercalation nanocomposites: from 1961 the ability of neutral unsaturated monomers, like acrylonitrile, methyl methacrylate (mma), and vinyl acetate, to

intercalate into montmorillonite was reported. The in situ polymerization take place by the initiator such as azo bis isobutyronitrile (AIBN), the polymer remaining strongly associated to the minerals substrate. These stable organic-inorganic materials are nowadays referred to as polymer-clay nanocomposites. From these pioneering works to the present the study of intercalation of organic polymers into different 2D host lattices has been very intense. The first one result from combination of polymers whose interest is centered on their mechanical or rheological properties, such as nylon-clay nanocomposites. Depending on the nature of each component, 2D host and guest polymer, the following procedures of synthesis can adopted:

- ❖ Direct intercalation from polymer solutions or by polymer melting
- ❖ In situ intercalative polymerization
- ❖ Delamination & entrapping-restacking

1.2.2 Organic derivative of inorganic solids:

This class of hybrids is formed by grafting of organic groups onto inorganic surfaces; the attachment of both phases is assured by covalent bonds. The first attempts to obtain these materials were based on the “esterification of silica” (1). After works made more stable compounds, that were obtained by the reaction of silica with a large variety of mono-, di- or tri- chloro (or alkoxy)- silanes containing diferrents organic groups, that my confer different functionality on the organic substrates. Thus, organosilanes containing $\equiv \text{Si} - \text{X}$ groups gave very stable bonds through Siloxane Bridge between the inorganic and inorganics parts linked to Si atoms. To help the reactivity between silanol groups and the organosilanes it is necessary to use an acid treatment on silicates. On 1964 an ingenious procedure was developed to obtain organic-inorganic solids involving the simultaneous hydrolysis of silicate and organosilane, these process could be applied also to prepare organic derivatives of various minerals (such as vermiculite, chrysotile, olivine). The organic derivatives of silicate obtained using organosilanes are extraordinarily stable towards chemical agents or thermal treatment.



Chapter 1: Bibliography

Table 1-1. Evolution of Hybrid synthesis since early XX century up to our days.

Year	Organic-inorganic Hybrids	Examples	Reference
1939	Clays minerals intercalated by organic cations	Montmorillonite/ quaternary ammonium species	Gieseking, 1939
1953	Organic derivatives of silica	Esterification of precipitated silica with alcohols	Iller, 1953
1961	Polymer-clay intercalation compounds	Montmorillonite/polyacrylonitrile	Blumstein, 1961
1967	Transition metal oxychlorides	FeOCl/amines	Hagenmuller et al, 1967
1973	LDH intercalated by organic anions	[Zn ₃ Al(OH) ₈]/ dicarboxylates	Miyata & Kimura, 1973
1976-1978	Organic derivatives of layered phosphates	Grafting of epoxides & direct synthesis of organophosphonates in α Zr-phosphate	Yamanaka, 1976 Alberti et al, 1978
1980	Organic derivatives of layered silicic acids	Interlamellar grafting of trimethylsilyl groups on H-magadite	Ruiz-Hitzky & Rojo, 1980
1986	Conducting polymers 2D intercalated materials	FeOCl / Polypyrrole	Kanatidis et al, 1986
1990	Ion-conducting polymers 2D intercalated materials	Layered silicates/ PEO	Ruiz-Hitzky & Aranda, 1990
1997	Polyoxometalates doping conducting polymers	[PMo ₁₂ O ₄₀] / polyaniline	Gomez-Romero & Lira-Cantu, 1997
2002	Silica grafted surfactants (SGS)	Self-assembled organo silica	Ruiz-Hitzky et al, 2002

Sol-gel hybrid materials is the widest category on the types of preparation for hybrids. It's based on organometallic compounds like alkoxides of silicon, titanium, zirconium among others, that acts as precursors, this class of hybrids are characterize by the presence of Mt-O-R, metal organic bonds in metal oxo-networks. The diversity on the kind of precursors, make the number of organics-inorganics materials almost unlimited, since they could be designed and controlled in different ways. The selection of the organic part confers different natures and properties. Other interesting feature of this kind of hybrids is the process sol-gel carried out in the presence of surfactants for the self-assembled organic-inorganic materials.

1.2.3 Classification

Based on the nature of bonds and interactions existing in the hybrid interface, hybrid materials can be divided in two main types (P. Judeinstestein, 1996; C. Sanchez, 1994):

Class I: corresponds to all the systems where no covalent or ion covalent bonds are present between the organic and inorganic components

Class II: in this materials at least a fraction of the organic and inorganic components are linked through strong chemical bonds.

1.2.4 Properties

The final properties of hybrid materials depend not only on the characteristics of initial components involved, but also significantly rely on the component's interface. Therefore, the component's synergy does influence their properties. For example, Judeinstein and Sanchez have described many applications of their hybrid materials.

Suitable mechanical properties are one of the foremost areas for hybrid materials. These studies are guided by the strong similarities which could be found with structural composites (Shea et al, 1992). The effect of mixing and/or grafting polymers to glass fibers or woven fabrics to reinforce their structure is a current issue. Some research on this kind of materials is focused to obtain specific properties or response to factors such a pH, light, electric field or temperature.

1.2.5 Technology driven exploration of hybrid materials

1.2.5.1 Hybrid Coatings:

The hybrids' main advantages for coatings is the lightweight, some structural properties, corrosion and resistant, use as barriers against oxygen and water, the films can be deposited at low temperatures. The electronic industry is one of the most interested, but not the only one, since others like the automotive and aerospace industries are also gaining interest on hybrid materials (Chiu et al., 2013; Zhang et al., 2010).

1.2.5.2 Hybrids for optical applications:

The main optical application is at wafer-scale in applications such as waveguides grafting, micro-optical devices, high refractive index materials and photo-chromic materials or photo detectors. (Wang et al, 2010)

1.2.5.3 Hybrids in electronic applications:

The hybrids materials could increase the performance in electronics through shrinkage of the circuits. Some examples of this materials applied to devices are low-k dielectrics, also in some silicon materials they are used to produces POSS derivatives. (Liu et al, 2001).

1.3 Strategies for the synthesis of Hybrid Materials

There are 2 different approaches that can be used for the formation of the hybrids

- Building block approach: in this technique, well defined building blocks is used to form the final hybrid material, in which the precursor still at least partially keep their original integrity on one or both structural units. The main advantage of this approach is the possibility to make prediction of the structure properties because no significant structural change during the matrix formation is observed.
- In situ formation of the components: contrary to the building block technique, this approach is based on the chemical transformation of the precursor used through the preparation of the hybrid materials. One of the most common cases is the preparation of the organic polymer, but also reaction that involved sol-gel reaction to produce the inorganic part. In the in situ approach the variation of one parameter could change completely the results in two very different materials. The final performance is strongly dependent on their process and its optimization.

1.3.1 In situ approach

In situ formation of the inorganic component: the widest used process is the sol-gel reaction. The sol-gel process is chemically related to an inorganic polycondensation reaction, in which a small molecules form polymers structures by the loss of subsistent. Usually the reaction results in a three dimensional cross-linked network.

The Figure 1-1 shows how the pH influence on the sol-gel reaction. This pH variation not only change the reaction mechanism but also affect the kinetics on the condensation reaction expressed on the gel point.

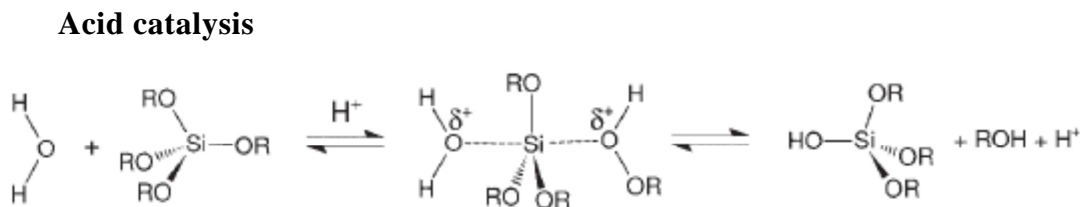


Figure 1-1. Acid Catalysis Mechanism

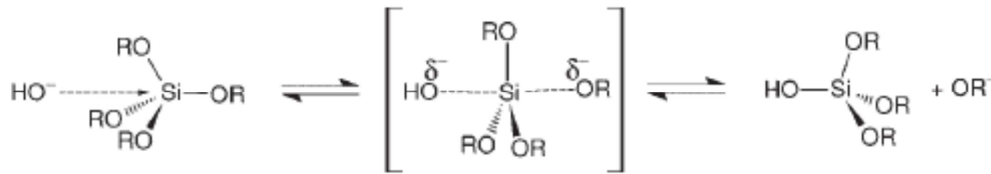
Base catalysis

Figure 1-2. Base Catalysis Mechanism.

Other important parameter on the sol-gel process is the precursor structure; larger substituent (R) decreased the reaction time due to the steric hindrance. The solubility and the miscibility on the water are also necessary for the reaction. Hence, for a well defined material the reaction condition has to be fine-tuned.

The next step on the sol-gel reaction is defined by gelation point, which is reached when the links between the sol-particles are formed and created a three dimensional cross-linked network. Released solvent (alcohol) can be trapped in the pores. The condensation reaction can go on for a long time until the final stage: this process is called ageing. The gel structure results of the drying process. Using a supercritical condition can give highly porous aerogel.

Other factor that affects the sol-gel reaction is the hydrolysis ratio that means the water quantity compared with the precursor molecules. It is determinant to completed the reaction just to oxide the precursor or not.

Hybrid Materials by the Sol-Gel process: Organic molecules other than the solvent can be added of the formed network upon gelation. Hence functional hydrolysable organic are not tolerated. However, a partial tolerance for the pH can be obtained if the sol-gel reaction is carried out in a buffer solution. Physical entrapment has the disadvantage that sometimes the materials obtained are not stable towards phase separation or leaching because of differences in polarity. While the formation of homogeneous materials with a chemical link between the inorganic component is in many case the preferred route, there are case where a controlled, phase separation between the entrapped organic molecules and the sol gel material is compulsory for the formation of the material.

Usually the organic functionalization has a large influence on the properties of the final hybrid material. An example, the size on the particle is affected if a tri or tetra

alkosilanes, is used, and also affected the density of the last material. In addition, the functional group incorporated changes the properties of the final material.

Hybrid material derived by combining the sol-gel approach and organic polymers: Compared with other inorganic network forming reaction, the sol-gel process show mild reaction condition and a broad solvent compatibility. These two characteristics offer the possibility to carry out the inorganic network forming process in presence of performed organic polymer or to carry out the organic polymerization before, during or after sol-gel process.

The reaction mechanism of the sol-gel process and typical organic polymerization, such as free radical polymerization, allow the temporal separation of the polymerization reaction, which offers many advantages in the material formations.

The identification of a solvent in which the organic macromolecules are soluble and which is compatible with either the monomers of preformed inorganic oligomers is a main parameter.

Organic polymers are immiscible with alcohols that are released during, the sol-gel process, this can be avoided if the solvent is switched from typically used alcohols to solvents like the THF, for example, in which many organic polymers are soluble and which is compatible with many sol-gel reactions. Phase separation can be also avoided if the polymers contain functional groups that are more compatible with the reaction conditions of the sol-gel process or even undergo an interaction with the organic material formed.

Formation of organic polymers in presence of preformed inorganic materials: If the organic polymerization occurs in the presence of an inorganic component to form the hybrid material, it is important to distinguish between several possibilities to overcome the incompatibility of the two species. The inorganic material can have no surface functionalization but the bare material surface, it can be modified with non-reactive organic groups, or it can contain reactive surface groups such as polymerizable functionalities.

If the inorganic component has non-reactive groups attached to its surface and it can be dissolved in a monomer, which is subsequently polymerized, the resulting material after the organic polymerization is a blend. In this case the inorganic component interacts only weakly or not at all with the organic polymer, hence, is a class I. Homogeneous materials are

only obtained in this case if agglomeration of the inorganic component in the organic environment is prevented. The strongest interaction is achieved if class II, for example with covalent interactions. Examples for such strong interaction are the use of surface-attached polymerisable groups.

If a porous 3D inorganic network is used as the inorganic component for the formation of the hybrid materials, a different approach has to be employed depending on the pore size, the surface functionalization of the pores and the stiffness of the inorganic framework. In many cases, intercalation of organic components into the cavities is difficult because of diffusion limits. Probably the most studied material in this respect is that of 2D layered inorganic materials that can intercalate organic molecules and if polymerization between the layers occurs even exfoliate producing nanocomposites. There are three methods for the formation of polymer–clay nanocomposites can be used:

- Intercalation of monomers followed by in situ polymerization
- Direct intercalation of polymer chains from solutions
- Polymer melt intercalation

The method applied depends on the inorganic component and on the polymerization techniques.

Hybrid materials by simultaneous formation of both components: Simultaneous formation of the inorganic and organic polymers can result in the most homogeneous type of interpenetrating networks. Usually the precursors for the sol-gel process are mixed with the monomers for the organic polymerization and both processes are carried out at the same time with or without solvent.

One problem that also arises from the simultaneous formation of both networks is the sensitivity of many organic polymerization processes for sol-gel conditions or the composition of the materials formed. Ionic polymerization, for example, often interacts with the precursors or intermediates formed in the sol-gel process. Therefore they are not usually applied in these reactions; instead free radical polymerization is the method of choice. This polymerization mechanism is very robust and can lead to very homogeneous materials. A very clever route towards hybrid materials by the sol-gel process is the use of precursors that contain alkoxides

which also can act as monomers in the organic polymerization. The released alkoxides are incorporated in the polymers as the corresponding alcohol while the sol-gel process is carried out.

1.3.2 Building block approach

Many future applications in particular in nanotechnology, focus on a bottom up approach in which complex structures are hierarchically formed by these small building blocks.

A typical building block should consist of a well defined molecular or nanosized structure and composition. In regard of the preparation of functional hybrid materials the building block should also deliver interesting chemical or physical properties in areas like conductivity, magnetic behavior, thermal properties, switching possibilities, etc...

Inorganic building block: Prime examples of inorganic building blocks that can keep their molecular integrity are cluster compounds of various compositions. Usually clusters are defined as agglomerates of elements that either exclusively contain pure metals in mixtures with other elements. The goal in the chemical design of these systems is the preparation of cluster carrying organic surface functionalization that tailor the interface to an organic matrix by making the inorganic core compatibles and by the addition of functional groups available for certain interaction with the matrix.

Two methods are used for the synthesis of such surface-functionalized molecular building blocks: either the surface groups are grafted to a preformed cluster or they are introduced during the cluster synthesis.

Surface functionalized metal cluster are one prominent model system for well defined inorganic building blocks that can be used in the synthesis of hybrid materials.

Recently the modification and embedment of transition metal oxide clusters and particles has become more and more important, because of their catalytic, magnetic or electric properties. Chemical approaches different to those of silicate systems are often required for the attachment of organic groups to the surface compounds. The reason for these differences is the changes reactivity of these species for example metal oxides often do not show highly nucleophilic oxygen atoms at their surface and charges are frequently delocalized over the whole cluster core. A variety of methods can be used for surface functionalization of pure

cluster or nanoparticles depending on the reactivity of the surface, which often changes with parameters such as the pH value. Compatibilizing agents such as surfactants are regularly used to increase the compatibility of the cluster or nanoparticles with an organic matrix. These molecules have two segments of which one undergoes interactions with the surface of the inorganic particle, for example by electrostatic or hydrogen bonding and other one commonly a non polar block, interacts with the surrounding organic phase.

Post synthetic modification: Post synthetic modification means that the cluster or nanoparticles is formed in a first step applying well-established procedures and the functionalization with organic groups is applied in a second step. Functionalization is required and allows a chemical reaction with the surface decorating molecules.

Another way to attach functional groups to the surface of a performed building block is the exchange of surface groups, similar to the above mentioned ligand exchange on gold clusters. In such a reaction the charges and coordination number balance of the surface atoms must be retained, which is more complicated in the case of metal oxides with their heterogeneous surface than with homogeneous surface of metal clusters and particles. Many stabilized metal oxide species such a titanium oxo-clusters can for example, exchange surface alkoxide groups with other alkoxides.

In the case of metal oxo-clusters or metal oxide particles containing metals in high oxidation states it is often difficult to attach functionalized surface molecules, like unsaturated bonds during their synthesis because of the strong oxidizing conditions either of the cluster itself or the oxidative reaction conditions during their synthesis. These groups may carry organic functionalities such as polymerizable double bonds. However, sometimes strong ligands can lead to the reorganization of a cluster surface or even to degradation of transition metal clusters or a partial degradation of the particles which has been show in several cases.

Functionalization of cluster and particles during their synthesis (in situ functionalization): In the post synthesis modification, functionalized building blocks are formed in two steps: the inorganic core is formed first, and the functional organic groups are introduced later in a different reaction. This is realized in the case of metal cluster or particles. If the metal core is prepared in presence of ligands, one limitation is that the organic groups have to withstand the reaction conditions of the clusters core formation. In situ functionalization is also a versatile route for many transition early transition metal oxo-

clusters. The main differences in these reactions are that surface-functionalization is included in these systems, similar to the metal cluster by functionalized ligands.

Interactions between metals or metal oxides core to molecules that act as surface functionalization are similar on a molecular scale and therefore do not usually change with size of the core. Thus, the chemistry developed for isolated and structurally characterized metal and metal oxide cluster can also be applied for the functionalization of larger nanoparticles.

Organic building blocks: Organic building blocks can also be used for the formation of hybrid materials. Typical examples are oligo and polymers as well as biological actives molecules like enzymes. Similar methods have to be applied as in the formerly discussed examples to increase the compatibility and the bonding between the two phases. The small description of the organic building blocks types.

- *Small molecules:* the modification of inorganic networks with small organic molecules can be defined as the origin of hybrid materials. The latter is achieved by the modification of the organic molecules with hydrolyzable alkoxy silane or chlorosilane groups. Phase separation is usually avoided by matching the polarity of the often hydrophobic molecules to that of the hydrophilic environment.
- *Macromolecules:* Oligo and polymers as well as other organic molecules often show different solubilities in specific solvents compared with monomers; most often the solubility of the polymers is much lower than that of the monomers. However, many formation mechanisms for hybrid materials and nanocomposites are based on solvent chemistry, for example the sol-gel process or the wet chemistry formation of nanoparticles. A particularly interesting group of macromolecules are block copolymers, consisting of a hydrophobic segment. They can be tailored in such a way that reveals totally different chemical characters and therefore, they are known as good compatibilizer between two components.
- *Particles and particles-like structures:* organic colloids formed from physically or chemically cross linked polymers can also be used as building blocks for inorganic-organic hybrid materials and nanocomposites. The good control over

their properties, such as their size the broad size range in which they can be produced from several nanometers to micrometers accompanied by their narrow size distribution makes them ideal building blocks for many applications.

Another type of organic macromolecular building blocks is the hyperbranched molecules so called dendrimers. Dendrimers are highly branched regular 3D monodisperse macromolecules with a tree like structure.

The end groups of dendrimers can also be used for an interaction with metal clusters or particles and these nanocomposites are formed often by simply mixing the two components.

Besides their role as cross linking building blocks dendrimers can form hybrid materials by themselves. For example in their outer or inner shell precursors for nanoparticles are grown within the branches of the dendrimers. (Kickelbick, 2007)

1.4 State-of-art techniques for the synthesis of hybrid materials

1.4.1 Sol-Gel process

The sol-gel method is a series of the hydrolysis-condensation reactions. Mainly, an alcoxide $M(OR)_4$ are used as a precursors, where M presents a metal with the valence n and OR presents alkoxy group type $(-OC_nH_{2n+1})$ (usually, methoxy or ethoxy). As an example, the formation of SiO_2 nanoparticles can be given (Livage, J., 2000): inorganic polymerization (condensation) causes the formation of SiO_2 nanoparticles with bigger size, which form a sol and finally, with the time, a gel can be formed. Brinker et al., 1990 have shown that a newly-formed gel can be used in production of glass and ceramic. Another definition, given by Sanchez et al, 1994, is a production method of dispersed materials by the growth of the oxopolymers. Generally, according to the nature of the molecular precursors involved, there exist two types of synthesis:

- “Inorganic” way: the precursor is in form of metallic salt, which is dissolved in water solution, the hydrolysis reaction is followed by precipitation, which is caused by the formation of oxo- bonds.
- “Organic” way: precipitation takes place in organic solution of organo-metallic precursor after reaction with water molecules and it's result of a series of

hydrolysis-condensation reactions. This reaction way is more interesting to use because of its simplicity of controlling (Livage J., 1994).

The both reaction ways have one thing in common: the processes are initiated by the hydrolysis reaction, which allows obtaining the highly reactive particles. The newly-formed highly reactive particles take part in the reaction of condensation, forming oxo-polymers. The sol-gel production method by “organic” way will be the only further used and the sol-gel process will be devoted to it.

The reactivity of the precursor is mainly defined by the electrophile characteristic of metal, caused by the presence of the alcoxy groups. In case of transition metals, the presence of d-orbitals and its unsaturation of coordination sphere have additional influence on the reactivity of the process. Thus, chemical mechanism is divided into two stages (Bradley, D.C., 1958; Corriu, R., 2009; Seebauer, E.G., 2009):

- Hydrolysis, which corresponds to the hydrolysis reaction.
- Inorganic polymerization, a stage of chains' growth.

1.4.1.1 Hydrolysis

This process is defined by the next reaction:

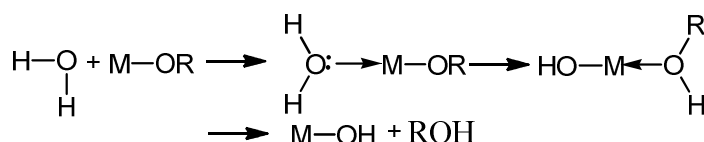


Figure 1-3. General representation of the Hydrolysis reaction

The reaction of hydrolysis can be initiated by the addition of water or water/alcohol mixture to the metal alcoxide or by changing of solution's pH. Its reaction mechanism is a nucleophilic substitution of type SN2. The metal alcoxide hydrolysis steps are shown in the Figure 1-3 : nucleophilic substitution (step 1) on the atom of metal with proton transfer (step 2) with separation of leaving group (step 3).

The velocity of nucleophilic substitution depends on unsaturation of coordination metallic center M of alcoxide, which is presented by difference between maximum value of coordination number N of the metal and its oxidation degree z. Thus, more (N-z) is, more the possibility of proton transfer (step 2) should be, and less activation energy, associated with nucleophile addition, will be.

The initial hydrolysis reaction can be accelerated by the use of catalyst: acid or base reaction medium or nucleophilic catalyst. In case of acid catalysis, the negatively charged alkoxy group can be easily protonated, this fact leads to decrease of electronic density on the metal atom, making it more electrophilic and increasing nucleofugality of leaving group. Logically, transfer of a proton does not influence the overall kinetics of the process. In case of base catalysis, a hydroxyl group replaces the water molecule because of its more nucleophilicity, thus accelerating the first step (Keefer, 1984). The nucleophilic catalyst, like Lewis bases: F⁻ or 4-dimethylaminopyridine (DMAP) creates a hypervalent transition state on the stage of nucleophilic coordination.

A very interesting fact is that catalysis not only speeds up the hydrolysis reaction rate, but also controls the shape of the newly-formed colloid particles. In case of silica colloids, the use of acid catalysis may lead to the formation of the final chain inorganic polymers; while condensation into branched inorganic polymers are more favorable in case of a basic and nucleophilic catalyst use.

1.4.1.2 Inorganic polymerization

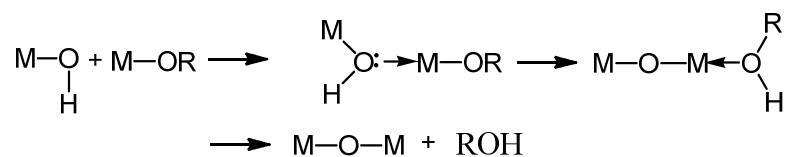
Inorganic polymerization starts even before hydrolysis reaction has been finished. Its mechanism is relatively complex, because four mechanisms (alcoxolation, oxolation, alcoolation and olation) may proceed in parallel (Sallar S., et al, 2004).

Polycondensation

The newly-formed hydroxyl group, bounded to metal atom is a better nucleophile than alkoxy group. Thus, similarly to the hydrolysis, hydroxyl group of metal-organic precursor reacts with non-substituted alcoxide. The reactive product will be either alcohol molecule or water molecule, thus two process may take place: alcoxolation and oxolation, respectively (Pierre, A.C., 1998; Brinker C. J. 1990).

Chapter 1: Bibliography

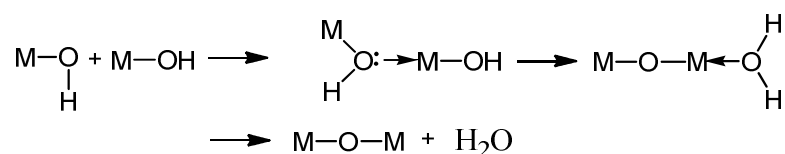
- Alcoxolation : This reaction takes place between two alcoxide molecules: partially hydrolyzed and non hydrolyzed. The reaction mechanism is shown next:



General representation of the reaction:



- Oxolation : This is the case of condensation reaction, where both alcoxide molecules are partially hydrolyzed:



General representation of the reaction:



Inorganic polymerization by coordination

The next inorganic polymerization mechanisms are only possible if the alcoxide coordination sphere is not completed, i.e. $(N-z > 0)$. At the same time, the steric hindrance of metal in its alcoxide molecule may avoid the proceeding of this reaction. But, under favorable conditions: alkyl ligands does not form a steric barrier for reaction to take place and coordination value $(N - z) > 0$, inter-metal bridge can be formed $\text{M}-\text{O}-\text{M}$. Two ways of coordination makes two mechanisms be possible: alcoxolation and ololation:

- Alcoxolation: An oxygen atom of the precursor's alkoxy group may be observed like "a bridge", which connects two metal atoms of alcoxide precursors. Thus, hydrolysis of the precursor does not need to be done before alcoxolation reaction to take place. $2\text{M}(\text{OR})_n = (\text{RO})_n\text{M} - \text{OR} - \text{M}(\text{OR})_{n-1}$

- Olation: Unlike previous reaction, olation reaction involves the partly hydrolyzed precursor. A mechanism is similar to alcolation reaction, by in this case “bridge”, which connects two metal atoms of alkoxides, is presented by the hydroxyl group.



The structure and morphology of the final products of these reactions highly depend on the contribution of every component involved. Thus, several experimental conditions: external (hydrolysis and condensation ratios, catalyst's nature, concentration of alcoxide, solvent, temperature) and internal (nature of metal and alkoxy groups, structure of molecular precursors) influence the inner structure of the obtained oxo-polymer net.

1.4.1.3 Micromixing approach

Mixing is a key parameter in tailoring the particle size distribution in precipitation processes (Bałdyga et al., 1995). It becomes more and more critical when the particle reactivity increases and the particle size decreases. Many theoretical and experimental efforts in understanding of the nano-sized solids precipitation have been made (Schwarzer et al., 2004; Wang et al., 2004; Artelt et al., 2006; Gradl et al., 2006; Marchisio et al., 2006; Schwarzer et al., 2006). Particular emphasize of these studies was given to the development of a relevant numerical model of turbulent mixing in relation to the particle size distribution. High reaction order (Soloviev et al., 2003) and rate of hydrolysis-condensation reactions (Livage et al., 1988) impose serious restrictions to the sol-gel reagents mixing in order to achieve the homogeneous reaction conditions, which are critical for attaining narrow particles polydispersity and reproducibility of the process kinetics.

The need of reproducible fabrication of size-selected monodispersed nanoparticles for different applications has motivated Rivallin et al. (2005a) to design a sol-gel limit reactor with rapid (turbulent) micromixing, which has been further developed by Azouani et al. (2010). The reactor consists of three main parts: two thermostatic containers, T-mixing element and container, which receives the prepared solution.

Figure 1-4 shows the particles size-distribution curves (PSD) at $Re=2 \cdot 10^3$, $3 \cdot 10^3$, $6 \cdot 10^3$ and $8 \cdot 10^3$ measured at $H=1.9$, $C_{Ti}=0.146M$ and $T=20^\circ C$. It appears from this figure that the mean particle size and the width of the distribution curve decrease from $R=3.2$ nm and $\Delta=2.2$ nm at $Re=2 \cdot 10^3$ to $R=2.0$ nm and $\Delta=1.0$ nm at $Re=6 \cdot 10^3$. As discussed

above, we relate the PSD evolution with Reynolds number to the net effect of an enhancement in the mixing processes on the particle precipitation. For $Re > 6 \cdot 10^3$ the measured PSD does not appreciably change with Re . In fact, PSD's obtained at high Reynolds numbers, tend to show slightly greater size and broader dispersion, e.g. $Re = 8 \cdot 10^3$, $R = 2.2$ nm, $\Delta = 1.2$ nm. In the limit of large $Re \geq 4.4 \cdot 10^3$ the colloids are almost monodispersed and the observed dispersion is essentially due to the limited data statistics ($t_{acc} \neq \infty$). The variations of the induction time during these measurements have attained 10% of its initial value ($\frac{\Delta t_{ind}}{t_{ind}} < 10\%$) (Rivallin et al., 2003). The TiO_2 nanoparticles prepared in the sol-gel reactor are almost monodispersed.

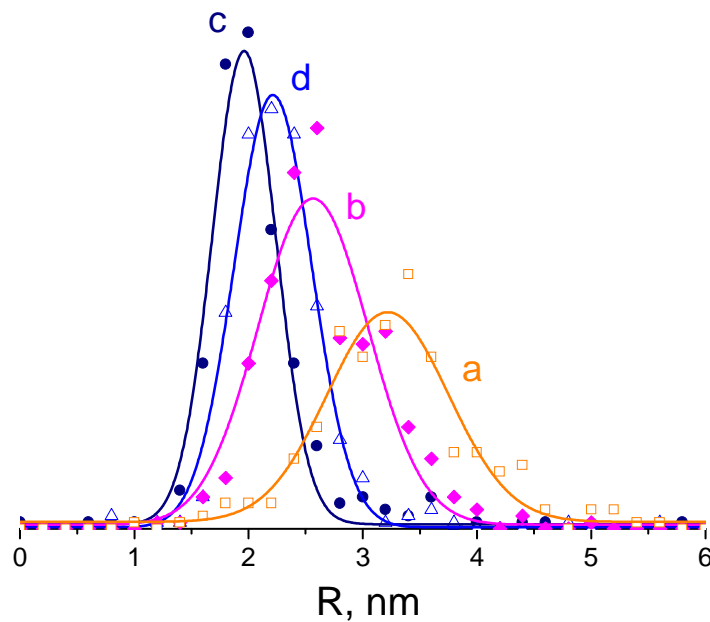


Figure 1-4. Particle size distributions for different injection rate correspondent to $Re = 2 \cdot 10^3$ (a), $3 \cdot 10^3$ (b), $6 \cdot 10^3$ (c) and $8 \cdot 10^3$ (d). Solid curves are Gaussian fits of experimental data.

1.4.1.4 Applications

Nanomaterials, defined as particles ranging from 1 to 100 nm diameter, have become widely used because of their unique physicochemical properties. Among those nanoparticles,

titanium dioxide (TiO₂) is frequently used in the production of paints, paper, plastics, welding rod-coating material and cosmetics just to mention a few. TiO₂ is the most commonly used semiconductor photocatalyst. Among the different nanomaterials, it is the most studied. Activated by UV-A irradiation, its photocatalytic properties have been used in various applications. A wealth of information on TiO₂ photocatalytic in activation of bacteria has been acquired over the last 20 years (Macwan et al 2011)

- Dental implant application: (Yang et al 2009)
- Polylactide nanofibers/nano-TiO₂ blends on biorecognition of anticancer drug daunorubicin (Song et al 2008)
- Antimicrobial nanomaterials for water disinfection and microbial control: potential applications and implications (Li et al 2008)
- Preconcentration and separation of cadmium (Kalfa et al 2009)
- For determination of chemical oxygen demand (Zhang et al 2009)
- Nano-gold supported on TiO₂ coated glass fiber for removing toxic CO gas from air (Kuo et al 2007)
- Application of nano-TiO₂ toward polluted water treatment combined with electro-photochemical method (Chen et al 2003)
- Photocatalytic oxidation of VOCs using nano-TiO₂ photocatalyst (Yu et al 2007)
- Aluminum-doped TiO₂ nanopowders for gas sensors (Bozzi et al 2005).
- Self-cleaning of modified cotton textiles by TiO₂ at low temperatures under daylight irradiation (Choi et al 2007)
- On the electrode of dye-sensitized solar cells (Meen et al 2009)
- Smart corrosion resistant coatings (Radhakrishnan et al 2009)

An exhaustive list will be too long to fit in this work and is not in the scope of this thesis to make a full revision of all the possible applications for TiO₂ materials. However, what is clear is that these materials have big potential of application in a wide variety of fields.

1.4.2 Polymerization and Co-Polymerization

The polymerization of organic compounds was first reported about the mid-19th century and consist on a process of reacting monomer molecules together in a chemical

Chapter 1: Bibliography

reaction to form polymer chains or three-dimensional networks (Young, R. J., 1987). However, it was not until about 1910 that the simultaneous polymerization of two or more monomers (or copolymerization) was investigated when it was discovered that copolymers of olefins and dienes produced better elastomers than either polyolefins or polydienes alone

Polymers and co-polymers can be classified according to the techniques used for monomer polymerization, namely Bulk, Suspension and Emulsion polymerizations. In bulk polymerization, only the monomer (and possibly a catalyst and/or initiator, but no solvent) is fed into the reactor. The monomer undergoes polymerization, at the end of which a (nearly) solid mass is obtained as the polymer product. As we shall see later, bulk polymerization is employed widely in the manufacture of condensation polymers, where reactions are only mildly exothermic and viscosity is mostly low thus enhancing ready mixing, heat transfer, and bubble elimination. Solution polymerization involves polymerization of a monomer in a solvent in which both the monomer (reactant) and polymer (product) are soluble. Suspension polymerization refers to polymerization in an aqueous media with the monomer as the dispersed phase. Consequently, the polymer resulting from such a system forms a solid dispersed phase. Emulsion polymerization is similar to suspension polymerization but the initiator is located in the aqueous phase (continuous phase) in contrast to the monomer (dispersed phase) in suspension polymerization. Besides, in emulsion polymerization the resulting polymer particles are considerably smaller (about ten times smaller) than those in suspension polymerization. (Ebewele, 2000)

This classification scheme, however, does not allow a complete differentiation between polymers and co-polymers. A more complete but still oversimplified scheme that is based on the different polymerization processes classifies polymers into three categories: condensation, addition, and ring-opening polymers. This scheme reflects the structures of the starting monomers. Probably the most general classification scheme is based on the polymerization mechanism involved in polymer synthesis. Under this scheme, polymerization processes are classified as step-reaction (condensation) or chain reaction (addition) polymerization (Young, R. J., 1987).

Even though several classifications exist based in the previously mentioned criteria, what is common to most of them is the method through which polymerization can be achieved and will depend on the selected monomers and the desired type of chains or condensates. These methods are: radical polymerization, thermal polymerization and photo

polymerization, which can also be used to carry on the co-polymerization of more than one monomer. These methods are discussed in deeper detail below.

1.4.2.1 Radical Polymerization

The chemistry and kinetics of free-radical polymerization is described in detail in two excellent books published recently.[Moad et Solomon, 2006] A simple mechanism of free-radical polymerization can be described in terms of the following four elementary reactions:

Initiation



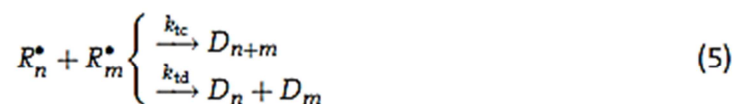
Propagation



Chain transfer to monomer



Termination by combination/disproportionation



In the above kinetic scheme, the symbols I , I^{\bullet} and M denote the initiator, radicals formed by the fragmentation of the initiator and monomer molecules, respectively. The symbols R_n and D_n are used to identify the respective ‘‘live’’ macroradicals and the ‘‘dead’’

Chapter 1: Bibliography

polymer chains, containing n monomer structural units, respectively. To describe the progress of the reaction and molecular weight or chain structural developments during polymerization, population mass balance equations should be derived for all chemical species present in the reactor. These constitute a set of simultaneous differential equations which are usually solved numerically provided that the appropriate rate constants of every elementary reaction are known. (Achilias et Kiparissides, 1994)

However, the term ‘rate constants’ is somewhat of a misnomer, as these so-called rate constants vary during the course of any polymerization. This variation was assumed in order to quantitatively describe the effect of diffusion-controlled phenomena on the polymerization kinetics. That means that k_i 's appearing in Equation (1) to (5), which are influenced by diffusional phenomena are to be regarded as ‘‘apparent rate constants’’ or ‘‘rate coefficients’’ rather than ‘‘rate constants’’. (Russel 2002)

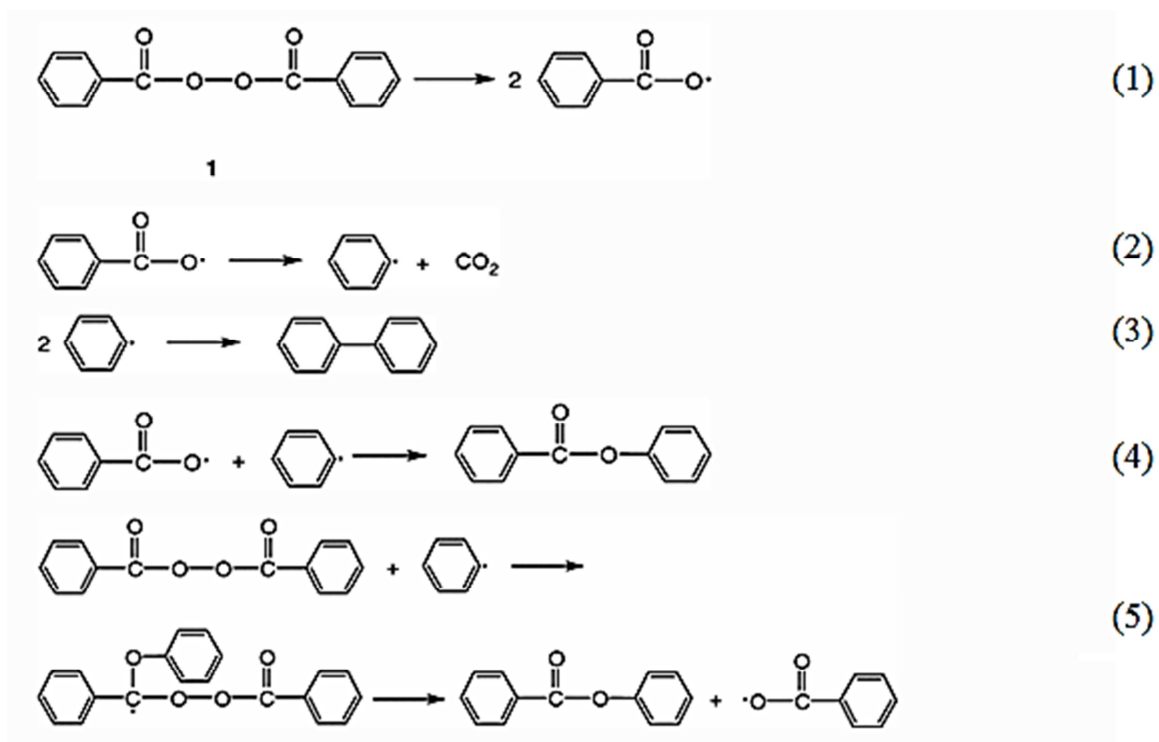
In free-radical polymerization, the presence of diffusion limitations is so well documented that different manifestations have been given particular names. The impact of diffusion on the termination step is named as the Trommsdorff or gel-effect, while the effects on the propagation and initiation reactions are known as the glass and the cage-effects respectively. Different theories for the modeling of such effects have been proposed, a fair review of the most relevant models is available from (Achillias, 2007).

Ideally, for radical polymerization to take place in the best conditions, the initiators should be relatively stable at room temperature but should decompose rapidly enough at polymer processing conditions to ensure a practical reaction rate. A large number of free radical initiators are available (Stevens 1999, Odian 2004); In this work two of the three available types are used: (1) thermal initiators, including peroxides and azo compounds create radicals when subject to a source of heat, (2) photoinitiators: compounds that form radicals under influence of light. A more detailed description of the two types of radical initiators is provided in the next subsections.

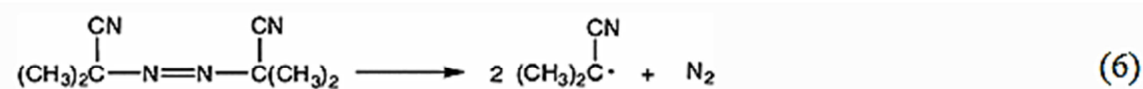
Thermal initiators for radical polymerization

There are different types of thermal initiators that can be used depending on the monomers to be polymerized; the most common are peroxides, hyperperoxides and azo compounds. The most commonly used peroxide is benzoyl peroxide, which undergoes

thermal homolysis to form benzoyloxy radicals (1). The benzoyloxy radicals may undergo a variety of reactions besides adding to monomer, including recombination (reverse of eq. 1), decomposition to phenyl radicals and carbon dioxide (2), and radical combination (3) and (4). These secondary reactions occur because of the confining effect of solvent molecules (cage effect), and as a result, the concentration of initiator radicals is depleted. Another “wastage” of initiator reaction is induced decomposition (5).



Among the azo compounds the most commonly used is α, α' -Azobis (isobutyronitrile) or AIBN this initiator decomposes at relatively low temperatures. The driving force for decomposition is the formation of nitrogen and the resonance-stabilized cyanopropyl radical, as shown in reaction (6).



The differences in the decomposition rates of various initiators are conveniently expressed in terms of the *initiator half-life* ($t_{1/2}$) defined as the time for the concentration of I to decrease to one half its original value. The rate of initiator disappearance is given by:

$$\frac{-d[I]}{dt} = k_d[I] \quad (7)$$

The half-life of the most commonly used thermal initiators at different temperatures is presented in Table 1-2 below:

Table 1-2. Half-life of the mos common initiators in respect to temperature.

Initiator	Half Life time at a given temperature			
	50 °C	70 °C	85 °C	100 °C
AIBN	74 h	4.8 h		7.2 min
Benzoyl Peroxide		7.3h	1.4h	19.8 min
Acetyl Peroxide	158 h	8.1h	1.1h	

The previous table shows the importance of choosing the initiator that better suits the application and the control of the parameters for its more efficient performance. In our case, AIBN was chosen to polymerize thermally the HEMA polymers and HEMA-EMA copolymers as will be explained in Chapter III.

Peroxides and azo compounds dissociate photolytically as well as thermally. The major advantage of photoinitiation is that the reaction is essentially independent of temperature. Furthermore, better control of the polymerization reaction is generally possible because narrow wavelength bands may be used to initiate decomposition (with less side reactions), and the reaction can be stopped simply by removing the light source. The reaction is fast (seconds) as compared to the thermal initiation (minutes or even hours). A wide variety of photolabile compounds are available, including disulfides (1), benzoin 8 (2), and benzyl 9 (3). Table 1-3 lists some commercial available photoinitiators and their decomposition wavelength. It is interesting to note that most of the initiators contain benzoyl groups which can form stable benzoyl radical through the resonance stabilization of phenyl ring.

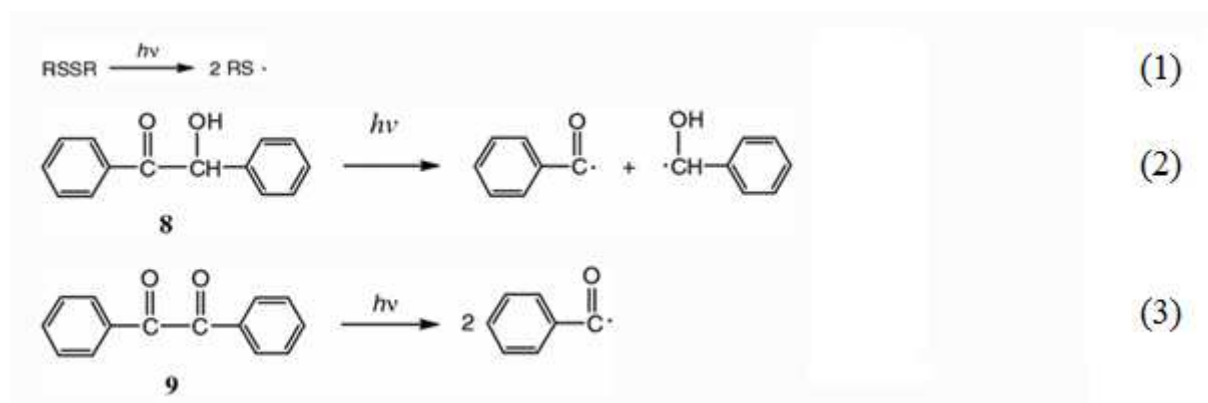


Table 1-3. Commercial photoinitiators and their initiating wavelength (Holman, 1984)

Chemicals	λ_{max} (nm)
1-hydroxy-cyclohexyl-phenyl-ketone	245
2-methyl-1-[4-(methylthio)phenyl]-2-(4-morpholinyl)-1-propanone	307
2-benzyl-2-(dimethylamino)-1-[4-(4-morpholinyl)phenyl]-1-butanone	324

1.4.2.2 Co-polymerization Routes

Macromolecular design and architecture through copolymerization of monomers has led to a number of commercially important polymers. Copolymer composition can be varied over wide limits, resulting in a wide range of property/process performance. A copolymer may be composed of comparable amounts of the constituent monomers. The properties of the resulting copolymer will be substantially different from those of the parent homopolymers. On the other hand, the copolymer may contain only a very small amount of one of the monomers. In this case, the gross physical characteristics of the copolymer probably approximate those of the homopolymer of the major constituent, while the minor constituent confers specific chemical properties on the copolymer.

Some considerations relevant for copolymerization kinetics are:

- The number of reactions involved in copolymerization of two or more monomers increases geometrically with the number of monomers. Consequently, the propagation step in the copolymerization of two monomers involves four reactions.
- The number of radicals to be considered equals the number of monomers. The terminal monomer unit in a growing chain determines almost exclusively the reaction characteristics; the nature of the preceding monomers has no significant influence on the reaction path.
- There are two radicals in the copolymerization of two monomers. Consequently, three termination steps need to be considered.
- The composition and structure of the resulting copolymer are determined by the relative rates of the different chain propagation reactions.

In this work Radical Polymerization is used all along in its thermal and photo radicalization versions. As will be explained on Chapter III, AIBN was used as thermal initiator of the radical polymerization for HEMA and HEMA-EMA based materials. For photo-activated radical polymerization (or photopolymerization) 4,4'-bis(dimethylamino) benzophenone was used as initiator. In the next section, a more detailed explanation of the methods found in literature specific of TiO₂ hybrid materials will be presented.

1.5 Hybrid Materials based on TiO₂

Literature about hybrid materials based on TiO₂ is constantly growing. Our research group has contributed in an important way to TiO₂ Hybrid materials development by several thesis works and publications. In this section, the basis of the hybrid material synthesis previously employed are briefly explained as well as the darkening phenomena, characteristic of the TiO₂ hybrids developed by our research group in the last decades.

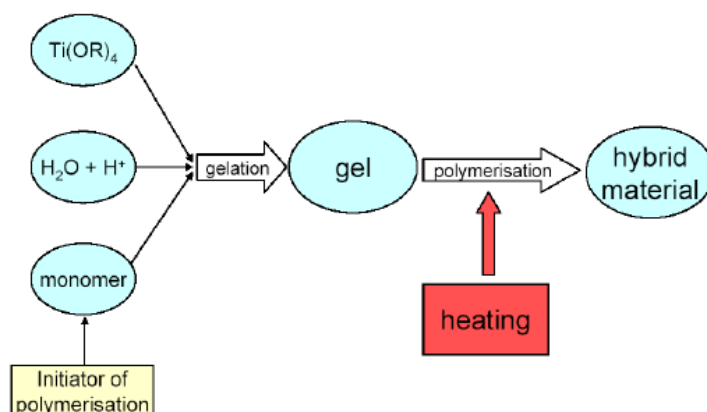
1.5.1 Kameneva synthesis route

The preparation method of the pHEMA-TiO₂ hybrid materials has been developed by Kameneva et al. (2006), based on earlier studies by Novak et al. (1991) on silica based materials. In these previous studies, the authors have prepared molecular precursors, tetraalkoxy silanes, where aliphatic groups contained unsaturated groups (possible to polymerize). A simple reaction of transalkolysis where initial ethoxy groups have been concurrently replaced by the alkoxy group, has been used for preparation of the precursor. As a result, the newly obtained molecular precursor has been hydrolysed; this fact has provided the inorganic

polymer network Si-O-Si. The excess of initial solvent (unsaturated alcohol) and the organic substituents on the surface of SiO₂ chain network (deprotonated form of the initial unsaturated alcohol) were used for the organic polymerization. Finally, the newly proposed approach of hybrid material elaboration has led to the process, which allows formation of interpenetrated networks of silica (SiO₂) and aliphatic chains (due to the organic polymerization), and a bulk polymer samples of hybrid materials obtained this way were free of unwanted surface issues: cracks and fissures. Hajjip et al. (1999) have followed the same synthesis path for the preparation of the HEMA-based hybrid material, where silica was used for the inorganic network formation.

In her work, Kameneva (2006) proposed the use of HEMA molecules for the titanium precursor, titanium tetra-isopropoxide (TTIP) modification and as a solvent. In general, the synthesis schema depicted in Figure 1-5 shows several major steps of this synthesis route:

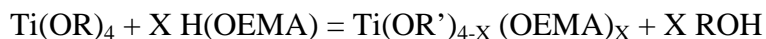
- Transalkolysis: a reversible reaction that takes place in the considered case between alkoxy groups of the TTIP precursor, alcohol and 2-hydroxyethyl methacrylate (HEMA).
- Hydrolysis-condensation reactions of the modified precursor, which led to the formation of inorganic TiO₂ oxo-network. During this stage, the alkoxy substituents (- OEMA) are partially replaced by hydroxyl groups.
- Organic polymerization: a radical reaction between the unsaturated C=C bonds, which led to the organic aliphatic chain (-CH₂-CH₂-) formation.



Chapter 1: Bibliography

Figure 1-5. Schema of hybrid materials elaboration proposed by Kameneva et al. (2006).

During the exchange reactions between HEMA and TTIP, the isopropoxy groups of TTIP are substituted by the alkoxide groups of HEMA:



Since the transalkolysis reaction is reversible, the process can be shifted to the reaction products (modified precursor) by evaporating of the released isopropanol under vacuum pumping. In this way, the substitution number X can be increased up to 4 of the total precursor modification (formation of Ti(OEMA)_4). A large difference between the boiling temperatures of isopropanol (81 °C) and HEMA (207-208 °C) validates this solution. It was experimentally observed by Raman spectroscopy that evaporation of isopropanol under 1-5 mbar pressure during 90 minutes was sufficient for the isopropanol elimination. The formation of the oxo- TiO_2 chains requires hydrolysis of the newly obtained titanium alkoxide. During this process isopropoxy and alkoxy (OEMA) groups may be partially hydrolyzed resulting in the hydroxyl group's formation. Hydrolyzed titanium precursor produce condensed titanium-oxo-alkoxy species, which can associate into the macroscopic inorganic gel.

The gelation time as a function of the hydrolysis ratio and proton ratio in particularly, the system $\text{Ti/HEMA/H}_2\text{O/HCl}=1/6/3/0.18$ demonstrated a gelation time of about 10 minutes.

The -OEMA substituents possess unsaturated double $\text{C}=\text{C}$ bonds, which can be polymerized. Kameneva et al. (2005) have used thermal polymerization process as the final stage in the hybrid elaboration scheme, for which 0.5 wt.% of 2,2'-azobis(2-methylpropionitrile) (AIBN) has been added to the monomer solution. The vinyl groups of the HEMA monomer participated in the formation of the aliphatic bushy 3D-polymeric structure according to the scheme presented in Figure 1-6.

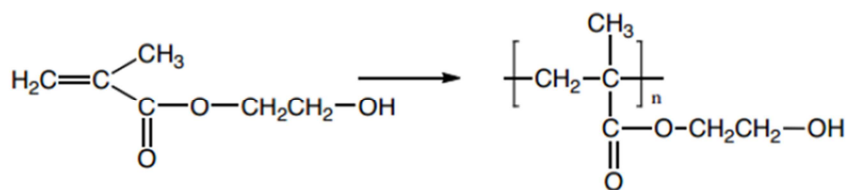


Figure 1-6. Schematic representation of HEMA polymerization.

The overall polymerization process includes several temperature treatment steps:

- heating temperature $T = 65\text{ }^{\circ}\text{C}$ during 20 hours;
- heating temperature $T = 120\text{ }^{\circ}\text{C}$ during 3 hours.

It was also proved that additional polymerization at $120\text{ }^{\circ}\text{C}$ during 3 hours did not improved significantly the monomer-polymer conversion rate.

After completing the synthesis, transparent light-yellow monolithic materials able to withstand mechanical processing and optical-grade polishing were obtained. An example of the hybrid sample is shown in Figure 1-7. A very good homogeneity of the material has been achieved, free of internal cracks and bubbles. According to the synthesis schema, the obtained materials belong to the Class II hybrids consisting of covalently interacting organic and inorganic chains.

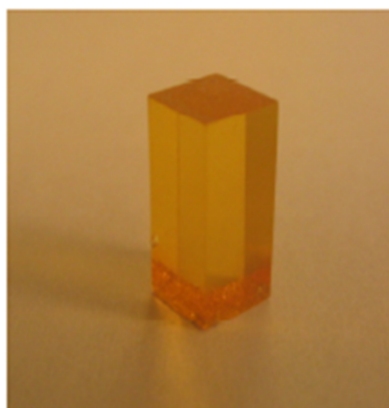


Figure 1-7. pHEMA-TiO₂ hybrids obtained by Kameneva et al. (2006).

1.5.2 Gorbovyi synthesis route

This method is based on the Kameneva method (Kameneva *et al.* 2005) that has been proposed for the TiO₂ gel based hybrid fabrication. However, the inorganic morphology was

poorly defined and some modification was done to the synthesis of the materials, because of this change, the products are highly sensitive to local composition of the reactive fluid. This is a case of oxo-TiO₂ nanoparticles prepared from the titanium tetraisopropoxide (TTIP) precursor. Gorbovyi synthesis route is based in the following steps modified from Kameneva method:

1. Generation of nanoparticles: Use of the sol-gel reactor described in the experimental methods, that assures an homogeneous reaction conditions of the mixed fluids and permits generation of monodispersed oxo TiO₂ nanoparticles. The thermostatic stock solutions containing TTIP and water in 2-propanol solvent are injected into the mixer through two input tubes. This injection is exocentric: the fluids form a vortex before entering in the main tube. The two reagents' flow rates are maintained equal varying from 2 to 12 ml s⁻¹ by applying an external gas pressure (N₂, purity 99.995%). The diameters of two input tubes (1.0 mm) and one main tube (2.0 mm) are chosen in order to assure a continuity of the Reynolds number. The static T mixer performance has been studied by several groups and a considerable narrowing of the particle size distribution. In application to the sol-gel process, its advantage is related to the hierarchical growth mechanism of the structural units (Azouani et al, 2007) in which reactivity step wisely decreases with increase of size. The conditions for the experiments for the sol particles were generated in 2-propanol solutions with TTIP at concentration $C_{Ti} = 0.15$ M and hydrolysis ratio $H = 2.0$ and at 20 °C. According to Azouani et al (2007), nanoparticles nucleate in these conditions; however, their growth is strongly prohibited. The fabricated nanoparticles are not crystalline, of general formula $TiO_{2(x+y)/2}(O^i Pr)_x(OH)_y$, and are composed of a metal oxide core with surface propoxy (Oⁱ Pr) and hydroxy (OH) groups.
2. Surface exchange and nanoparticle stability. The solvent exchange is carried out at the next stage. HEMA (97% purity, Aldrich) was preliminarily distilled in order to eliminate impurities and traces of hydroquinone (hQ), which is an inhibitor of spontaneous polymerization of the monomer. As we have recently shown, traces of hQ induce yellow coloration of the pHEMA-TiO₂ hybrids due to the formation of the hQ-Ti complex (Kutnetzov et al, 2009), which does not induce charge separation and partially screens the interband absorption of TiO₂. The solvent

exchange does not influence the particle size and aggregation state. Figure 1-8 shows the ACF of the concentrated 1.5 M HEMA–TiO₂ colloid, which was obtained after the 2-propanol substitution by HEMA with the volume ratio HEMA : 2-propanol = 1 : 10. Obviously, the quality of the ACF (signal-to-noise) increases because of the 10-times higher nanoparticle concentration. Because of the higher HEMA dynamic viscosity η the measured ACF decay time τ looks longer; however, the particle radius $R = 2.5$ nm defined by $R = k_B T q^2 \tau / 3\pi\eta$ (where k_B , T and q are correspondingly the Boltzmann constant, temperature and scattering vector) is conserved after the solvent exchange.

3. Hybrid preparation. A polymerization of the HEMA–TiO₂ precursor was realized thermally with the addition of an AIBN initiator to the nanoparticulate precursor. Non-colored transparent hybrids were obtained after 24 h of heating at a temperature of 75 °C. Mabilieu *et al.* (2008) have proposed to monitor the monomer polymerization by Raman spectroscopy, observing characteristic vibrational peaks of C=C at 1407 and 1641 cm⁻¹, associated with C=CH₂ stretching and C=C aliphatic stretching vibrations, respectively. Higher temperature treatment is known to provide diffusion possibilities and allows better steric adjustment for the efficient organic polymerization of HEMA moieties. We have observed that both longer (75 °C/ 48 h) and higher temperature (90 °C/24 h) treatments decrease the non-polymerized organic component by up to 30% (temperatures above 110 °C were skipped in the present study, since they produce non-desirable yellowish coloration of samples). No systematic quantitative estimations of the extent of polymerization were carried out because no safe procedure is available for peak normalization between different samples. However, residual HEMA monomers were always observed in most concentrated hybrid samples ($C_{Ti} \geq 1.5$ M) indicating that the corresponding organic polymerization is extended but incomplete. (Gorbovyi et al, 2011)

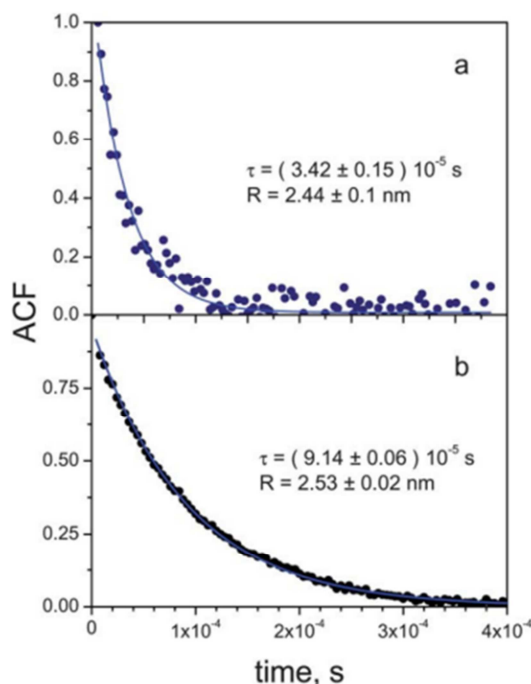


Figure 1-8. Characteristic ACF of oxo-TiO₂ nanoparticles after preparation in the sol-gel reactor ([Ti] = 0.15 M, H = 2, T = 20 °C, 2-propanol solution) (a) and after surface exchange with HEMA ([Ti] = 1.5 M) (b). Taken from Gorbovyi et al. 2011)

1.5.3 Light induced darkening of pHEMA-TiO₂ gel based hybrids

Kameneva *et al.* (2005) and Kuznetsov *et al.* (2009) have shown that the TiO₂ gel-based hybrids become dark under UV irradiation, which is explained by the accumulation of polaron-like Ti³⁺ centers evidenced by EPR measurements. Figure 1-9 shows absorption spectra of the different hybrids, which span from UV-A to near-IR spectral range. The spectral changes are reversible and the materials recovers transparency after a long time (weeks to months). Although gels are fundamentally different from titanium oxide solids, certain similarities of their properties exist. Indeed, the gel darkening threshold energy $E_{\text{gel}}=3.24$ eV (Bityurin *et al.*, 2003) is very close to the bandgap energy of the anatase solids, $E_g=3.2$ eV. The absorption of a photon with $h\nu > 3.2$ eV results in the electron transition from the valence band due to the O₂- 2p orbital to the conduction band due to the Ti₄₊ 3d orbital (Daude *et al.*, 1977).

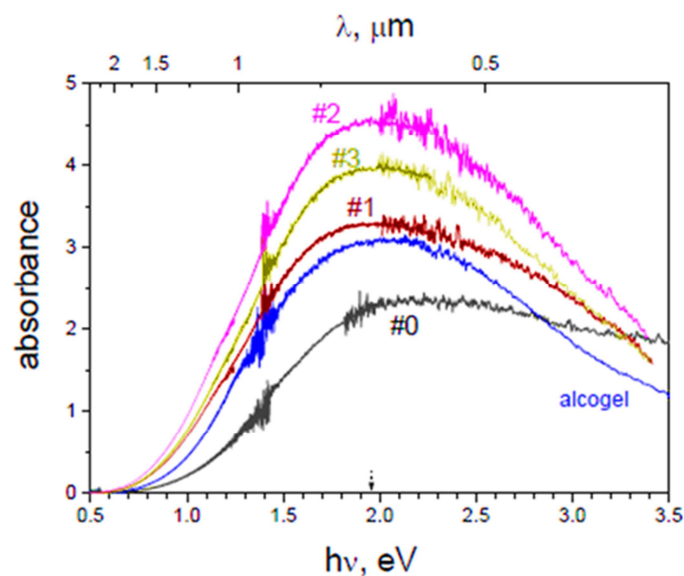


Figure 1-9. Laser-induced absorption of different pHEMA-TiO₂ hybrids (labels #0, #1, #2 and #3 designate hybrids based on Ti₁₆-cluster isolated condensed species, linear gel chains at the gelation point and branched gel chains after aging) and of wet alcogel. Taken from Gorbovyi, 2012.

The schema of the photo induced processes in TiO₂-based hybrids is shown in Figure 1-10. The absorption of a photon $h\nu_1$ (1) results in the electron transition from the valence band due to $2-O-2p$ -orbital to the conduction band due to $4+ Ti 3d$ -orbitals. A light hole $+h$ with a lifetime $+h \tau$ is believed to escape rapidly into the organic PHEMA component as $+h_{tr}$ (3) or to recombine with already trapped electron (6). The CB-electron can recombine with either “fast” hole (2) or (if its energy is sufficiently high: $g_a h\nu - E \geq E$) with already trapped hole (9). If not annihilated, it is trapped by the Ti^{4+} center (binding energy D_e) with quantum efficiency η (4). Ti^{3+} has very long lifetime $\tau \geq 10^7$ s and its spontaneous (“dark”) relaxation (5) is slow, while reexcitation in the CB (7) may be dominant. This process is described by absorption cross-section σ_b . The successfully reexcited CB electrons can migrate to the localized hole $+h$ and recombine with it (9) with the quantum efficiency η_b . If not, the electrons are retrapped by a Ti^{4+} center with the probability $1-\eta_b$.

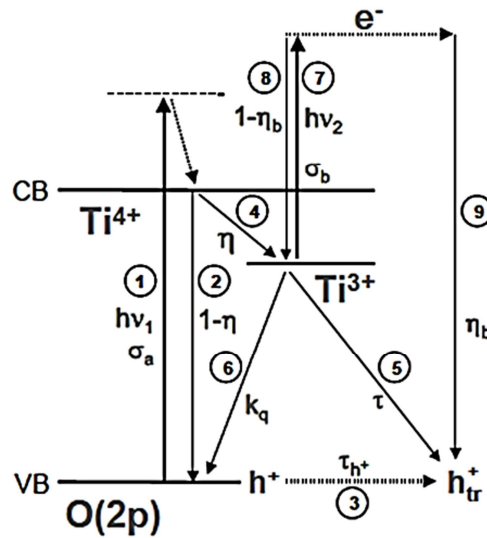


Figure 1-10. Schema of relevant photoinduced processes in TiO_2 hybrids. Taken from Gorbovyi, 2012.

A comparison made of different pHEMA- TiO_2 hybrids allowed to evidence correlations between their nanoscale morphology and photonic sensitivity. The experimental data are shown in Table 1-4. Indeed, the hybrids prepared of smallest Ti_{16} clusters show the lowest charge separation efficiency and maximum charges loading between the considered samples. On the other hand, the maximum efficiency and loading demonstrate the hybrids with quasi-linear gel chains. Isolated large condensed species (aggregates of nanoparticles) take intermediate position between these two limit cases.

Table 1-4. Photonic sensitivity of different hybrid samples. Taken from Gorbovyi, 2012.

Inorganic component	Charges separation efficiency	Maximum charges loading, $\text{Ti}^{3+}/\text{Ti}^{4+}$
Ti_{16} clusters	6 %	4.6 %
Isolated condensed species	12 %	8.2 %
Linear gel chains (gelation point)	12 %	14 %
Branched gel chains (after aging)	12 %	12 %
Alcogel	25 %	7.3 %

The reference Ti_{16} clusters sample can be described as a nanocomposite where the inorganic nano-domains are well dispersed in the organic polymer. Because the starting inorganic components are preformed species, the size and the nature of the hybrid interface are well defined, as reported by Trabelsi *et al.* (2005).

1.6 Conclusions

The literature analysis shows a possibility to produce TiO₂ hybrids with different type of polymers and polymerization reactions. Among the possible candidates and polymerization reactions HEMA and EMA monomers have been chosen for this study. Their introduction is especially interesting because of different hydrophilic and hydrophobic characters of these monomers. The thermal polymerization has been most widely studied. The NBB approach based on NPs, developed in PgD by Gorbovyi (2012), gives the best charge separation efficiency and charge loading.

Chapter 2 : Experimental Techniques

Chapter 2: Experimental Techniques

The principle of characterization methods and equipment that has been used in this work will be presented in this chapter. The description of the equipment and its utilization will not be fully described since we assume the reader was familiarized with most of the equipment. However, we will pay special attention to the procedures, equipment and techniques appearing to be less common or that constitute a fundamental step in the preparation of the materials described in this work and we will offer a more detailed description.

2.1 Glove-box

The glove box is an instrument that permits experiments in an enclosed environment having a controlled atmosphere, to avoid the accumulation of oxygen and humidity. The purification system is constituted by a nitrogen recirculation system, filters and a copper catalytic matrix. Working inside the glove box, avoids collateral reaction catalyzed by humidity or oxygen presence. The equipment used for the synthesis requiring controlled atmosphere was a MBRAUN LABstar Glove Box Workstation with an attainable purity level $\text{H}_2\text{O} < 1 \text{ ppm}$, $\text{O}_2 < 1 \text{ ppm}$.

2.2 Sol-Gel reactor

The schema of the developed reactor with temperature and atmosphere control and in-situ particles granulometry is shown in Figure 2-1. The reactor consists of three main parts: two thermostatic containers, T-mixing element and container, which receives the prepared solution.

Reservoirs

Reservoirs (inner and outer covers made of inox) are placed at upper point of the experimental set. Temperature of containers may be regulated by thermostat. They are used to store hermetically the prepared solutions of reagents under controlled conditions. The solutions of reagents (TTIP and H_2O) in 2-propanol have been prepared in a glove-box, which allows performing precursors preparation under controlled conditions (in case of TTIP solution, impact of humidity should be avoided). The newly prepared reagent solutions are transferred to respective reactor containers with the help of syringes. A permanent nitrogen flow U ($\text{H}_2\text{O} < 5 \text{ ppm}$) allows putting the reactor system under controlled conditions (non humid atmosphere). An injection may be performed only after delay of 30-60 min: time required for temperature stabilization of all system.

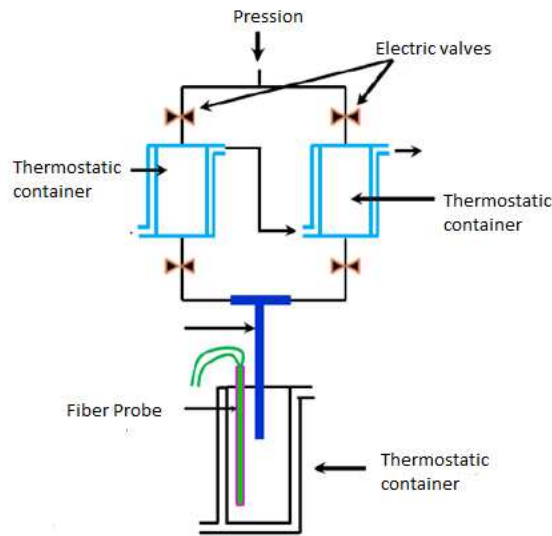


Figure 2-1. The principal schema of the sol-gel reactor.

T-mixer

The T-mixer consists of two inlets (internal diameter of each arm 1 mm, and their length is 20 mm) and one outlet (internal diameter 2 mm, its length is 200 mm). Choice of the arm's diameter has been based on the importance of controlled condition (the same Reynolds number) $\left(Re = \frac{4Q\rho}{\mu\pi d} \right)$, where Q: flow of fluid ($m^3.s^{-1}$), ρ : density ($kg.m^{-3}$), μ : dynamic viscosity (Pa.s) and d : diameter of outlet (m). The T-mixer, which is used in the reactor, is shown in the Figure 2-2. Specially designed inner volume of T-mixer allows formation of the tangential inlet jets, which induce the formation of a vortex promoting micromixing. The time of the mixture was determined based on the neutralization reaction between a strong acid and a strong base in the presence of a color indicator (Pohorecki, R., 1983; Li, K.T., 1986; Rousseaux, J.M., 2000). The micromixing time is in range 4-8 milliseconds, if Reynolds number is $4000 < Re < 10000$. It is less than the characteristic time of the TTIP hydrolysis time.

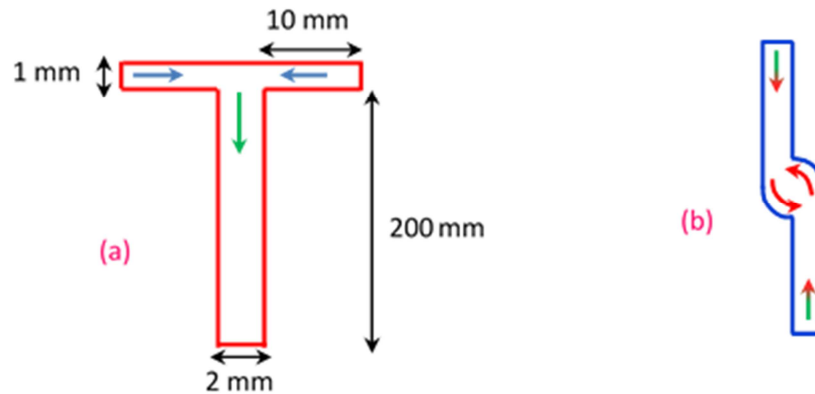


Figure 2-2. Schematic representation of the T-mixer, used in the sol-gel reactor: (a) side view; (b) top view..

Solution holding container

The holding container is a double-walled glass, cylindrical form flask of an inner diameter of 5.5 cm and a total volume of 250 cm³. The temperature control is performed by a thermostat with a capacity of 4.5 litres (Haake, DC10K15), which allows coolant circulation in both reservoirs, and in the container, which holds sol of TiO₂ particles. Special slot is also intended for the fiber optic probe which allows in-situ measurements to be performed. The moisture contamination when transferring the sample in the optical cell for classic measures is thus avoided.

2.3 Dynamic Light Scattering (DLS)

Hydrodynamic radius of a small particle can be measured by dynamic light scattering method (DLS) in case of the studied particle is smaller than wavelength of incident light. Behavior of larger particle is not the same as a particle of a smaller size: the peaks of the light scattering spectrum, in case of large particles, have broad nature, while scattering of light, observed in the small particles, produces relatively sharp peaks in light scattering intensity spectra. In general, the effect of light scattering may give two types of information: intensity of diffused light by particles (static light scattering, SLS) and hydrodynamic radius of the particle (DLS). The intensity of dynamic light diffusion of DLS has been used for measurement of hydrodynamic radius of particles. In general, this method is based on the Doppler Effect. While being in Brownian motion a particle may influence the spectrum of diffused light: because of the Doppler Effect, it becomes broader (Figure 2-3). Thus, the particles, which are getting closer to the observation point, diffuse light with $\lambda' < \lambda$ in

contrary, molecules, which will move into opposite direction, will diffuse light with different wavelength. As the result, heterogeneity of the total light diffusion, produced by molecules in Brownian motion, will cause the broadening of its spectrum. The Stokes Einstein equation describes the relation between the particle radius and diffusion coefficient (in case of spherical particle observation):

$$D = \frac{K_B T}{6\pi\mu R}$$

Where μ (Pa.s) – dynamic viscosity of the medium, T (K) – medium temperature and $K_B = 1,3806.10^{-23}$ J*molecule⁻¹K⁻¹ is Boltzmann's constant. It is clear that the size of the particles has influence on the effect of signal broadening. This relation shows that with the constant temperature and in the same medium, the diffusion coefficient and the radius of the particles are in opposite relation.

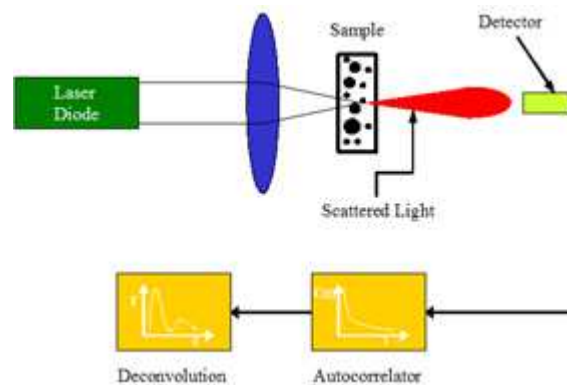


Figure 2-3. Broadening of the spectrum, caused by Doppler Effect.

2.4 Transmission Electron Microscopy (TEM), Scanning electron microscopy (SEM)

This characterization method is used to analyze material microstructure with a resolving power of a several angstroms. TEM is based on the principle of electron diffraction; the image of the sample is formed from the interaction of the electron transmitted through the specimen. TEM image allows providing information concerning the inner structure of materials and provides information about its morphology (size and a form of the grains). There exist several different operational modes: Selected area electron diffraction (SAED) is used to study crystallographic structure; Electron energy loss spectroscopy (EELS) that give some characterization possibilities. The transmitted electrons can be rejected based upon their voltage (which, due to constant charge is their energy) using magnetic based equipment

(EELS spectrometer). This device allows selection of particular energy range, which can be associated with the way the electron has interacted with a sample. Presence of different chemical elements in the sample results in the special range of energy of transmitted electrons. Thus, this effect can be used to provide information on elemental composition based upon the atomic transition during electron-electron interaction. A bright zone of an image corresponds to region, where diffusion of electrons takes place.

The scanning electron microscopy (SEM) is a technique that allows to reproduce an image of a sample's surface by scanning it with a beam of electrons with a very high resolution allowing the magnification of the object even hundreds of thousand times (Figure 2-4). The electrons focused on the sample's surface, interact with the atoms that make them produce signal that contains information about topology, composition and other properties of the sample.

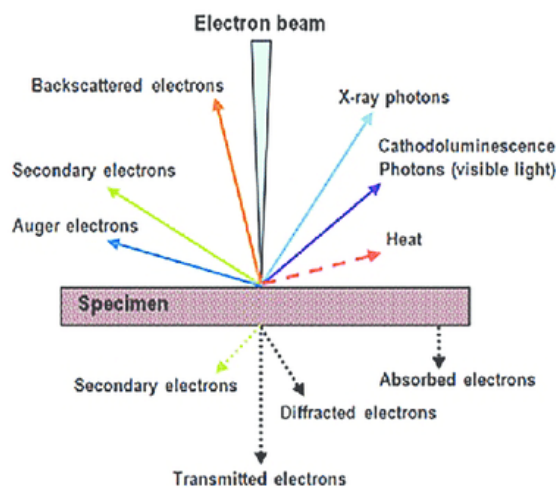


Figure 2-4. Electron effects present in SEM.

The beam of electrons has an energy ranging from 0.2 keV to 40 keV and is focused into a spot of about 0.4 nm to 5 nm in diameter. To form the final image electrons will “scan” every surface point, thus each topological unit of a sample corresponds to its virtually reproduced surface presentation (GN-MEBA group and Brisset F., 2008; Goldstein J., 2003). The SEM images presented in this work, have been produced by a microscope Zeiss Supra 40VP and Leica 440 with an acceleration voltage ranging from 1 to 30 kV.

2.5 RAMAN spectroscopy

Raman spectroscopy is a technique used to study vibrational, rotational and other low frequency modes on the material molecules. It is a nondestructive analysis technique, based on detection of inelastic scattered photons, which are produced after interaction between the beam of monochromatic light (laser source) and the sample. The difference of wavelength of the incident photons and the diffused ones gives information about the chemical nature of the sample involved. At the same time, the position of the peaks on RAMAN spectra (specific wave number) does not relies on the frequency and intensity of the monochromatic source, which has been chosen for analysis. The Raman effect occurs when light impinges upon a molecule and interacts with the electronic cloud and the bonds of the molecule. A spontaneous Raman Effect is a form of light scattering: a photon excites the molecule from the ground state to a virtual energy level. When the molecule relaxes, it emits a photon and it returns to a different rotational and vibrational state. The difference in energy between the original state and a new one leads to a shift in the emitted photon's frequency away from the excitation wavelength.

While performing Raman analysis, information about several parameters should be taken into account:

- A part of the light of the same wavelength as incident beam diffused by a sample, a Rayleigh diffusion (elastic diffusion way);
- A small part or diffused photons have different wavelength than the incident ones.

In case when vibrational state of a molecule is more energetic then the initial state, the emitted photon will be shifted to a lower frequency in order for the total energy of the system to remain balanced. This shift in frequency is called a Stokes shift. Contrarily, in case of vibrational state of less energetic position than the initial one, the emitted photon will be shifted to a higher frequency. So, this shift is called Anti-Stoke shift.

A necessary option is required: a change in the molecular polarization-amount of deformation of the electron cloud for the Raman Effect to take place. The amount of the polarizability change determines the intensity of Raman scattering.

Opposite to infrared, where the interaction between a molecule and light is determined by the dipole moment. Utilization of Raman spectroscopy allows analyzing transitions that might be not active in IR spectroscopy. (Nakamoto K., 2009) Graphic presentation of several

principles: Rayleigh diffusion, Stokes diffusion and anti-Stokes diffusion is shown in Figure 2-5.

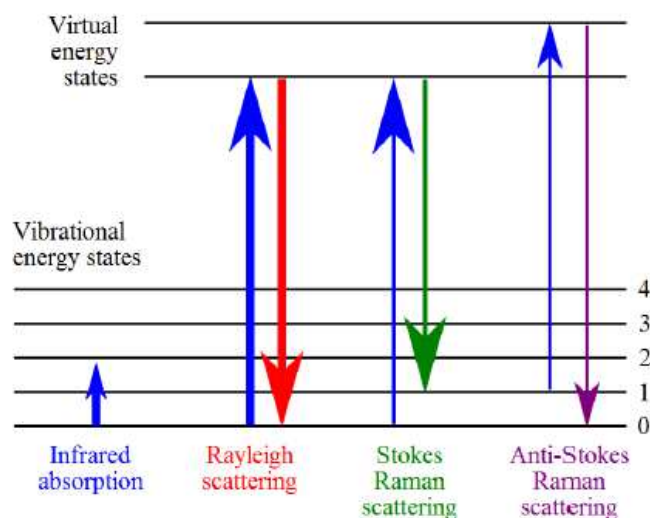


Figure 2-5. The principles of Rayleigh diffusion, Stokes diffusion and anti-Stokes diffusion.

The spectrometer HR800 (HORIBA Jobin Yvon) with the spectral and space resolution of 0.25 cm^{-1} and $\sim 5 \text{ }\mu\text{m}$ respectively, was used for characterization of the hybrid material samples. The spectrometer is equipped with “X-Y directional manipulator”, a system of confocal and adjustable slits and a Peltier-cooled CDD camera. The Notch filters have been used to cut Rayleigh frequency. The wavelength of monochromatic light used were 632.8 nm (using built in He/Ne laser as a light source), 514.488 nm and 363.8 nm supplied by the use of filters coupled with Argon laser.

2.6 Thermal Gravimetric Analysis and Differential Scanning Calorimetry (TGA-DSC)

The thermal analysis is a set of techniques where a physical or chemical property is determined and controlled in function of the time, temperature or/and heat flow. Some of the characteristics that we could determine with this technique are transition points, enthalpy, heat capacity, thermal expansion, mass loss or gain, crystallization, viscosity, denaturation, determine purity, investigate polymorphic transition, studies of hardness and decomposition.

The Thermal gravimetric analysis (TGA), is a destructive technique of characterization that permit know about the decomposition, oxidation reduction and thermal condition for obtain stable compounds. The instrument consist in a very sensitivity balance,

an oven, a temperature control a system to control the atmosphere, a microprocessor and a thermocouple placed the nearest possible to the sample. In certain designs the gases could go to Infrared spectrometer or a system of Gas chromatography.

The differential scanning calorimetry (DSC), this method determines the difference between the amount of heat flowing to the sample and a reference (crucible empty), in this way it's possible to test substance transition (endothermic or exothermic) such as system will measure the sample's thermal energy lost or gain in respect to the reference. Figure 2-6 shows at left the sample holder rod for TGA-DSC experiments and at right the working principle of the DSC measurements. The temperature sensing elements known as RTD are Platinum as Metal 1 and Pt-Rh alloy as Metal 2, the potential U is the potential difference between the reference and the sample in μV that can be transformed later to energy units by a calibration curve taking known fusion points of various metals as reference.

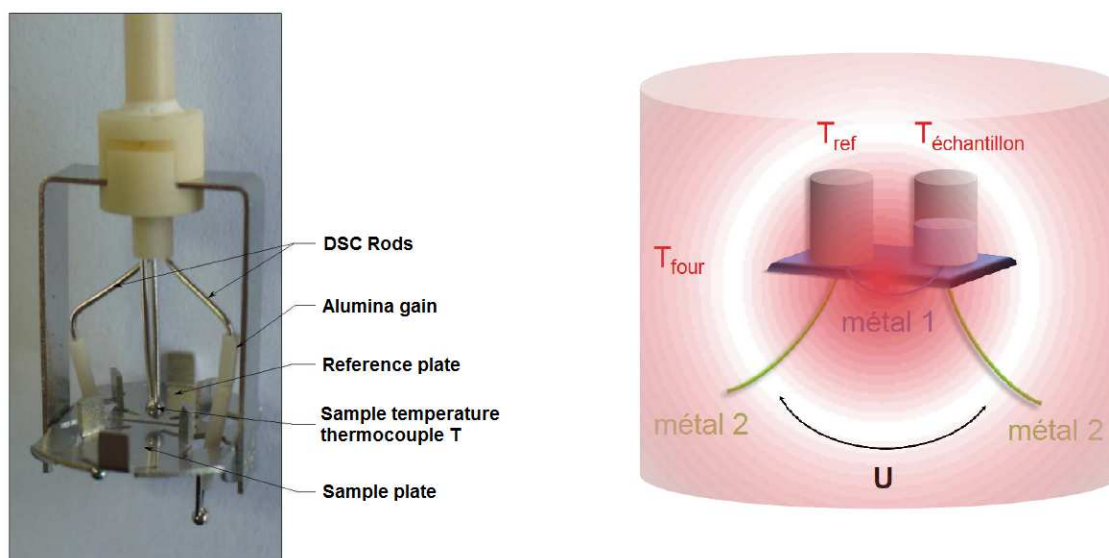


Figure 2-6. Right: DSC measuring principle, U is the potential difference in μV between the two crucibles. Left: TGA-DSC sample holder used in the experiments of Chapter IV, the thermocouples are RTD type of Platinum/Platinum Rhodium, the sample plates are in Pt and the DSC rods in Pt-Rh.

2.7 Gas Chromatography - Mass Spectrometry

The Gas chromatography mass spectrometry (GC-MS) is an instrumental technique, that include a gas chromatograph (GC) coupled to a mass spectrometer (MS) by which complex mixture of chemicals may be separated identified and quantified. This makes it ideal for the analysis of hundreds of relatively low molecular weight compounds found in environmental materials. In order for a compound to be analyzed by GC/MS it must be

sufficiently volatile and thermally stable. Sometimes the sample must be treated before the analysis to extract into a solvent or eliminated undesirable substance that could contaminated the sample.

The sample solution is injected into the GC inlet where it is vaporized and swept onto a chromatographic column by carrier gas the sample flows through the column on condition to separate the compounds in the mixture, depending on the interaction with the column and the carrier gas. The gases through pass to the chromatography column are conducted for a transfer line to ion source of mass spectrometer; there are 2 types of ion production that are electron ionization (EI) and chemical ionization (CI). This information may be used to identify compounds and identify the components of the mixer. (Universite de Bristol web page ref)

2.8 Fourier Transformed Infra-red Spectroscopy

Fourier transform infrared spectroscopy (FTIR) is a technique based in the interaction on specific interaction between irradiation of infrared zone range and the matter we want to analyze. Instead of sample irradiation with a monochromatic beam-containing bunch of photons with different frequencies and measures how much of that beam is absorbed by the sample. Studying of the matter in different aggregate states; gas, liquid solid can be used for characterization of specific components. In case of organic molecules, knowledge of characteristics vibrational frequencies of bond allows to find out the special functional groups that are presented in its structure. The basic components of Fourier transform infrared spectrometer are presented on the next figure (II-3 thesis Pablo). Light emitted by the polychromatic infrared is directed to a beam splitter- a semi- transparent mirror. It divides an incident beam into two beams of the same intensity and directs them to moving mirrors, respectively. Light is reflected from the mirrors back to the beam splitter and (ideally) 50% of the original light passes into the sample compartment. After that, the light is refocused on to detector. The difference in optic path length between the two ways to the interferometer is known as the retardation. By varying the retardation, thus with a help of interference, the separation of a specific wavelength from an initial photons bunch can be performed. Finally, the spectra in the form of interferogram can be transformed into classic IR spectra with the help of mathematical procedure: Fourier transformation. Comparing to the classic dispersive method, FTIR spectroscopy allows decreasing considerably the acquisition time for the spectra, but the sensitivity of the method is similar to classic.

2.9 TGA-DSC coupled to GC-MS and FTIR

The three previously mentioned techniques can be coupled together to obtain a more powerful analysis instrument, this kind of installations is rare but could allow to follow closely the phenomena typically analyzed in TGA-DSC experiments with the advantage of being able to analyze at the same time the evaporated byproducts. In this kind of systems the sample in the TGA-DSC is heated in a ramping or continuous mode, while heating, the gases produced as reaction byproducts are continuously analyzed by the FTIR and/or sampled and injected to the GC-MS.

The information obtained correlates the temperature, mass and energy flow of the sample with the chromatographic and spectrometric data of the gases produced while heating. This could be then used to determine the decomposition mechanism of a sample by determining the nature of the byproducts at a certain temperature, mass loss or energy flow.

In this work a TGA-DSC coupled to GC-MS and FTIR was used to investigate the solvent exchange process, the influence of the nanoparticle concentration on the polymerization process and on the decomposition of the hybrid material and the influence of nanoparticle content in solvent retention in polymerization. This work was performed using the analysis platform at ChimieParisTech (ENSCP) in collaboration with the laboratory of Prof. Michel Cassir the I2E (Interphases – Électrochimie – Énergie). The equipment used was a Setaram Evolution™ coupled to a Thermo Fisher Scientific Nicolet iS10® FTIR and to a Trace 1300®-ISQQD GC-MS. The whole system is shown in Figure 2-7.

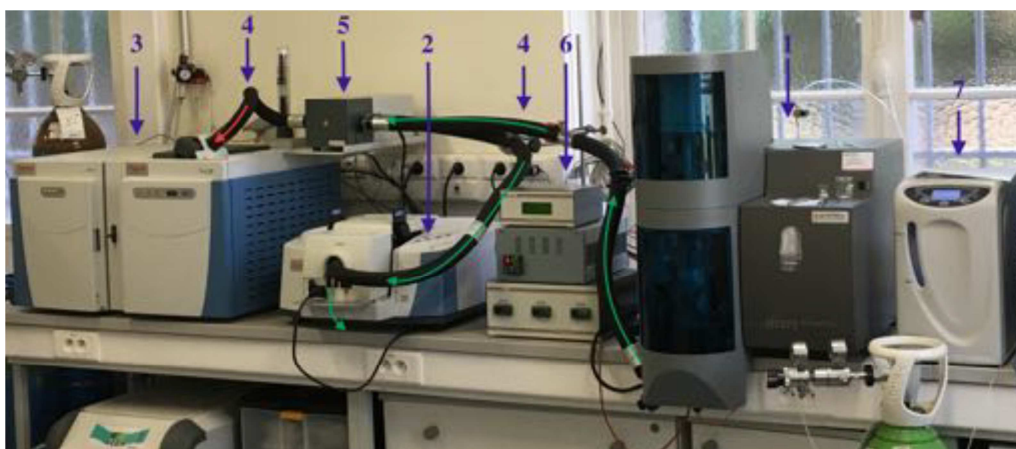


Figure 2-7. Coupled TGA-DSC/GC-MS/FTIR system as used at ChimieParistech

In the image shown above we can find the following components that constitute the system:

1. TGA-DSC : Capable of working with different atmospheres like partial vacuum, primary vacuum, Ar, He, H₂, O₂, Air, N₂, CO₂, CO, CH₄ and a mixture of maximum 2 of the former, among other possibilities allows us to perform a wide range of TGA-DSC experiments. Coupling with other techniques can be performed only when working with positive pressure with non-explosive atmospheres. An example of a TGA-DSC experiment coupled to FTIR is shown below in Figure 2-8. In the figure the mass loss is shown in black and the heat flow is shown in blue, we can distinguish two endothermic reactions (peaks pointing down) on the heat flow curve related probably to evaporation of two different components of the mixture. The phenomena takes place at different temperatures, each one is accompanied by a mass loss, such mass loss and heat flow is characteristic of evaporation. In other cases where an exothermic or endothermic phenomena is present without mass loss the interpretation is different meaning the presence of crystallization, polymerization, oxidation, reduction or fusion.

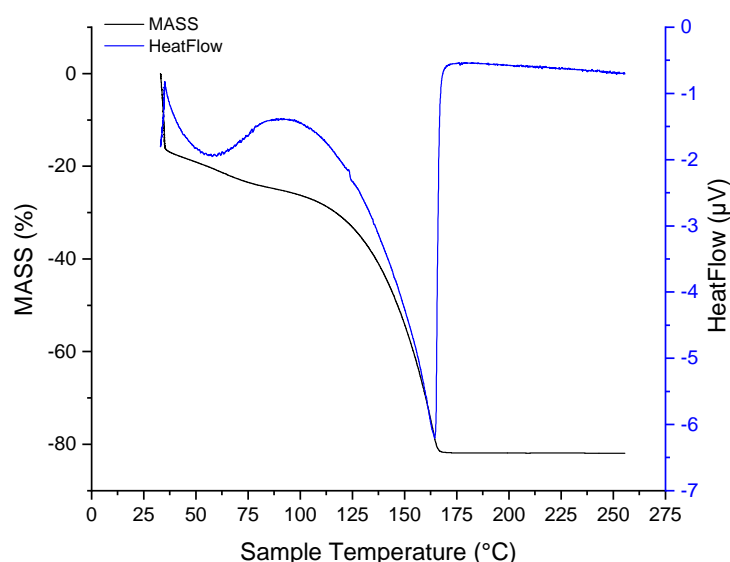


Figure 2-8. Thermogram of TGA-DSC coupled with FTIR experiment of a 1:1 mixture of isopropanol and HEMA in a temperature program of 30 to 250 °C at 4 °C min⁻¹.

Chapter 2: Experimental Techniques

2. FTIR : This equipment is capable of synchronizing a continuous spectra acquisition over the full TGA-DSC experiment. The data is then presented in a Gram-Schmidt graph, each point on this graph is a FTIR transmission spectra in the Gram-Schmidt each point represents the normalized addition in respect to the highest value of the area under the curve of all the peaks appearing on each FTIR spectra. In this way, the Gram-Schmidt allows the visualization of the general behavior of the sample where the peaks indicate that the sample has degassed something detectable by the FTIR at a certain moment in time. We can after come back to the specific FTIR spectra of any of the points in the Gram-Schmidt and search in the database for compounds that could match the spectra of the emitted gas. An example of Gram-Schmidt diagram and the FTIR spectra appearing on the first peak is shown in Figure 2-9.

As we can see when comparing Figure 2-8 and Figure 2-9, the first mass loss from 30 to 80 °C corresponds well to the moment of the maximum gas emission of the first peak in the Gram-Schmidt diagram, in this case, the spectra of that point was identified as isopropanol or 2-propanol. This example gives an idea of what can be possible to analyze when coupling the TGA-DSC to the FTIR.

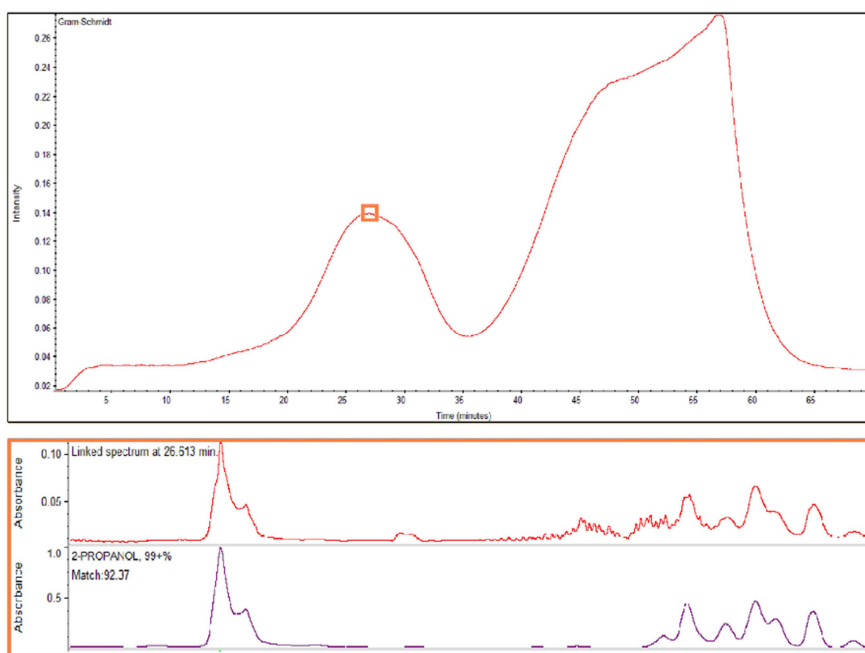


Figure 2-9. Above: Gram-Schmidt representation, below: FTIR spectra of the maximum point of the first peak identified as isopropanol. TGA-DSC coupled with FTIR experiment of a 1:1 mixture of isopropanol and HEMA in a temperature program of 30 to 250 °C at 4 °C min⁻¹.

3. GC-MS : when coupling to this equipment, the gases outgazing from the sample are analyzed, small samples of $1\mu\text{L}$ from the gas flowing from the TGA-DSC are injected into the system. Then, the column configured in temperature and pressure separates the molecules in the sample, this column can be chosen to better suit the type of organic components to be separate. After separation each molecule arrives to the mass spectrometer and its spectra is recorded. The spectra can be compared with a database to find the molecule, or the most probable molecule that corresponds to the experimental spectra. This technique together with the FTIR coupling allows the identification of almost all the components present in the gases coming from the TGA-DSC experiment, which is very useful when working with unknown decomposition processes or investigating the interactions of the solvents and monomers in polymerization. The equipment is capable of working in two different modes: i) a continuous mode, where there is an injected sample every X seconds for a period of time equivalent to the TGA-DSC experiment and ii) a timed mode, in which one sample is taken at a specific time of the TGA-DSC experiment. Each mode has a dedicated purpose, the continuous mode is used as an exploratory experiment, where we will identify the moments at which the gas is emitted from the sample and to have a rough idea of the molecules in those gases. The disadvantage of this method is that it does not allow a full separation of the components in the column, in consequence the mass spectra is not sufficiently clear and does not allow full identification of components.

An example of this mode is presented in Figure 2-10 where the Total Ion Current (TIC) diagram (in black) of a 1:1 isopropanol – HEMA sample with initiator heated from 20 to 110 °C at a speed of $5\text{ }^{\circ}\text{C min}^{-1}$. The TIC is, as the Gram-Schmidt, a representation of all the intensities of all the mass spectra peaks added together to constitute a point in a count scale over time graph. The TIC representation can be filtered to shown only the addition of the mass spectra containing a specific mass peak. In Figure 2-10 the second TIC (in red) is filtered to shown only the addition of the spectra that contain the ion mass 60 which is characteristic of isopropanol, in the third TIC (in blue) the ion mass 69 characteristic of 2-hydroxyethyl methacrylate (HEMA). Comparison of the three

TICs gives us an idea of the moments at which isopropanol and HEMA could be outgazed from the sample in a more important quantity.

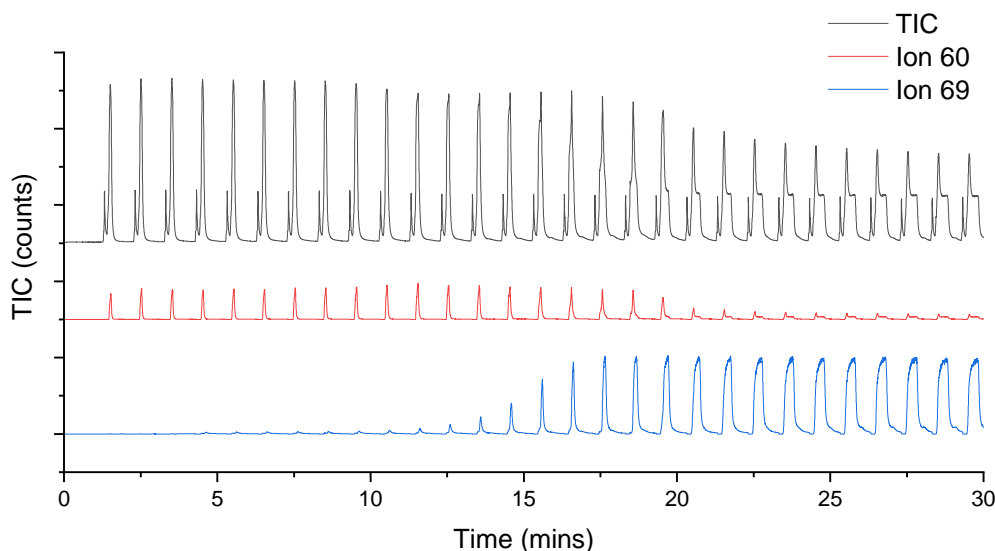


Figure 2-10. Total Ion Current (TIC) of a 1:1 isopropanol – HEMA sample with initiator heated from 20 to 110 °C at a speed of 5 °C min⁻¹. In black: TIC of the experiment, in red: TIC of Ion 60, in blue: TIC of Ion 69.

Once the times or temperatures of interest in the TGA-DSC experiment are identified within the thermogram, the GC-MS continuous mode and the FTIR data we can target specific moments of the TGA-DSC experiment to perform longer GC sequences that will separate the gases in the sample and give better mass spectra that can be well identified. This mode is used in Chapter IV to better understand the hybrid solvent exchange, and polymerization.

4. Gas transfer lines: heated steel 1/8" pipes coated internally with Si are heated to a temperature above the condensation point of the possible gases emitted by the sample. This line are isolated and allow a maximum temperature of 250 °C to be used. These heated lines are in charge of transferring the gases from the TGA-DSC to the other components.
5. Heated injector valve: A pneumatically actuated valve with a loop of 1 μL capacity is located inside a small oven and heated at the same temperature of the

lines, the valve is in open position in which the flow of gas is allowed to pass by the loop and exits to the FTIR. When the GC-MS mode is disabled, the gas flows continuously to the FTIR, when the GC-MS mode is enabled the valve switches at a specific time injecting the gas contained in the loop into the GC-MS for a very small period of time (typically 1s) when the injection is finished the valve comes back to the original position.

6. Synchronization control and heating control: These units are from the top to the bottom: i) the synchronization unit, ii) heating control of the TGA-DSC transfer valve, iii) heating control of the lines and pneumatic valve. The synchronization unit is in charge of organizing the coupling of the GC-MS, the FTIR and the TGA-DSC, it is programmed with the sequence to be followed (continuous or timed) and sends the signals to the pneumatic valve and the GC-MS to inject a sample and run the GC-MS. It also indicates to the FTIR when to start acquiring the spectra once the TGA-DSC is ready and running the experiment. This system allows keeping a consistent time-zero start point and keeps track of time, allowing to synchronize all the events to take place in the coupled TGA-DSC/GC-MS/FTIR experiment.
7. Hydrogen generator: To perform experiments in reducing atmosphere, the amount of hydrogen in a mixture of Ar or N₂ can be controlled automatically by the TGA-DSC allows performing a wide variety of experiments.

As has been shown in this section, the coupled TGA-DSC/GC-MS/FTIR experiments opens a wide variety of possibilities to identify components coming from the thermal processes carried out in the TGA-DSC. Further on this thesis this system is used to perform a series of experiments related to the solvent exchange and polymerization, were it will allows us to better understand some of the basic processes in the synthesis of hybrid materials.

2.10 Conclusions

All the previously mentioned analysis methods are available at the laboratory. Together, they could be used to optimize the TiO₂ hybrid synthesis and understand the relating problems of the synthesis, such as short gelation/precipitation time of the hybrid colloids, high water sensistivity, appearance of cracks in polymers, affecting photonic

Chapter 2: Experimental Techniques

response by preparation, etc. The understanding of different variables involved in the synthesis and their control is essential to the success of the synthesis.

The use of combined techniques such as the TGA-DSC coupled to GC-MS and FTIR available through the collaboration with ENSCP and the laboratory of Pr. Michel Cassir, will give us a maximum of valuable information with a very small quantity of samples minimizing the amount of synthesis to be performed in the laboratory. However, the complexity of the system will produce complex sets of data to be analyzed that will require significant time to explore. The effective techniques and instrumentation can permit to advance with the comprehension of the main issues related to the hybrids elaboration with emphasis of their organic component.

Chapter 3 : Material Synthesis

The material synthesis constitutes a medullar part of the work performed for all the experimental section of this thesis. Final material properties have their origin in this part of the process. Special care should be taken by anyone willing to reproduce this thesis results when following the synthesis procedures described herein.

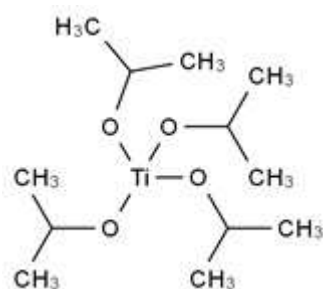
We will first have a look to the chemicals used in this work, their characteristics and handling/storage recommendations are cited. Even though the chemicals used were new and were maintained in optimal conditions for its preservation, the degree of purity of some of them is not the ideal to perform such delicate material synthesis, in consequence, purification steps were added to the synthesis process and will be fully described in this chapter.

3.1 Chemicals and their characteristics

Titanium tetra-isopropoxide [TTIP]

Formula: C₁₂H₂₈O₄Ti

Molecular Weight: 284.22 g mol⁻¹



Handling and storage : Handle and storage under nitrogen, and protected from moisture and in a cool place, keep container tightly closed in a dry and well ventilated place, manipulated away from source of ignition.

Melting point: 14-17 °C

Reative density: 0.96 g mL⁻¹ at 20 °C

Boiling point: 232 °C

Flash point: 45 °C

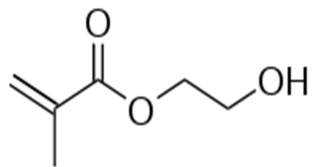
Vapour pressure: 1.33 hPa at 63 °C

Sigma-Aldrich safety data sheet according to regulation (EC) no 1907/2006.

Revision date 30 03 2016 version 6.0; No country specific data

2-(Hidroxyethyl)methacrylate [HEMA]

Formula: C₆H₁₀O₃



Melting point: 11.99 °C

Boiling point: 67 °C at 4.7 hPa

Autoignition: 375 °C at 1.024 hPa

Water solubility: 100 g L⁻¹ at 20 °C

Sigma-Aldrich safety data sheet according to regulation (EC) no 1907/2006.

Revision date 30 03 2016 version 6.0; No country specific data

Molecular Weight: 130.14 g/mol

Handling and storage : storage temperature between 2-8 °C, keep the container closed, dry and well ventilated place and away from ignition source; for handling avoid contact with skin and eyes and in fresh place and avoid inhalation of vapors.

Relative density: 1.073 g mL⁻¹ at 25 °C

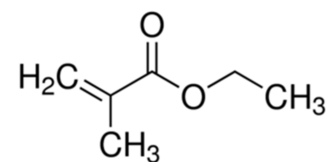
Flash point: 106 °C close cup

Vapor pressure: 0.08 hPa at 20 °C

Viscosity: 6.36 mm² s⁻¹ at 20 °C

Ethyl Methacrylate [EMA]

Formula: C₆H₁₀O₂



Melting point: -59.99 °C

Boiling point: 118 -119 °C

Molecular Weight: 114.14 g mol⁻¹

Handling and storage: the storage temperature recommended between 2-8 °C, tightly closed, covered from the light and the heat and away from ignition source, in the handling process avoid the contact with eyes and skin avoid vapors inhalation.

Relative density: 0.917 g cm⁻³ at 25 °C

Flash point: 19 °C close cup

Autoignition: 400 °C at 1,013 hPa

Vapor pressure: 15 mmHg at 20 °C

Vapor density: 3.94 (air= 1.0)

Water solubility: 4.69 g L⁻¹ at 20 °C **Viscosity:** 0.7 mm² s⁻¹ at 20°C

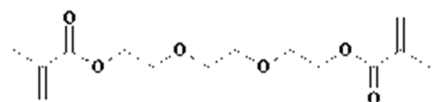
Sigma-Aldrich safety data sheet according to regulation (EC) no 1907/2006.

Revision date 31 03 2016 version 6.0; Generic EU MSDS, no country specific data, no OEL data.

Triethylene Glycol Dimethacrylate [TEGDMA]

Formula: C₁₄H₂₂O₆

Molecular Weight: 286.32 g mol⁻¹



Handling and storage: store temperature between 2-8 °C, protected from the light and away from ignition source; for the handling avoids the contact with the eyes and skin.

Boiling point: 172 °C at 7 hPa

Flash point: 167 °C close cup

Auto ignition: 255 °C at 1, 025 hPa

Water solubility: 3.6 g L⁻¹ at 20 °C

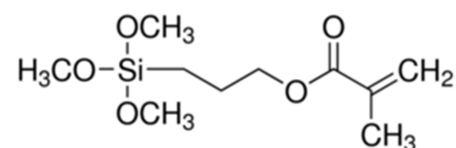
Viscosity: 9.15 mm² at 20 °C

Sigma-Aldrich Safety data sheet according to regulation (EC) No. 1907/2006, version 6.1, revision date 06/11/2017; Generic EU MSDS, No country specific Data, no OEL data.

3 (Trimethoxysilyl)propyl methacrylate) [MAPTMS]

Formula: C₁₀H₂₀O₅Si

Molecular weight: 248.35 g mol⁻¹



Handling and storage: Keep cool place tightly close in a dry and under inert gas, this reactive is sensitive to the heat, the handling avoid the inhalation of vapors or mist.

Boiling point: 190 °C

Flash Point: 92 °C closed cup

Melting point: -19.99 °C at ambient P **Autoignition:** 275 °C at 1013.5 hPa

Vapour density: 8.57 (air=1.0)

Vapour pressure: 0.23hPa at 25 °C

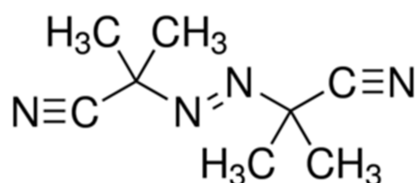
Relative density: 1.045gcm⁻³ at 25 °C **Water solubility:** 0.0862 gL⁻¹ at 20°C

Sigma-Aldrich Safety data sheet according to regulation (EC) No. 1907/2006, version 6.1, revision date 31/03/2016; Generic EU MSDS, No country specific Data, no OEL data.

Azobisisobutyronitrile [AIBN]

Formula: C₈H₁₂N₄

Molecular Weight: 164.21 g mol⁻¹



Handling and storage: For safe handling avoid contact with the eyes and skin; avoid the formation of dust and aerosols. Provide appropriate ventilation where dust is formed and keep away from ignition source and heat source. For the storage keep between 2- 8 °C in dry and well ventilated place. Reactive to the moisture and air, avoid organic peroxides and self-reactive hazardous materials.

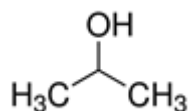
Vapour pressure: 0.81 Pa at 25 °C

Boiling point: Decomposes below boiling point.

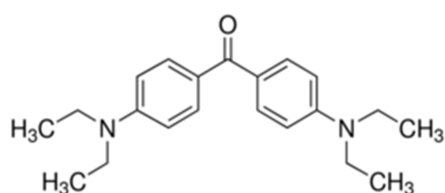
Relative density: 1.11 g/cm³

Melting point: 102 -104 °C decomposition

Sigma-Aldrich safety data sheet according to regulation No.1907/2006 version 6.1, revision data 06/02/2017, generic EU MSDS no country specific Data no OEL data.

Isopropanol**Formula:** C₃H₈O**Molecular weight:** 60.10 g mol⁻¹**Handling and storage:** Avoid the contact with eyes and skin, and vapors inhalations. Keep away from source of ignition and in a cool place in a dry and well ventilated place.**Melting point:** -89.5 °C**Vapor pressure:** 58,7 hPa at 25 °C**Boiling point:** 82 °C**Flash point:** 12.0 °C**Auto ignition:** 425 °C**Relative density:** 0.785 g cm⁻³ at 25 °C**Water solubility:** very soluble

Sigma-Aldrich safety data sheet according to regulation No.1907/2006 version 5.6, revision data 02/08/2018, generic EU MSDS no country specific Data no OEL data.

4 4-bis(dimethylamino)benzophenone**Formula:** C₁₇H₂₀N₂O**Molecular weight:** 268.35 g.mole⁻¹**Handling and storage:** Avoid the contact with eyes and skin, and vapors inhalations. Keep away from source of ignition and in a cool place in a dry and well ventilated place.**Melting point:** 90 - 95 °C**Decomposition:** > 300 °C**Auto ignition:** 480 °C**Flash point:** 151 °C**Water solubility:** 400 mg/L (20°C)

Sigma-Aldrich safety data sheet according to regulation No.1907/2006 version 5.9, revision data 21/02/2018.

3.2 Purification processes

3.2.1 Distillation of monomers

The distillation is one of the most widely method of purification of liquids or low melting solids, especially of organic chemicals. The vacuum distillation is the expression used for denoted a distillation under reduce pressure, and is used when a substance is unstable for been boiling at atmospheric pressure.

The distillation apparatus, showed in the Figure 3-1, consist of a distillation flask, usually fitted with a vertical fractionating column to which is attached a condenser leading to a receiving flask. A thermometer is placed just below the junction point of the column and the condenser.

To achieve the maximum separation by a distillation it is important to consider:

- The kind of column chosen and if it is or not packed, as well the volume of the sample and column (the volume of the column must be smaller than the any component in the sample that want to separate.)
 - Heat loss from the column and if need to be prevent.
 - For vacuum distillation must be carefully controlled the pressure to avoid flooding or cessation of reflux.
 - The kind of condenser chosen and the refrigeration liquid, and it temperature.
- (Armagero et Lin Li Chan, 2013)

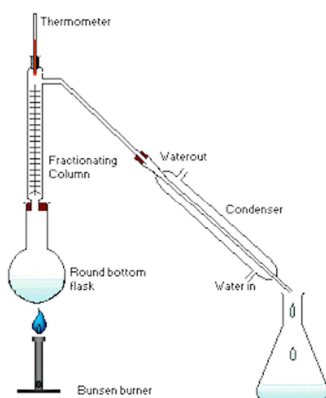


Figure 3-1. Schematic of the distillation setup.

HEMA and MAPTMS were distilled in vacuum with a fractionating column at respectively 67 and 110°C. It is important to distillate only the first 2/3 parts of the initial volume to avoid the contamination of the distilled sample by dimers, inhibitor or low molecular weight polymers that are generally present in the last third of the initial volume which is discarded.

Once distilled the maximum storage time of the product is 7 days if an only if properly refrigerated at temperatures between 4 and 10 °C.

3.2.2 AIBN recrystallization

One common type of purification method for any reactant typically present in form of crystals is the recrystallization, in general it consist in the dissolution of the material to be purified in a solvent such as alcohols, organic solvents or even water. Then, the stirred mixture is modified to propitiate the precipitation of the desired reactant in form of crystals. The parameters that could be modified are pH, concentration, temperature, or solvent among others. The resulting crystals can be recovered by filtration, decantation or solvent evaporation, which are the most common.

For this thesis work, the AIBN was recrystallized to obtain a higher purity by the method known as the “Methanol (MeOH) AIBN recrystallization” (De Souza Machado, 2008). In our case, 5 g of AIBN powder were dilute in 20 ml of MeOH by stirring for a period of 1 h, then the solution is filtered by using filter paper and a fast funnel type filter support. The eluent is then refrigerated at 4 °C for a period of 24 h then filtered again with filter paper. The obtained solution is then cooled down abruptly, in our lab this was achieved by fast immersion of the round bottom flask in liquid nitrogen for periods no longer than 5 s while stirring the flask by hand. After each immersion visual inspection was performed, avoiding freezing of the sample and monitoring the growing of small needle-like crystals suspended in the solution. The fast cooling process is repeated 2 or 3 times until the solution becomes turbid. After this, the flask is immersed in an ice bath, solvent extraction is then performed by connecting the flask to a vacuum pump. Crystals will start growing in the solution and will precipitate in the walls and bottom of the flask. Once solvent is eliminated, the resulting crystals are collected in a new amber-colored flask and stored in refrigeration where they can last around 3 months.

In case the stored crystals start changing color becoming white and turning into a powder, the reactant should be recrystallized again.

3.3 TiO₂ nanoparticles synthesis

A reactor of a fast micro-mixing has been used in the preparation scheme. Previously, the kinetic studies have shown that this TiO₂ synthesis way allows preparing series of the gels with a well-defined size of the nanoparticles: 2, 3.2, and 5.2 nm of diameter (Azouani *et al.* 2010). Actually, the total synthetic process is characterized by a rapid nucleation period, and it ends with a nanoparticle growth period-induction time. At the end of this period precipitation will take place. Therefore, it's very important to find the appropriate reaction conditions, which would be suitable for preceding the solvent exchange reaction. The main experimental parameters, used in the TiO₂ nanoparticles suspension production phase, are show in Table 3-1.

Table 3-1. Parameters used in the synthesis of TiO₂ nanoparticles

Parameters	
Pressure of injection	4 bars
Temperature	20 °C
Concentration of TTIP	0.146 M
Hydrolysis ratio	2

Based on the experimental condition, we can conclude that:

- Expected TiO₂ particle size (radius) is 2.6 nm
- Reaction stoichiometry allows to produce stable TiO₂, nanoparticles with no residue of TTIP
- Expected induction time for the TiO₂ suspension solutions is 24 hours, which is suitable for proceeding the solvent exchange production phase.

The sol-gel reactor developed by Rivallin et al (2003) and Azouni et al (2010) has been used to produce the suspension of TiO₂ nanoparticles. The complete scheme of the reactor is mentioned in Chapter 2.

The solution of TTIP in 2-propanol and water in 2-propanol have been prepared in a glove box (MBraun) with the follow conditions:

- Pressure: 1.2 -1.5 bars
- H₂O vapors concentration: less than 0.5 ppm
- O₂ concentration: less than 2.0 ppm

These solutions have been transferred with the help of syringes into double-wall inox reservoirs that are been thermostat with the help of cryostat and distilled water has been used as a coolant. The solutions in the reservoirs were set under the flow of nitrogen to avoid the humidity contamination. The thermostatic reactor holds all 100 mL of TiO₂ nanoparticles suspension after the end of a hydrolysis reaction. After the hydrolysis the size of the nanoparticles could be measure by DLS technique.

3.4 Solvent Exchange

The calculated volume of a newly prepared suspension of TiO₂ nanoparticles in 2-propanol has been transferred to the graduated syringe under flow of inert gas (N₂). The procedure of mixing of the nanoparticles colloid with purified monomer solution was conducted in a glove box. The added volume of monomer solution was equal to 5 ml.

The solvent exchange procedure was performed in a round-bottom flask (total volume 200 ml.). The flask has been equipped with a magnetic stirrer and a vacuum valve. A single stage membrane pump (supplier: KNF N 840.3FT.18) has been used for pressure reducing down to 1-10 mbar. A LN₂ trap has been used to condensate 2-propanol vapor. The exchange reactor temperature control (T=20 °C) has been realized with a simple water bath.

At this stage, the TiO₂ nanoparticles concentration can be adjusted to a desirable value by admission of an increased colloid volume, with subsequent pumping until its reduction to that of monomer solution (5 ml). The information about components concentration in the stable hybrid solution after the solvent exchange stage is given in Table 3-2, Table 3-3 and Table 3-4

As a convention, sample name is composed in first place by the monomer mixture followed by the TiO₂ initial volume in that sample, for example: HEMA 5x, HEMA-EMA 10x or even HEMA-TEDGMA 20x.

Chapter 3: Material Synthesis

Table 3-2. Concentrations of HEMA and TiO₂ for each sample prepared.

HEMA			
Sample	Volume initial TiO ₂ per ml of monomer synthesis.	TiO ₂ concentration in the final Hybrid material M	HEMA:TiO ₂ molar ratio
5x	5	0.73	11:1
10x	10	1.46	5.5:1
20 x	20	2.92	2.7:1
30 x	30	4.38	1.8:1

Table 3-3. Concentration of HEMA-EMA and TiO₂ for each sample prepared.

HEMA-EMA				
Sample	Volume ratio HEMA:EMA	Volume initial TiO ₂ per ml of monomer synthesis.	TiO ₂ concentration in the final Hybrid material M	HEMA-EMA:TiO ₂ molar ratio
5x	1:1	5	0.73	11:1
10x	1:1	10	1.46	5.5:1
20 x	1:1	20	2.92	2.7:1
30 x	1:1	30	4.38	1.8:1

Table 3-4. Concentration of HEMA-TEGDMA and TiO₂ for each sample prepared

HEMA-TEGDMA				
Sample	Molar % TEGDMA	Volume initial TiO ₂ per ml of monomer synthesis.	TiO ₂ concentration in the final Hybrid material M	HEMA-TEGDMA:TiO ₂ molar ratio
5x	10	5	0.73	12.5:1
10x	10	10	1.46	6.24:1
20 x	10	20	2.92	3.14:1

The solvent exchange could be performed with a multiple valve in different flask, and the initial volume don't affect the extraction time with the same initial quantities of the monomers, that means that solvent exchange for all concentrations could be performed at the same time. The molar ratio was calculated, assuming complete elimination of isopropanol. In reality a complete isopropanol exchange and elimination is not possible as will be proven in Chapter IV however, these calculations are a good approach to have an idea of the final content of TiO_2 .

3.5 Radical Thermal Polymerization

As described in Chapter I, section 1.4.2, Radical Thermal Polymerization is a complex and delicate process in which monomer and initiator purity as well as solvent and initiator concentration together with the temperature are critical parameters directly linked to the conversion ratio and the size of the polymer chains obtained. Hence, accurate control of the previously mentioned variables has to be taken in account to keep an acceptable repeatability of the process for each produced sample.

For these series of samples (HEMA, HEMA-EMA and HEMA-TEGMA), polymerization followed the next steps:

1. AIBN initiator is mixed with one of the colloids obtained from the solvent exchange (HEMA 5x, 10x and 20x) in a concentration of 0.1 % M in a small glass container.
2. The mixture is then degasified by freezing the sample in liquid nitrogen, once the colloid is freeze and solid, it is removed from the liquid nitrogen and vacuum is applied to the container. Once the mixture is liquid again, vacuum is stopped and the process is repeated as many times as necessary (generally 5) until bubbles does not show up when the sample unfreezes. This step has the objective of removing the dissolved gases in the mixture (mainly oxygen) that could affect the radical formation or reactivity.
3. Now the colloid is ready to be polymerized, it can be poured in between two microscope plates separated by a specially calibrated separator to form a thin film

of a specific thickness. Or can be left in the glass container to obtain a small cylinder.

4. Whatever container or shape chosen, in order to polymerize the sample it has to be heat treated in an oven, the best results were obtained when the oven was preheated at the chosen polymerization temperature. It is important to avoid air contact of the colloid when polymerizing. In this case the oven was preheated at 90 °C for HEMA 5x, 10x and 20x then sample was introduced in the oven for a period of 12 h.

In the case of HEMA 20x, it was observed that at this polymerization temperature the obtained polymer was full of cracks specially in the case of the thin films. To avoid this, polymerization temperature for the HEMA 20x samples was reduced to 65 °C and samples were held in the oven for 16 h. These parameters proved to be the best compromise between polymerization ratio and cracking reduction. However, cracking was not completely avoided for the HEMA 20x samples.

All the previously mentioned procedures were carefully followed for all the synthesis prepared for all the experiments performed, conditions varied slightly only due to ambient temperature and ambient relative humidity that was not fully controlled in the laboratory. In the next chapter, the organic constituent of the hybrid materials produced with these methods will be studied.

3.6 Conclusions

Knowing the physico-chemical properties of all the reactants allows to have a clear vision of their limitations, possible behaviours and the variables to take care of to perform all the experiments in the most efficient and safe way. As mentioned by Gorbóvyi in his thesis manuscript, the control of the sol-gel reaction by micromixing is important for the photonic properties of hybrid materials. However, it is also necessary to take in account the purity of the monomers and initiators as crucial elements for obtaining the best quality polymers, also degasification played an important role in the preparation of the colloid to be polymerized.

Temperature and pressure are essential parameters to take in account in all stages of the synthesis of hybrids, from purification to storage of colloids, since the particle size could

change with moisture content and parasitic reactions could interfere with proper polymerization. Special care is suggested and a thorough understanding of the parameters involved in each step is mandatory to obtain the best results.

Chapter 4 : TiO₂ hybrids with HEMA organic component

The detailed understanding of all key stages of the hybrid materials preparation has not been attained until now. One important issue concerns an interaction of the organic and inorganic components with solvent in the liquid solution. In this chapter, we analyse chemical interactions in the isopropanol/H₂O/HEMA/TiO₂ system on the solvent exchange stage, which has not been explicitly considered in previous studies devoted to the nanoparticulate Titania hybrids. For example, Kameneva (2009) and Gorbovy (2012) have supposed a complete replacement isopropanol by HEMA under vacuum pumping in the hybrid solution, leading to covalently attached monomer ligands to TiO₂ nanoparticles. In the following sections, we investigate the influence of nanoparticles on colloid and polymer behavior on the organic polymerization stage.

4.1 Solvent exchange on HEMA-TiO₂ hybrids

In this section, the solvent exchange process will be studied in HEMA-TiO₂ hybrids. First, the best solvent exchange parameters will be chosen based on the thermogravimetric experiments at constant temperature and partial vacuum. Then, a complex experimental installation of coupled TGA-DSC/GC-MS/FTIR will be used to analyze the material content, and especially the residual isopropanol, and influence of the residual solvent on the polymerization process and material stability.

4.1.1 Thermogravimetric study of solvent extraction

This series of experiments had as objective to understand if the isopropanol extraction during the solvent exchange process is complete or not and knowing if it occurred following a step-like or smooth progressive behavior. These experiments allowed us to define optimal conditions for this stage of the material synthesis. In these experiments, four samples were prepared as follows:

1. 1 ml of HEMA + 10 ml of isopropanol (HEMA x10 w/o NP)
2. 1 ml of HEMA + 20 ml of isopropanol (HEMA x20 w/o NP)
3. 1 ml of HEMA + 10 ml of TiO₂ NP solution (HEMA x10 NP)
4. 1 ml of HEMA + 20 ml of TiO₂ NP solution (HEMA x20 NP)

These samples were analyzed in separate runs on the ChimieParistech/I2E coupled TGA-DSC/GC-MS/FTIR platform. The TGA-DSC was used in partial vacuum mode. This

experiment consisted in keeping the temperature of the sample constant at 30 °C, and then reducing the pressure in the sample chamber to a constant value of 62 mbar to simulate the conditions of the solvent exchange process; the change in weight of the sample and the energy transfer was followed for a period of 2 h. This time was calculated to exceed at least 1 hour longer the point, from which the mass of the sample remains constant. The isopropanol mass content on samples can be calculated from the volumetric content of the mixture in the following way:

Table 4-1: Calculated mass % of isopropanol on tested samples from their volumetric proportions

HEMA x10 w/o NP			
	Volume (ml)	Density (g/ml)	Mass (g)
HEMA	1	1.073	.073
Isopropanol	10	0.785	.85
	Total mass		.92
	Isopropanol fraction		.880
	Isopropanol mass %		7.97%

HEMA x20 w/o NP			
	Volume (ml)	Density (g/ml)	Mass (g)
HEMA	1	1.073	.073
Isopropanol	20	0.785	5.7
	Total mass		6.77
	Isopropanol fraction		.936
	Isopropanol mass %		3.60%

HEMA x10 NP			
	Volume (ml)	Density (g/ml)	Mass (g)
HEMA	1	1.073	1.073
Isopropanol	10	0.785	7.85
Ti*			0.070
	Total mass		8.99
	Isopropanol fraction		.8729
	Isopropanol mass %		7.29%

HEMA x20 NP			
	Volume (ml)	Density (g/ml)	Mass (g)
HEMA	1	1.073	.073
Isopropanol	20	0.785	5.7
Ti*			.140
	Total mass		6.91
	Isopropanol fraction		.9283
	Isopropanol mass %		2.83%

* Ti mass was calculated based on the Ti molar content of the nanoparticle solution and the volume of this solution taken to prepare x10 and x20 samples. Since the real Ti volume is unknown, isopropanol volume was not adjusted to account for the Ti volume. However, Ti volume will be very small introducing a negligible error in this calculation. With this inconsideration, we can take the calculated isopropanol mass content as a fair approximation to the real content.

Figure 4-1 shows the relative (%) mass loss and heat flow curves of samples HEMA x10 w/o NP and HEMA x20 w/o NP. The mass loss can be described as a one-step process taking around 15 minutes with a mass loss of 87.19% for HEMA x10 w/o NP and of 88.11%

for HEMA x20 w/o NP. In both cases, the mass loss is very close to the isopropanol mass in the samples, which was calculated to be 87.97% and 93.60% for respectively HEMA x10 w/o NP and HEMA x20 w/o NP. This indicates that the available isopropanol was successfully extracted in the given experimental conditions and the extraction process required the same time for samples with different HEMA content.

The heat transfer curves in Figure 4-1 indicate in both cases an endothermic process corresponding to the evaporation of isopropanol solvent, which has the same completion time and intensity. This supports that the presence of HEMA in samples does not affect significantly the extraction process. When the endothermic process vanishes, the mass loss stops clearly, which evidences that isopropanol evaporation is the only factor of the observed mass loss.

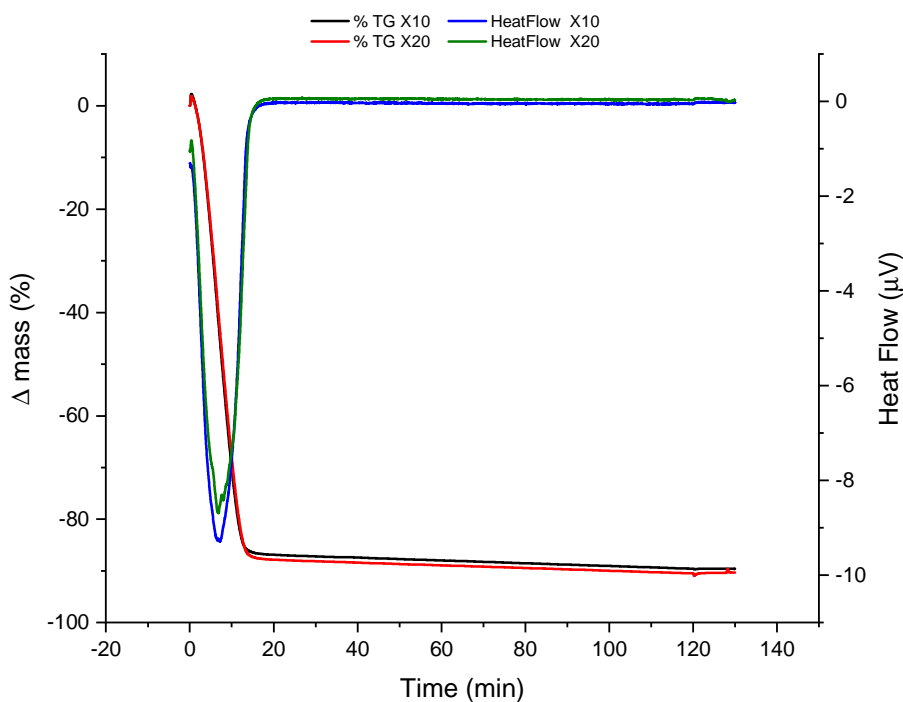


Figure 4-1. TGA-DSC of HEMA x10 w/o NP and HEMA x20 w/o NP samples ($T = 30\text{ }^{\circ}\text{C}$, $P = 62\text{ mBar}$).

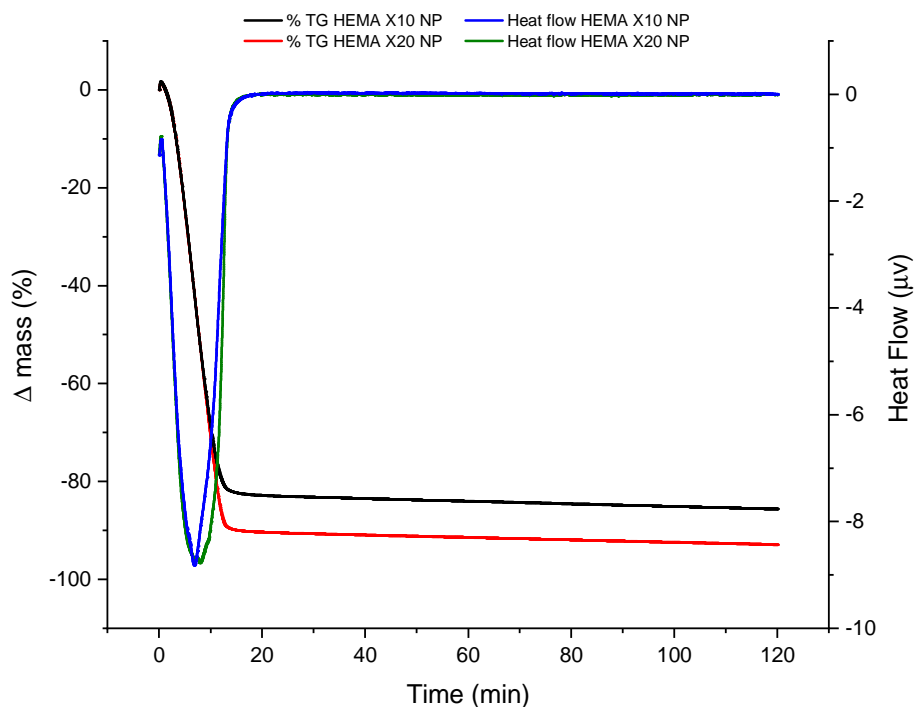


Figure 4-2. TGA-DSC of HEMA x10 NP and HEMA x20 NP ($T = 30\text{ }^{\circ}\text{C}$, $P = 62\text{ mBar}$).

TGA-DSC measurements shown in Figure 4-2 indicate that samples with nanoparticles HEMA x10 NP and HEMA x20 NP followed the same extraction process. As we can see in this figure, the mass loss of samples HEMA x10 NP and HEMA x20 NP was respectively 83.2 % and 90.7 %, which are very close to their respective isopropanol contents of 87.29% and 92.83%. As it can be noticed, the extraction process in both samples took almost the same time. However, the presence of nanoparticles affects the solvent exchange in colloids. The relative mass loss decreased in the colloids, which can be explained by an additional residual mass of TiO₂ nanoparticles and solvent retention on the particles surface. Moreover, the endothermic peak shifted to longer times confirming the solvent retention. In Table 4-1 the residual mass loss in % for all the samples is calculated. As can be observed, the difference between experimentally removed isopropanol and theoretical maximum mass of isopropanol in the samples seems to vary without direct correlation to nanoparticle presence or concentration. However, it is clear that since all samples were treated in the same way and that TGA-DSC curves shown a reasonable stabilization after the main mass loss, this difference is not casual, but cannot be explained with the limited set of data available at the moment.

Table 4-2. Experimental mass loss, calculated mass loss and their difference expressed as residual isopropanol mass for samples with and without nanoparticles.

Sample	Experimental Mass loss %	Calculated isopropanol mass %	Residual isopropanol mass %
HEMA x10 w/o NP	87.19 %	87.97 %	0.78 %
HEMA x20 w/o NP	88.11 %	93.60 %	5.49 %
HEMA x10 NP	83.20 %	87.29 %	4.09 %
HEMA x20 NP	90.70 %	92.83 %	2.13 %

The heat transfer indicates one endothermic process, taking place during the mass loss and terminated when it attains its maximum. These results confirm that the isopropanol evaporation is the major phenomena, to which this endothermic process can be assigned.

The presented TGA-DSC experiments showed that the solvent exchange process is a one-step mass loss accompanied with an endothermic reaction attributable to the isopropanol evaporation. The nanoparticles affect this process, which was observed by the broadening of the endothermic peak and a difference in residual isopropanol mass. The solvent (both isopropanol and HEMA) retention on the particle surface may explain this effect. However, the available information at this stage of the study is not enough to conclude on this behavior.

4.1.2 TGA-DSC / GC-MS / FTIR analysis of solvent

This section describes the TGA-DSC / GC-MS / FTIR coupled measurements conducted with the isopropanol-HEMA solvent of 1:1 composition, which served to be a reference for understanding the colloids behaviour, no initiator was used in this experiment. The optimum parameters used in the TGA-DSC measurements were fixed after a series of tests where the speed of the heating ramp and the final temperature were varied. These parameters are specified in Table 4-3.

Table 4-3. Parameters used in TGA-DSC experiments

Parameter	Value	Units
Initial temperature	30	°C
Final temperature	250	°C
Heating ramp	4	°C min ⁻¹
He atmosphere at a flow	50	ml min ⁻¹
Pre-stabilization time	15	min
Cooling from 250 °C to 30 °C	30	°C min ⁻¹

To characterize the by-products issued of the heating process in TGA-DSC series, they were connected with on-line GC-MS and FTIR analysis. The conditions proposed by

Michelsen *et al.* 2007 for the characterization of HEMA for dental resins were first explored and then adjusted to our setup; the final parameters used are specified in Table 4-4.

Table 4-4. Parameters used in GC-MS experiments

Parameter	Value	Units
He flow rate	4	ml min ⁻¹
Split flow	10	ml min ⁻¹
Split ratio	10:1	
Injector temperature	250	°C
Hold time	5	Min
Column initial temperature	50	°C
Column final temperature	120	°C
Column heating ramp	50	°C min ⁻¹
Purge flow	5	ml min ⁻¹
Mass range	50 to 350	Mz

The column used for the experiments was TR-V1® of 30 m length by 0.25mm diameter and 1.4µm of film thickness. This Thermo Fisher Scientific™ column is the equivalent to that used by Milchensen *et al.* In the proposed experimental conditions, according to (Michelsen *et al.* 2008), the GC peak of HEMA appears between minutes 3 and 4, and that of the initiator Monomethyl ether hydroquinone (MEHQ) at minute 5 (Milchensen *et al.* 2007).

Four reference temperatures were chosen for the sample analysis in the MS timed mode (see Chapter 2). The first one at 30 °C, that is 30 seconds after the beginning of the experiment and it should detect volatile products (alcohols) contained in the sample. The second at 90 °C sampling 30 minutes after the former, corresponded to the polymerization temperature of HEMA. The third one taken at 160 °C at 47 minutes of experiment runtime corresponded according to Gonzalez-Henriquez *et al.* (2014) to the HEMA monomer decomposition. Finally, the last chromatogram was taken at 235 °C after 65 minutes corresponded to the decomposition of pHEMA polymer (Mohapatra *et al.* 2005).

In the thermograms shown in Figure 4-3 the TG signal shows two mass losses, the first one between minute 0 and 15 where isopropanol evaporates during the stabilization time, sample loosed in this first step 28.1 % of its initial mass. The evaporation is accentuated when the temperature ramp begins and stops at minute 30. At a temperature of 90 °C the endothermic peak characteristic of isopropanol evaporation phenomena (first peak in the heat

flow diagram in blue) appears clearly only when the ramp starts. This is due to the working principle of the TGA-DSC sample support plate. From minute 32 to minute 48 the second mass loss appears abruptly, the sample loosed in this step 53.54 % of mass. The endothermic peak with onset at 133 °C shows a fast evaporation between 92 and 175 °C that can be attributed to the HEMA evaporation. According to Gonzalez-Henriquez *et al.* 2014 HEMA decomposes before evaporation at 160 °C. According to Wypych *et al.* 2011 the mass loss of HEMA evaporation/decomposition occurs between 85 and 100 °C which is in good agreement with our data.

In Figure 4-3, the sampling points on the time-scale chosen for the successive on-line GC-MS analysis are denoted with the numbers in a circle. Each injection to the GC-MS apparatus corresponded to a given temperature of the sample, defined in the figure by the black curve. The samplings were performed in a similar way; however, in practice, small temporal deviations occurred due to the synchronization mismatch, as summarized in Table 4-5.

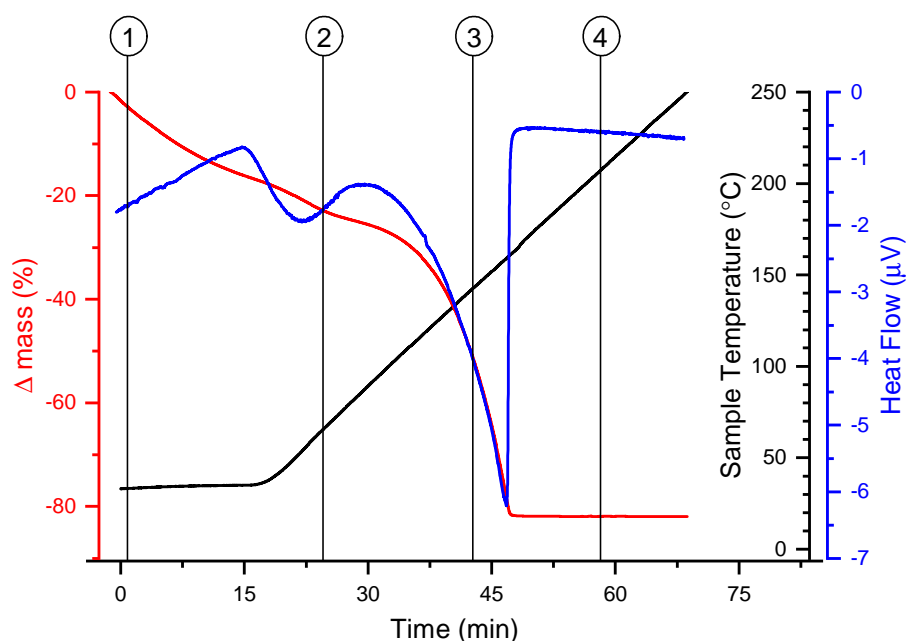


Figure 4-3. TGA-DSC curves of solvent isopropanol:HEMA=1:1. The sample temperature increase is shown by black line. The injections points for GC-MS analysis are labeled with numbers in a circle.

Table 4-5. Time and temperature of injections in GC-MS experiments

Injection point	Time when taken (minutes)	Sample temperature (°C)
1	0.81	32.3
2	24.3	60.4
3	43.3	115

4	58.3	208
---	------	-----

FTIR spectra of products were acquired on-line during TGA-DSC measurements in parallel to GC-MS analysis. It is important to keep in mind that the FTIR sensitivity is much lower than that of GC-MS; because of that, compounds in very small quantities or with similar bounds configuration were rather difficult to distinguish. However, FTIR data provided a deeper insight to the general behaviour of the process in complement to GC-MS. Because the complete analysis is very time-consuming and required much data processing, the experimental data were treated only at the selected times.

Figure 4-4 shows a general 3D view of the experimental FTIR spectra $I(t, \nu)$, where t -axis represents the experiment elapsed time, ν -axis represents wavenumber in cm^{-1} and I -axis represents absorbance. Together these three axes provides a complete information about the experiment: e.g. $I(\nu)$ spectra of any time t , Gram-Schmidt curves $I(t)$ and 2D color map of the products absorbance.

The peaks around 3000 cm^{-1} corresponds to OH group asymmetric stretching vibration $\text{CH}_2\text{-OH}$, its intensity becomes significant from 20 to 35 minutes from the process beginning, attaining the maximum at 26 minute, and then decreases almost to zero and increases again. It is important to notice that the spectral shape and full width at half maximum (FWHM) of this peak is not conserved at later times after the first period of the appearance. The modifications apparently indicate a change of the nature of the detected molecules. The peaks around 1000 and 1500 cm^{-1} start appearing at 39 minute; these peaks are characteristic of respectively C-O and C=O bounds in asymmetric stretching vibration mode C-O-C and C=O stretching respectively. The progressive spectral modifications and appearance of different peaks during the experiment runtime indicate a complex processing consisted in two stages, at which different compounds were emitted by the sample: the first stage takes place between 0 to 35 minutes and the second one from 39 to 62 minute.

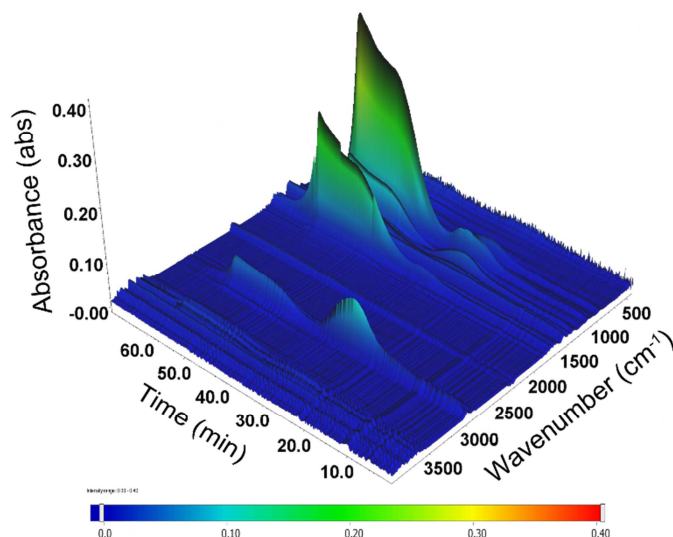


Figure 4-4. 3D representation of FTIR spectra acquired during TGA-DSC series of 1:1 isopropanol:HEMA solvent.

FTIR spectra obtained at the selected points of GC-MS injections are shown in

Figure 4-5 in red lines. The FTIR spectra of reference compounds, to which the spectra were attributed are shown in the same figure by black lines. The spectrum 1, measured at 0.8 minute from the process beginning, shows the presence of water and isopropanol. The characteristic peak of isopropanol at 2975 cm^{-1} is of a relatively low intensity, which makes appreciable intensity of the structured water bands around 1600 and 3800 cm^{-1} . In contrast, later at about minute 24, the intensity of the isopropanol peak increased hiding a weak structured water absorption in background. At minute 43, the spectrum changes: the isopropanol peak at 2975 cm^{-1} vanishes and smooth bands at about 2960 and 2892 cm^{-1} appear together with two very strong peaks at 1744 and 1160 cm^{-1} which are characteristic of 2-hydroxyethyl-methacrylate vapors. Spectra at minute 58 (point 4, not shown in figure) can be assigned to a mixture of different species, mainly HEMA and, at least, one decomposition product methyl methacrylate, which cannot be firmly confirmed in this study because of similarities with HEMA bands.

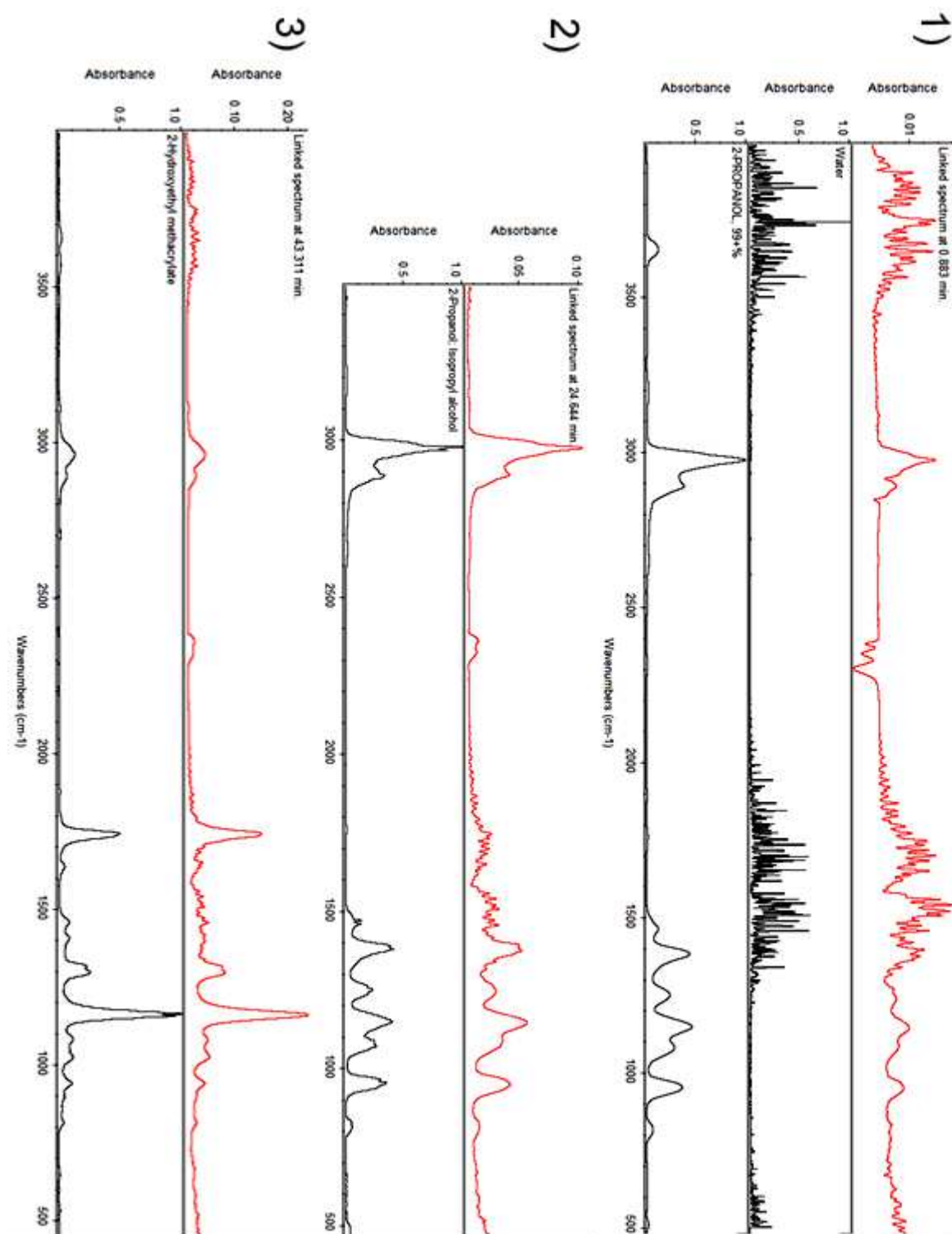


Figure 4-5. FTIR spectra of 1:1 isopropanol:HEMA solvent obtained at the GC-MS injection times (in red) and spectra of reference products: 1) 0.8 minute, 2) 24 minute, 3) 43 minute.

GC-MS chromatograms (Total Ion Current – TIC) of the four injection points, specified in Table 4-5 and TGA-DSC series of Figure 4-3, are shown in Figure 4-6. Each

peak on the TIC of each injection has a characteristic mass spectrum, which was analyzed with the help of Chromeleon® software and the NIST libraries furnished with the equipment.

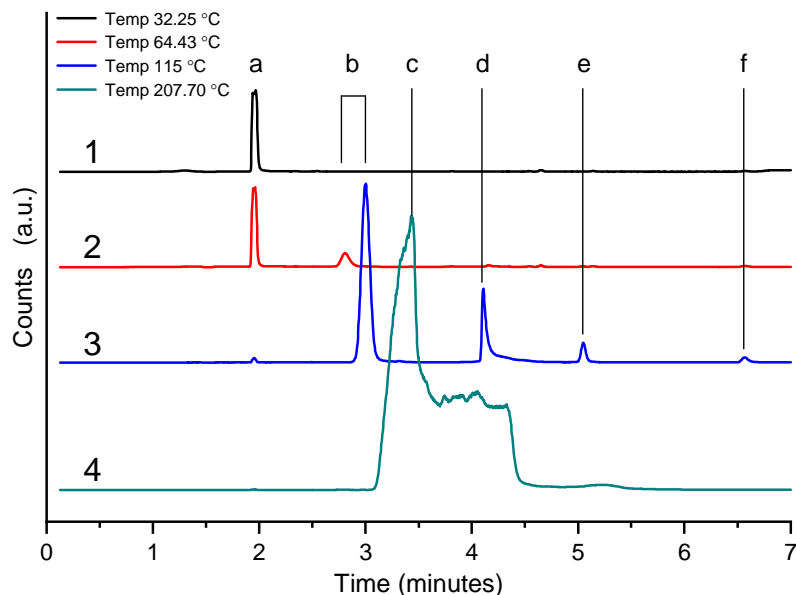


Figure 4-6. Chromatograms of 1:1 isopropanol-HEMA solvent during TG-DSC series at selected injections points.

The peak labeled (a) appeared at 2nd minute in the four chromatograms corresponds to isopropanol. According to available data, in GC-column used in the experiment HEMA showed up at 3rd minute, which corresponds to the peak labeled (b); the small peaks appeared between 3rd and 4th minutes in chromatograms 1-3 were also assigned, by using the available database, to HEMA monomers. In contrast, chromatogram of 4th injection the full separation of products was not achieved due to an excess of gases produced by the sample. The mass spectra of the wide peak labeled (c) was also assigned to HEMA, while the adjacent shoulder was attributed to by-products of the HEMA decomposition. The chromatogram 3 already evidenced the beginning of HEMA decomposition with the additional peaks of 2-methyl propionic acid at 4th minute (d), 2-hydroxy ethyl acetate at 5th minute (e) and methyl methacrylate at 6.5 minute (f), which is an impurity from HEMA synthesis (Montheard *et al.* 1992) and also a decomposition product. The depicted above molecules are chemically shown in Figure 4-7. We notice that the inhibitor methyl hydroquinone (MEHQ), which according to Milchensen *et al.* (2007) could be expected appearing in the chromatograms of the commercial HEMA, was absent. This confirms the effectiveness of the applied purification process of HEMA distillation.

Chapter 4: TiO₂ hybrids with HEMA organic component

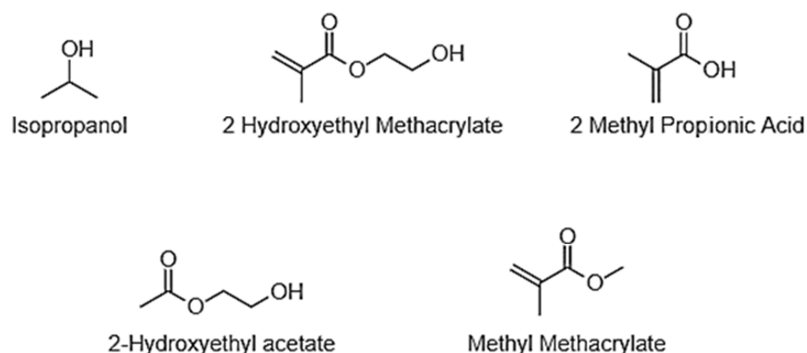


Figure 4-7. Relevant products of chromatograms in Figure 4-6.

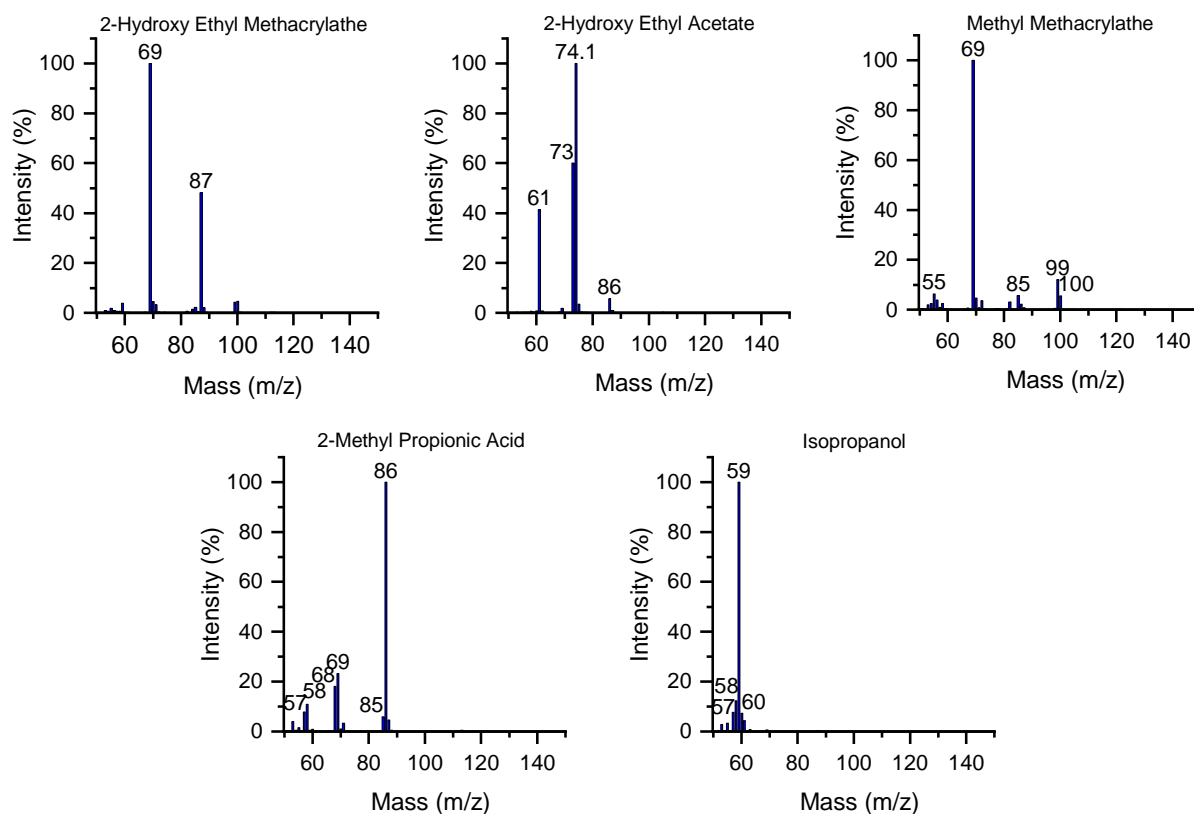


Figure 4-8. Mass spectra acquired for each by-product of the samples during the experiment.

The TGA-DSC/FTIR/GC-MS experiments performed in this chapter indicate that isopropanol remains in 1:1 isopropanol-HEMA solvent even at temperatures as high as 200 °C. In the same time, the decomposition products of HEMA begin to appear earlier than

expected, at temperatures as low as only 115 °C, which contrasts with the literature data about the decomposition onset at 160 °C (Gonzalez-Henriquez *et al.* 2014). The simultaneous release of isopropanol and HEMA is observed at relatively low temperatures between 64 and 115 °C, which may be explained by their specific interaction resulting in the formation of an azeotropic mixture isopropanol-HEMA. Our measurements evidence that the dominant released product 1:1 isopropanol-HEMA solvent in the temperature range below 111 °C is isopropanol, from 111 to 127°C it is isopropanol and HEMA in similar weighted fractions, and from 127 to 223 °C it becomes HEMA and the decomposition products, between which 2-methyl propionic acid and 2-hydroxy ethyl acetate were identified. The traces of water and methyl methacrylate by-product of HEMA synthesis remain even after the purification by distillation while hydroquinone inhibitor was eliminated.

4.1.3 TGA-DSC/GC-MS/FTIR analysis of colloid

In this section, we study the of HEMA-TiO₂ colloids after the solvent exchange stage including the analysis of the remained isopropanol and influence of the nanoparticles concentration. This study was carried out without initiator to avoid polymerization since our interest was brought to the analysis of interactions in the colloid submitted to a temperature ramp. The three samples were prepared in the following way:

1. 1 ml of HEMA + 10 ml Isopropanol followed by solvent extraction to a final volume of 1 ml. (HEMA x10 w/o NP)
2. 1 ml of HEMA + 10 ml of NP solution followed by solvent extraction to a final volume of 1 ml. (HEMA x10 NP)
3. 1 ml of HEMA + 20 ml of NP solution followed by solvent extraction to a final volume of 1 ml. (HEMA x20 NP)

These samples were studied by TGA-DSC coupled to GC-MS and FTIR using the experimental parameters specified in section 4.1.2 for the analysis of the 1:1 isopropanol-HEMA solvent.

The TGA-DSC thermogram of the prepared samples shown in Figure 4-9 evidence that the mass loss proceeds in an apparently one-step process at temperatures between 90 to 175 °C. The total mass losses of samples are: 78 % in HEMA x10 w/o NP, 84 % in HEMA x10 NP and 73 % in HEMA x20 NP. This mass loss can be attributed to the HEMA decomposition/evaporation (Gonzalez – Henriquez *et al.* 2014). In the same time, a smaller

relative mass loss of HEMA x20 NP compared with HEMA x10 NP can be connected with bigger content of inorganic nanoparticles resulted in the larger solvent retention on the nanoparticles surface and/or larger remaining mass. In contrast, the stronger mass losses in HEMA x10 NP colloid compared with HEMA x10 w/o NP solvent may signify a significant retention of isopropanol molecules on the particle surface after the solvent exchange stage, which are additionally released from the colloids, in contrast to the solvent without nanoparticles. This assumption is additionally supported by mass loss kinetics at low temperatures <100 °C, which increased in the order HEMA x10 w/o NP, HEMA x10 NP and HEMA x20 NP: the alcohol molecules weakly bound to the particles surface can be readily released at these temperatures and more concentrated colloids x20 released more alcohol compared to less concentrated x10 and even less than pure solvent without nanoparticles.

The complementary heat flow analysis brought an important information about the presence of different process responsible for the observed mass loss. Indeed, sample HEMA x10 w/o NP shows two well-defined endothermic processes: the first one between 30 and 90 °C correspondent to the isopropanol evaporation, previously discussed in section 4.1.2 , and the second one between 110 and 176 °C, which can be attributed to the evaporation/decomposition of HEMA. The presence of nanoparticles in HEMA x10 NP and HEMA x20 NP samples significantly modified the heat transfer. The first low-temperature endothermic process related to the isopropanol evaporation remained but become less pronounced. In addition, a new evaporation peak appeared at higher temperatures as a shoulder of the major peak related to the the beginning of HEMA evaporation/decomposition at 160-170 °C (point 3): this peak was found at 150 °C in HEMA x10 NP and at 133 °C in HEMA x20 NP colloids.

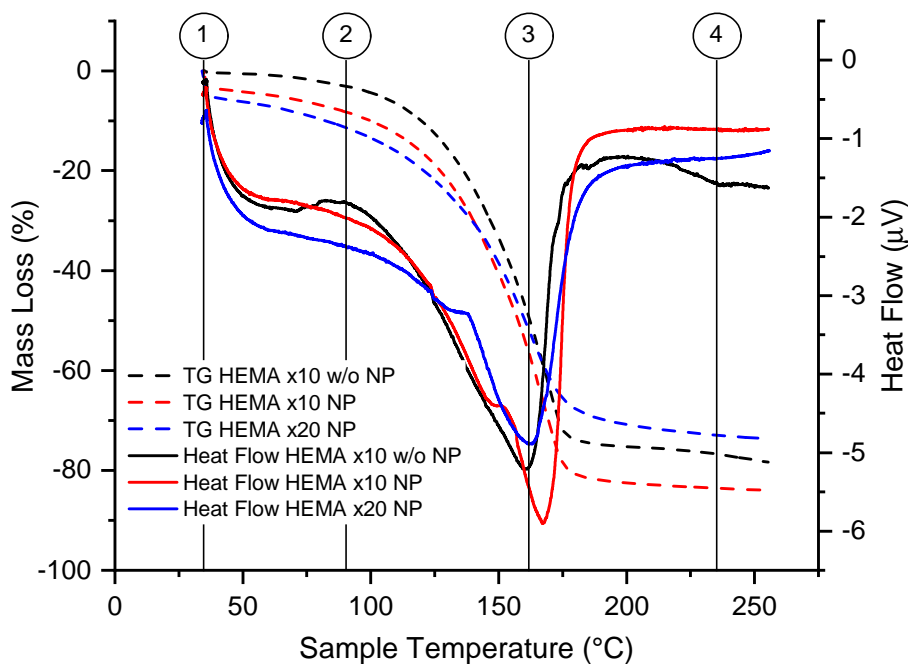


Figure 4-9. TGA-DSC curves of HEMA x10 w/o NP, HEMA x10 NP and HEMA x20 NP.

The understanding of the shoulder appearing on the heat flow curve in nanoparticle containing samples, shown in Figure 4-9, is easier if we analyse the first derivative of the mass loss shown in Figure 4-10. The dTG curve of sample HEMA x10 w/o NP (black line) does not seem to present any shoulder; however, the peak is wide enough to cover two well-resolved contributions of the nanoparticulate samples, indicating that the two evaporation / decomposition processes may coexist in this temperature range. The presence of the inorganic nanoparticles separates the two contributions making the low-temperature shoulder of the main peak due to the HEMA evaporation / decomposition process to appear. In need, in dTG curves the shoulder of HEMA x10 NP sample appears at 149 °C, while that of HEMA x20 NP sample shifts down to 134.3 °C, which is consistent with shoulders appearing in the heat flow series (Figure 4-9). The unknown evaporating species should have a very close evaporation enthalpy to that of HEMA. In this particular case, 2-hydroxy ethyl acetate with the evaporation enthalpy 48.8 kJ mol⁻¹, which is slightly lower than that of 49.5 kJ mol⁻¹ of HEMA, could be the released byproduct. The complex mass loss process is modified by the presence of nanoparticles, which influence the kinetics by promoting the catalytic HEMA transformation and evaporation of 2-hydroxy ethyl acetate product.

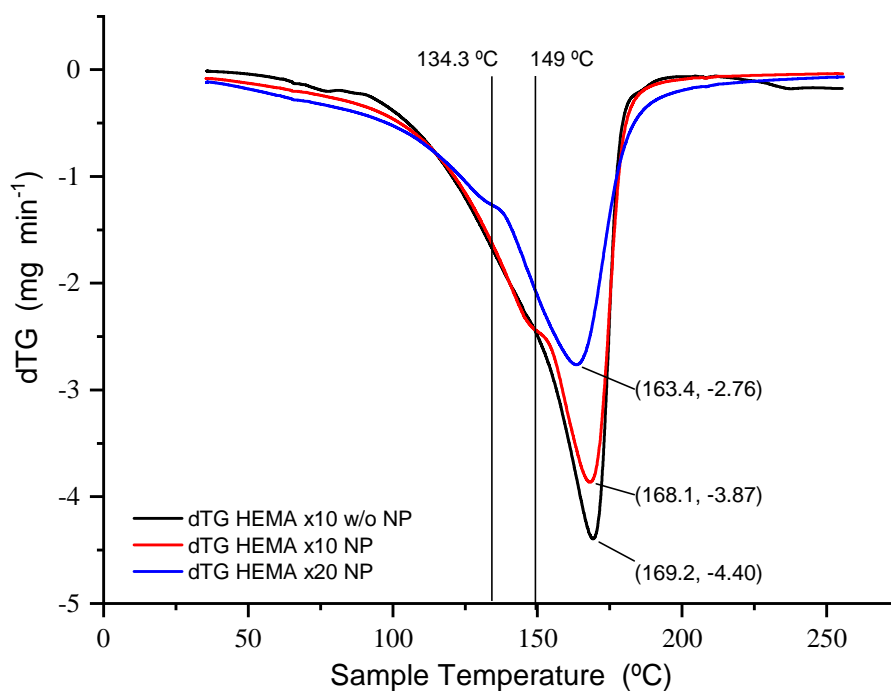


Figure 4-10. First derivative of mass loss curves (see Figure 4-9) of tree samples HEMA x10 w/o NP, HEMA x10 NP and HEMA x20 NP.

During TGA-DSC experiment gas sampling for GC-MS analysis was taken at the points marked in Figure 4-9 by numbers 1, 2, 3 and 4, which respective temperatures were 34 °C, 90 °C, 160 °C and 235 °C. In the same time, gaseous products released during the experimental series were analysed in a continuous mode by FTIR.

We first discuss the GC-MS analysis of three samples HEMA x10 w/o NP, HEMA x10 NP and HEMA x20 NP at the sampling points of Figure 4-9. The chromatogram in Figure 4-11 corresponds to point 1 with the temperature 34 °C. According to our previous analysis of the solvent, the major peak appeared at 2nd minute belongs to isopropanol. The second weaker peak at 3.8 minute detected only in samples containing nanoparticles, HEMA x10 NP and HEMA x20 NP, was assigned to isopropyl methacrylate. The third peak with a very low intensity, appeared at 6.6 minute in all samples, was assigned to methyl methacrylate, which, as previously mentioned, is an impurity of the HEMA synthesis. The difference in spectral positions of these peaks was not expected at low temperatures.

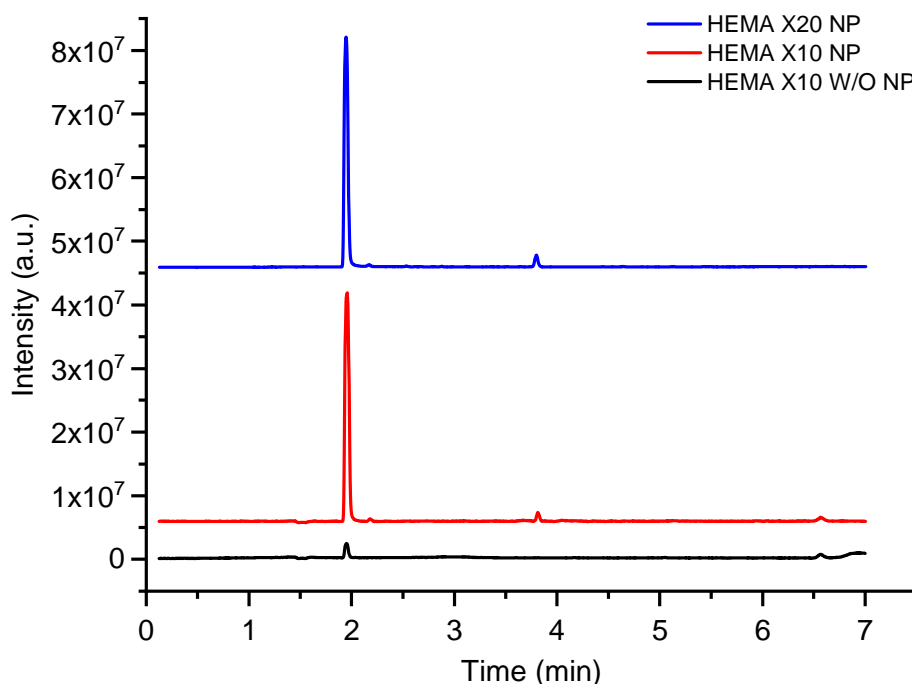


Figure 4-11. Chromatogram of gas probes at 34 °C in TGA-DSC series of samples HEMA x10 w/o NP, HEMA x10 NP and HEMA x20 NP.

The chromatograms presented in Figure 4-12 belong to gas sample taken at 90 °C. Those of the nanoparticulate colloids showed the major peak of isopropanol at 2nd minute, while it was much weaker in solvent without nanoparticles. Since the three samples followed the same solvent extraction process to the same final volume, the higher content of isopropanol in gas samples of the samples containing NPs at 90 °C suggests that NP retain much solvent, required more time and higher activation energy to be released. The last sample manifests the dominant peak of HEMA monomers at 2.8 minute, which intensity progressively decreased with an increase of the nanoparticles concentration: ~6 times weaker in HEMA x10 NP colloid and completely vanishing in HEMA x20 NP colloids. This finding additionally supports the assumption of the solvent retention on the nanoparticle surface: HEMA in this last case. The increment of another peak at 3.8 minute with an increase of the NP concentration, assigned to isopropyl methacrylate. This appearance of these species may be explained by the fragmentation or decomposition of HEMA, as depicted in the Figure 4-13, which could be promoted by the inorganic nanoparticles.

Chapter 4: TiO₂ hybrids with HEMA organic component

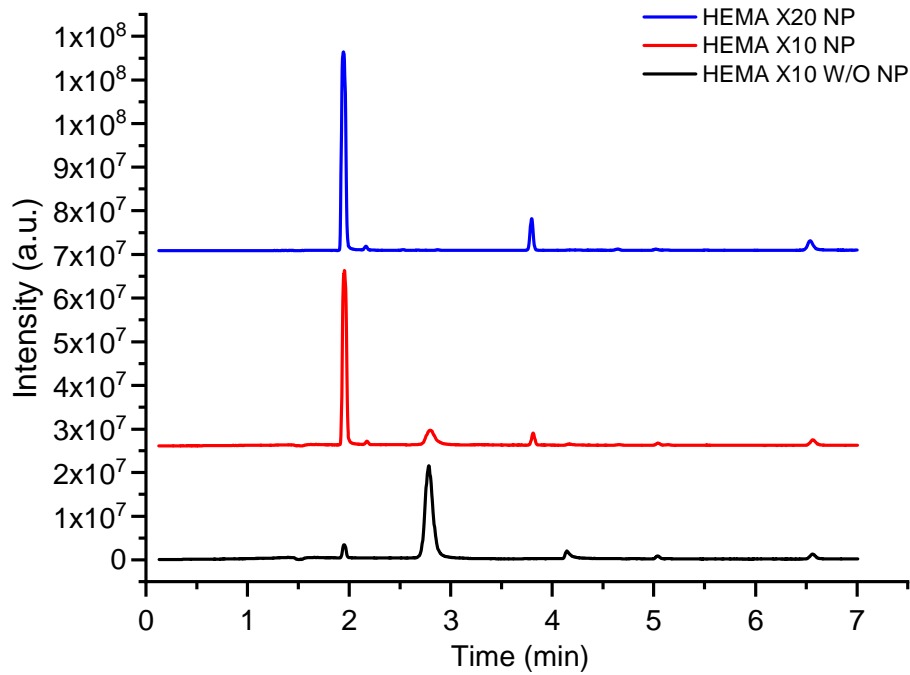


Figure 4-12. Chromatograms of a gas probes at 90 °C in TGA-DSC series of samples HEMA x10 w/o NP, HEMA x10 NP and HEMA x20 NP.

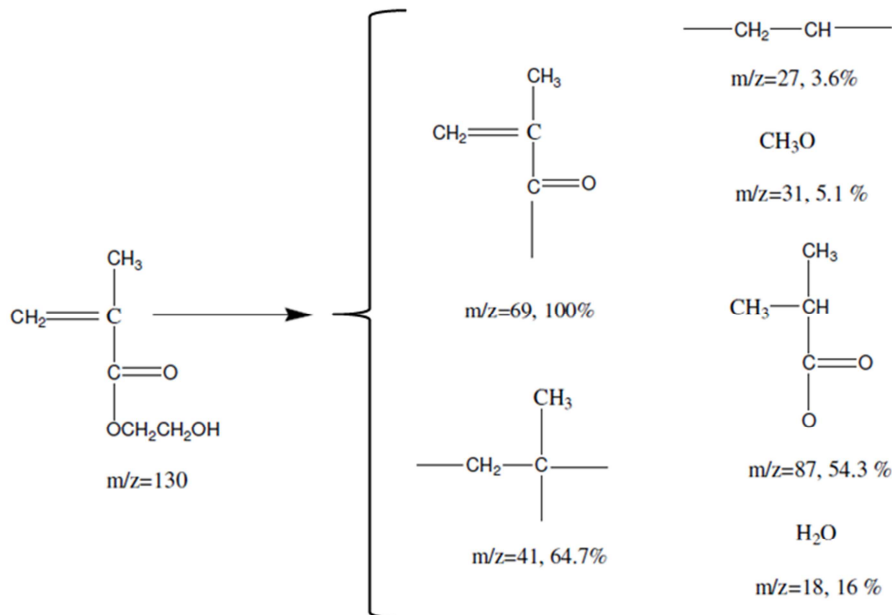


Figure 4-13. Schematic representation of HEMA fragmentation by pyrolysis analyzed by GC-MS taken from Vargün (2009).

At 4.15 minute, the peak identified as 2-methyl propionic acid in pure solvent appeared very weak in HEMA x10 NP colloid and not observed at all in a more concentrated HEMA x20 NP colloid. A small peak of 2-hydroxyethyl acetate at 5.1 minute apparently also weakened in presence of nanoparticles. Consequently, the related modifications of HEMA are prohibited on the particles surface, opened a new reaction channel towards isopropyl methacrylate indicated above. The peak of methyl methacrylate (impurity of HEMA) appeared at 6.55 minute in the three analysed samples with the similar intensity, which validates the experimental calibration.

At the third point of the chromatographic analysis taken at a temperature of 162 °C, the presence of isopropanol was not expected. Nevertheless, the isopropanol peak at 2nd minute clearly appeared in the colloidal samples, increasing with the nanoparticles concentration as Figure 4-14 shows. This evidences that the nanoparticles effectively retain this solvent even at such inappropriately elevated temperatures. In agreement with the previously discussed chromatograms at lower temperatures, the HEMA signal at 3rd minute appeared weaker in the colloids; however, the nanoparticles concentration affected weaker the release of the surface groups. These chromatograms confirm the catalytic contribution of the nanoparticles to the isopropyl methacrylate formation (peak at 3.8 minute) as well as the inhibition of 2-methyl propionic acid (4.15 minute) and 2-hydroxyethyl acetate (5.1 minute) formation. The validation of the experimental calibration provided the peak of methyl methacrylate (impurity of HEMA) at 6.55 minute, which appeared with the same intensity in all three analysed samples.

The injection at the highest temperature of 235 °C in Figure 4-15 showed no appreciable peak of isopropanol at 2nd minute. However, a zoom on the measured curves evidenced that it is still present in very small quantities in all three samples. The fine analysis confirmed an increase of the peak intensity from solvent to colloids, validating our suggestion of the solvent retention and stabilization against the decomposition at the nanoparticles surface. The peak at 3rd minute changed its low-T shape and strengthened indicating the release of many products issued of the HEMA decomposition.

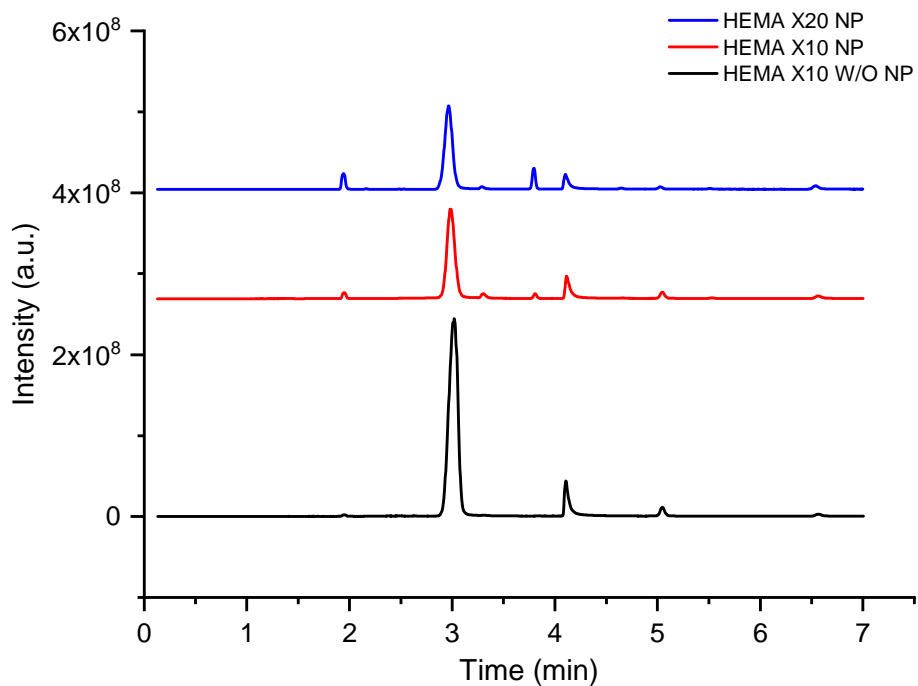


Figure 4-14. Chromatograms of a gas probes at 162 °C in TGA-DSC series of samples HEMA x10 w/o NP, HEMA x10 NP and HEMA x20 NP.

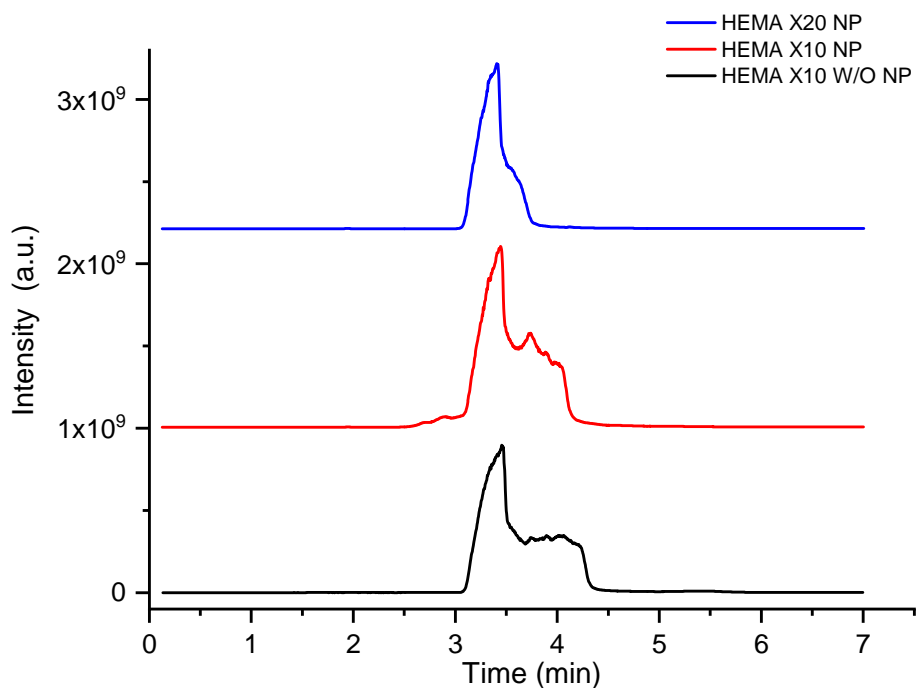


Figure 4-15. Chromatograms of gas probes at 235 °C in TGA-DSC series of samples HEMA x10 w/o NP, HEMA x10 NP and HEMA x20 NP.

To better visualize the influence of the NP concentration on the release of isopropanol and HEMA decomposition, we plotted the peak area for each sample at different gas sampling temperatures. As it was explained in Chapter II, the peak area in chromatography is proportional to the species concentration. The quantitative information about the concentration could be obtained for each peak after an appropriate calibration. In framework of our discussion, we applied a qualitative comparison of concentration evolution of the released species with temperature. The Log plot of relative concentrations of isopropanol and HEMA *vs* sample temperature is shown Figure 4-16 for samples HEMA x10 w/o NP, HEMA x10 NP and HEMA x20 NP. These data show that the isopropanol concentration (left part of the figure) in all gas probes in samples containing the nanoparticles is 10 times higher compared with that of solvent without the nanoparticles. This tendency to the concentration increase is especially strong at lower temperatures and softened at 235 °C. These results clearly indicated the nature of a thermally activated process, which consists in the species release from surface sites of the TiO₂ nanoparticles. In the same time, the similar shapes of the curves suggest that this activation behavior is mediated by the azeotropic nature of isopropanol-HEMA solvent, while nanoparticles serve to be a reservoir of an excessive isopropanol.

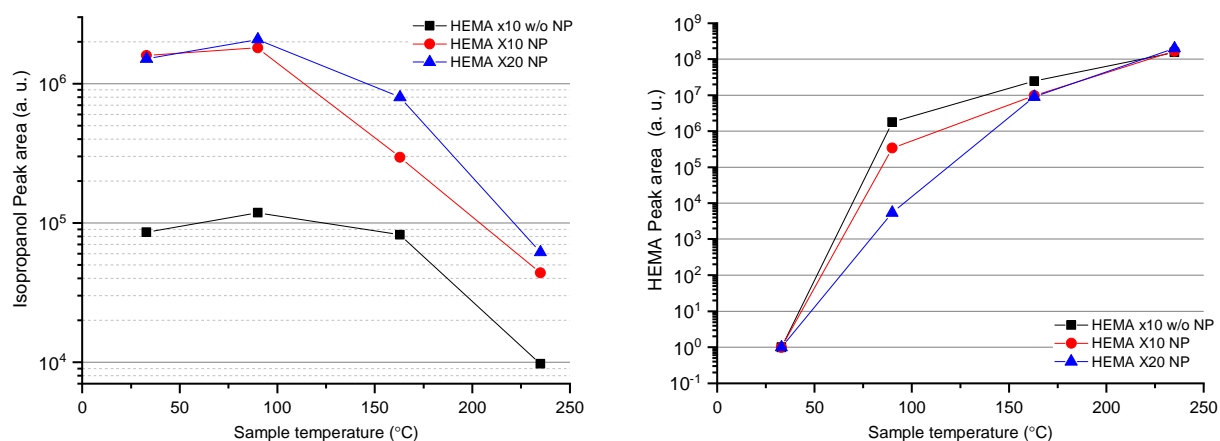


Figure 4-16. GS peak areas of isopropanol (2nd minute) and HEMA (3rd minute) of HEMA x10 w/o NP, HEMA x10 NP and HEMA x20 NP samples at different temperatures.

The right part of Figure 4-16 plots concentrations of the released HEMA. It shows that at 34 °C HEMA is almost not detectable in the probe, but its concentration rapidly increases

with temperature over the entire range of analysis. The activation behavior of the release process is clearly visible; however, the effect of the temperature increase appeared to be stronger at relatively low temperatures $T \leq 100$ °C and seemingly softens at higher temperatures, as if it required smaller activation energy. Moreover, with an increase of the nanoparticles concentration the activation process becomes better defined with a smaller dispersion of activation energy. A tentative explanation of this behavior can be given. In fact, the decomposition of HEMA at temperatures above 100 °C results in a release of gaseous products, which peaks partially superposed with that of HEMA and, therefore, contributing with different activation energies to the gaseous species concentration. In contrast, as previously discussed, the nanoparticles preserve the surface species delaying their thermal decomposition to even higher temperatures. The concentration and number of the released by-products consequently decreased. This would result in the activation energy closer to that of the major released HEMA component.

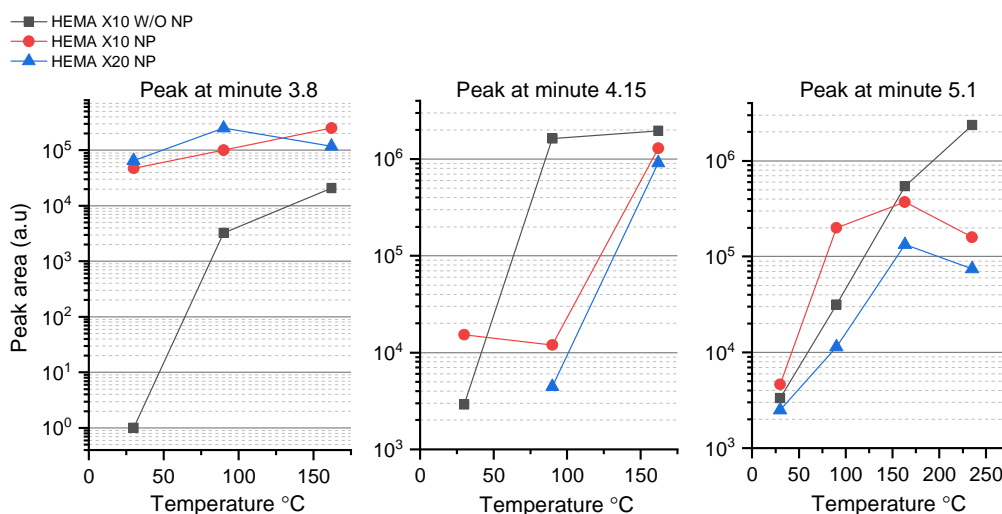


Figure 4-17. Peak area at 3.8, 4.15 and 5.1 minutes of HEMA x10 w/o NP, HEMA x10 NP and HEMA x20 NP samples at different temperatures.

The three graphs in Figure 4-17 show area of the small chromatogram peaks of gas probes of the same three samples characterised in Figure 4-16. The peak at 3.8 min does not significantly showed up in HEMA solvent but clearly appears in the nanoparticulate colloids. The MS analysis permits its attribution to isopropyl methacrylate (IM) molecule, which structurally differs from HEMA by a departure of hydroxyl group, which is apparently due to an interaction of HEMA with TiO₂ nanoparticle. Our experimental data in Figure 4-17

evidenced an important decrease of the activation energy of the HEMA-IM transformation in presence of nanoparticles, indicating significant catalytic activity at the solid-liquid interface. The peak at 4.15 min, attributed to 2-methyl propionic acid (MPA), was stronger in pure solvent and attained a comparable intensity only at temperatures ~ 150 °C in the colloids. Its evolution with temperature in HEMA solvent is rather similar to that of the peak at 3.8 min, however, nanoparticles strongly modify the reaction branching from MPA to IM at moderate temperatures < 150 °C. This reaction selectivity confirms catalytic activity of the solid component of our hybrids. The peak at 5.1 min was identified with 2-hydroxy ethyl acetate. This peak behavior with an increase was similar for all presented samples in the temperature range $T \leq 175$ °C. The differences appeared at high temperatures > 200 °C correspondent to the gas chromatograms probes in Figure 4-18 cannot be clearly rationalized because of the heavy organics combustion and poor peaks resolution.

These experiments brought us to a conclusion about three possible forms of isopropanol in our solutions:

1. Free isopropanol: a fraction of isopropanol that remains as solvent in the colloids, instantaneously non-interaction with the nanoparticles.
2. Interacting isopropanol with HEMA: a fraction of isopropanol interacting with HEMA forming an azeotrope complex.
3. Isopropanol-TiO₂: a fraction of isopropanol bound to nanoparticles, either chemisorbed in form of a surface ligand or physisorbed at the surface.

These interactions apparently affected all our experiments showing that isopropanol was continuously outgassed from the sample even at temperatures as high as 150 °C and remained up to a limit one 250 °C of the sample decomposition, while theoretically the hybrid solution it is expected to be purified from isopropanol at 90 °C. A strong isopropanol-HEMA interaction is evidenced by a slow isopropanol release from pure solvent. As a consequence, HEMA appears in released products at relatively low temperatures 90 °C and decomposed at around 160 °C (Gonzalez-Henriquez et al. 2014). The nanoparticle concentration preserves isopropanol concentration in the colloid, which preferentially stays at the particles surface. The problem of non-complete exchange may be an obstacle of the material application, since even small traces of non-controlled surface contaminants may significantly affect the functional properties of the hybrid material.

The interactions in the hybrid solutions appears to be strong in the temperature range of HEMA polymerization, which makes interesting to analyse the polymerization of the nanoparticulate hybrid solutions.

4.2 Influence of NP on HEMA polymerization studied by coupled TGA-DSC/GC-MS/FTIR

As discussed in the previous section, the presence of TiO₂ nanoparticles unusually affects the solvent composition under heating. In this section, the influence of nanoparticles on the polymerization stage will be studied by employing most adequate experimental techniques of section 4.1.

For a series of these measurements, four samples were prepared in the following way:

1. 1 ml of HEMA + 10 ml isopropanol followed by the solvent extraction to a final volume of 1 ml, than completed by 0.1 mol % of recrystallized AIBN (sample labelled HEMA x10 w/o NP-P).
2. 1 ml of HEMA + 10 ml of NP solution followed by the solvent extraction to a final volume of 1 ml, than completed by 0.1 mol % of recrystallized AIBN (HEMA x10 NP-P).
3. 1 ml of HEMA + 20 ml of NP solution followed by the solvent extraction to a final volume of 1 ml, than completed by 0.1 mol % of recrystallized AIBN (HEMA x20 NP-P).
4. Solvent extraction was performed on 100 ml of NP solution (prepared as explained in Chapter III), than dried at 70 °C for 24 h at ambient atmosphere; the obtained fine powder was kept in vacuum in a sealed ampoule until utilization in TGA-DSC (TiO₂ Powder).

For samples 1, 2 and 3, the coupled TGA-DSC/GC-MS/FTIR analysis was used with the same experimental parameters and sampling time as described in the previous section. Sample 4 was analysed by using TGA-DSC method.

In Figure 4-18, the mass loss and heat transfer are shown for the four selected samples HEMA x10 w/o NP-P (a), HEMA x10 NP-P (b), HEMA x20 NP-P (c) and TiO₂ powder (d).

As we can observe in Figure 4-18a, HEMA x10 w/o NP-P showed a very small mass loss of ~2.3 % due to a partial evaporation of solvent. On the heat flow plot, only one very narrow peak of an exothermic phenomenon is present with an onset of 96.1 °C, which corresponds to the polymerization of HEMA (Achilias et Siafaka, 2017), with the released heat of polymerization (area under peak) of 69.4 $\mu\text{V s mg}^{-1}$. The nanoparticles containing samples HEMA x10 NP-P (b) and HEMA x20 NP-P (c) also show an exothermic polymerization peak, which, however, is significantly broader and shifted to higher temperatures; the respective mass loss of these samples is much stronger as compared with that of the pure monomer solution and increased with the nanoparticle concentration in the hybrid solution. This difference evidences an impact of the nanoparticles on the polymerization process. The values of the polymerization onset temperature and released heat are reported in Table 4-6. The temperature of the polymerization initiation decreased with an addition of nanoparticles and further proportionally decreased with an increase of the nanoparticle concentration by about 6 °C per 1.5 mol nanoparticles. In the same time, the released heat also decreases in presence of nanoparticles. This apparently indicates that the respective polymerization efficiency and reaction rates decreased. In our case, this may be due to a slower diffusion of species and/or polymer chains propagation in presence of the inorganic nanoparticles, which plays a role of adsorber/quencher. The large mass loss in presence of nanoparticles may be connected to the shift of polymerisation to higher temperatures, which make the monomer evaporation process more effective. Consequently, more monomers leave the hybrid solution before polymerisation solidifies the sample prohibiting evaporation.

Table 4-6. Onset temperature and released heat of radical polymerization of selected hybrid solutions and HEMA solvent (measurements presented in Figure 4-18).

Sample	On set temperature (°C)	Released Heat ($\mu\text{Vs mg}^{-1}$)
HEMA x10 w/o NP-P	96.1	-69.4
HEMA x10 NP - P	90.3	-28.3
HEMA x20 NP - P	84.6	-21.9

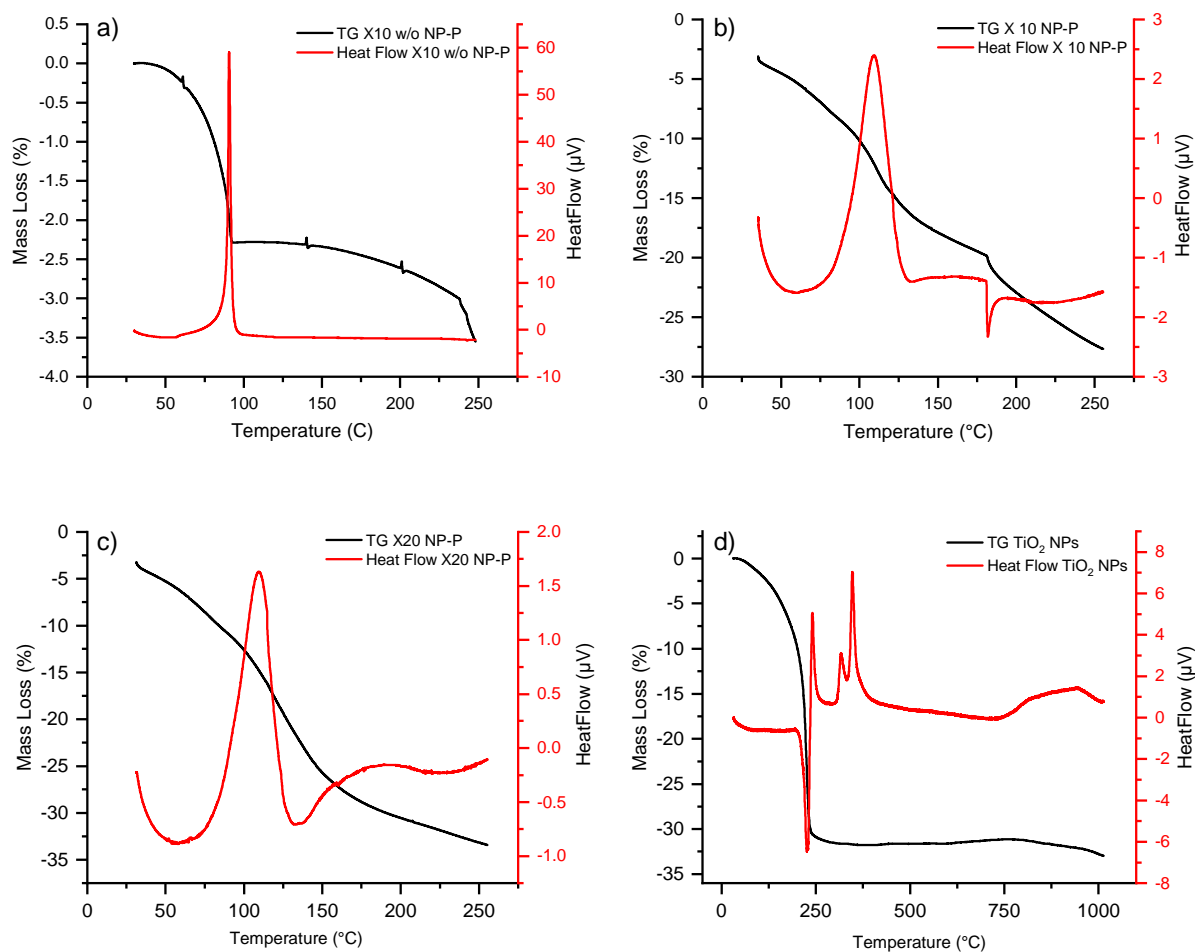


Figure 4-18. TGA-DSC curves of HEMA x10 w/o NP-P (a), HEMA x10 NP-P (b), HEMA x20 NP-P (c) and TiO₂ powder (d). Measurements were performed at 4 °C min⁻¹ under air atmosphere.

The TiO₂ powder in Figure 4-18(d) showed an important mass loss of 31.8 % and the endothermic peak with the onset temperature at 216.5 °C, which suggest the desorption of adsorbed water, isopropanol and possibly other organics remaining after the nanoparticles synthesis (Wang *et al.* 2008) (Ba-Abbad *et al.* 2012) (Phattepur *et al.* 2018). After the principal mass loss, three exothermic peaks with onset temperatures 235.7 °C, 308.9 °C and 340 °C appear, which can be attributed to birning of the surface organics and amorphous to anatase phase transition in TiO₂. The mass loss of three polymerized samples samples is summarized in Table 4-7.

Table 4-7. Mass loss of nanoparticulate hybrids, HEMA solvent and TiO₂ powder.

Sample	Mass loss at 225 °C (%)	Mass loss at 250 °C (%)
HEMA x10 w/o NP-P	2.84	3.55
HEMA x10 NP-P	25.3	27.3
HEMA x20 NP-P	31.8	33.2
TiO ₂ Powder	22.0	30.9

The Gram-Schmidt curves in Figure 4-19 of the hybrid samples containing the TiO₂ nanoparticles illustrate our general assignment of the respective mass loss to the evaporation process. The more precise information concerning the released species in course of the radical polymerization were obtained via FTIR and GC-MS measurements.

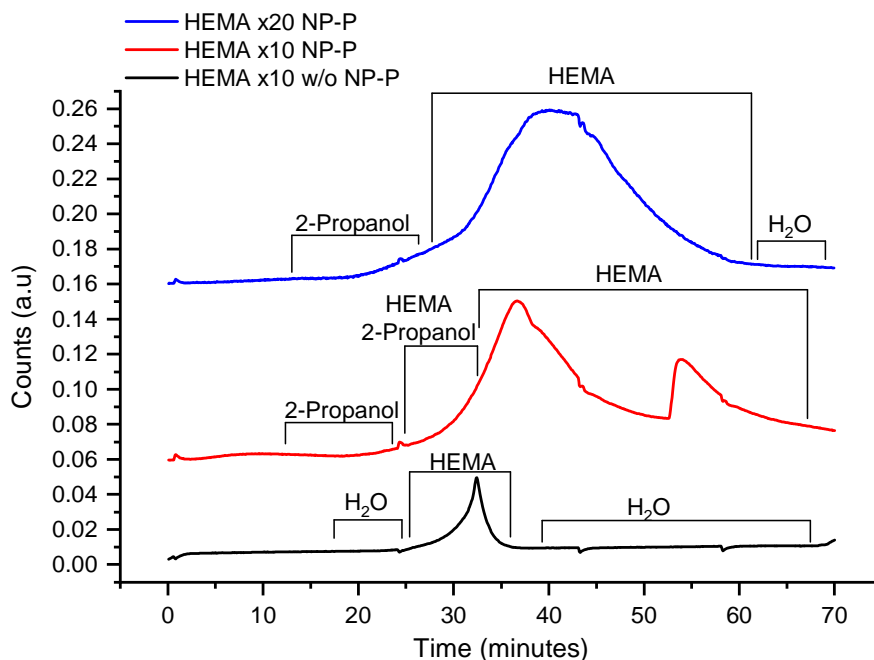


Figure 4-19. Gram-Schmidt representation of polymerization of three hybrid solutions during TGA-DSC series. The most significant released species are indicated.

This overall view of the FTIR experiment can give us a clear idea about the moment, where sample released more vapour; this release will be reflected in an increase on the Gram-Schmidt intensity and can be directly set in correlation with TGA-DSC series. As shown in Figure 4-19 the measured curves were quite different. In the case of HEMA x10 w/o NP-P (Figure 4-19, black line), only the released water was detected, before the major peak mainly composed of HEMA. This peak corresponds to the time of the TGA-DSC series when the

small mass loss takes place (see Figure 4-18a, $75 < T < 100$ °C). After this peak, only water was identified on the FTIR spectra. In sample HEMA x10 NP-P (Figure 4-19, red line) isopropanol was released in the beginning of the experiment, followed by a mixture of isopropanol and HEMA, before the apparition of two large peaks where only HEMA could be identified. As can be seen from the comparison with TGA-DSC in Figure 4-18b, the two peaks of sample HEMA x10 NP-P corresponds to the two principal mass losses at temperatures ~ 100 and 180 °C. In respect to sample HEMA x20 NP-P, isopropanol is present in the first part of the experiment, while no zone of its mixture with HEMA could be identified; the main peak was mainly due to the evaporation of HEMA, with an addition of water that became more important to the end of the experiment. This corroborates with the observation of one single one mass loss step in TGA-DSC measurements in Figure 4-18c. The results of FTIR and TGA-DSC experiments correlate; however, as has been stated before FTIR does not have a high sensitivity and detect only the most abundant species in the released gases. Therefore, for a better understanding an influence of nanoparticles on the polymerization process, a closer look on the GC-MS data will be done next.

As in previous GC-MS experiments, injections of gaseous probes from TGA-DSC were performed at four different temperatures: 22 °C, 90 °C, 163 °C and 235 °C. Figure 4-20 shows probes of three selected samples taken at 22 °C. In the case of the polymerizable organic solvent (HEMA x10 w/o NP-P), only a very small peak appeared at 2nd minute corresponding to isopropanol. In contrast, in the hybrid solutions HEMA x10 NP-P and HEMA x20 NP-P the isopropanol peak intensity was strongly increased by a factor of 10 and 100 times, respectively. This apparently signifies the isopropanol retention by the TiO₂ nanoparticles, since they were not outgassed during the solid hybrids preparation. Furthermore, samples containing the nanoparticles showed a weak peak at 3.8 minute attributed to isopropyl methacrylate, which was however stronger than in the organic solvent without nanoparticles, and increased with the nanoparticles concentration. This indicates that the nanoparticles promote the HEMA decomposition. No other significant peaks were found in the analysed chromatograms.

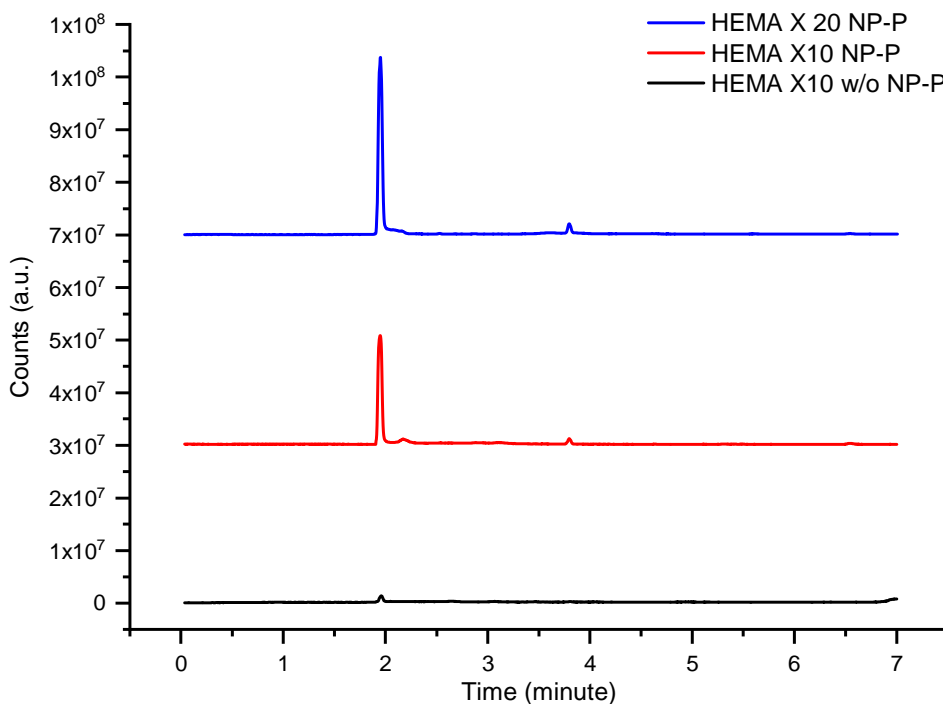


Figure 4-20. Chromatograms of a gas probes at 22 °C in TGA-DSC series of samples HEMA x10 w/o NP-P, HEMA x10 NP-P and HEMA x20 NP-P.

Figure 4-21 shows chromatograms of the three samples taken at the temperature 90 °C, which corresponds to the polymerization onset temperature and, therefore bring information about material solidification. As can be seen in this figure, a significantly smaller amount of isopropanol (compared with that at 25 °C) is present in the polymerized organic solvent at this temperature. The species peaked at 6.6 minute and correspond to the major HEMA impurity - methyl methacrylate.

As in chromatograms at lower temperature, in samples containing the nanoparticles the isopropanol peak (2nd minute) enhances ~10 times in both polymerized hybrids HEMA x10 w/o NP-P and HEMA x10 NP-P. Also the smaller peak of isopropyl methacrylate (3.8 minute) increased in the polymerized hybrids, indicating the beginning of HEMA decomposition at this rather low temperature. We notice that in polymerized organics without nanoparticles this by-product was not observed. This appearance of isopropanol in the solid hybrids at 90 °C may indicate that TiO₂ nanoparticles captured the solvent, remained after the exchange stage, during the polymerization stage and progressively release it in the diffusional-like process enhanced by heating.

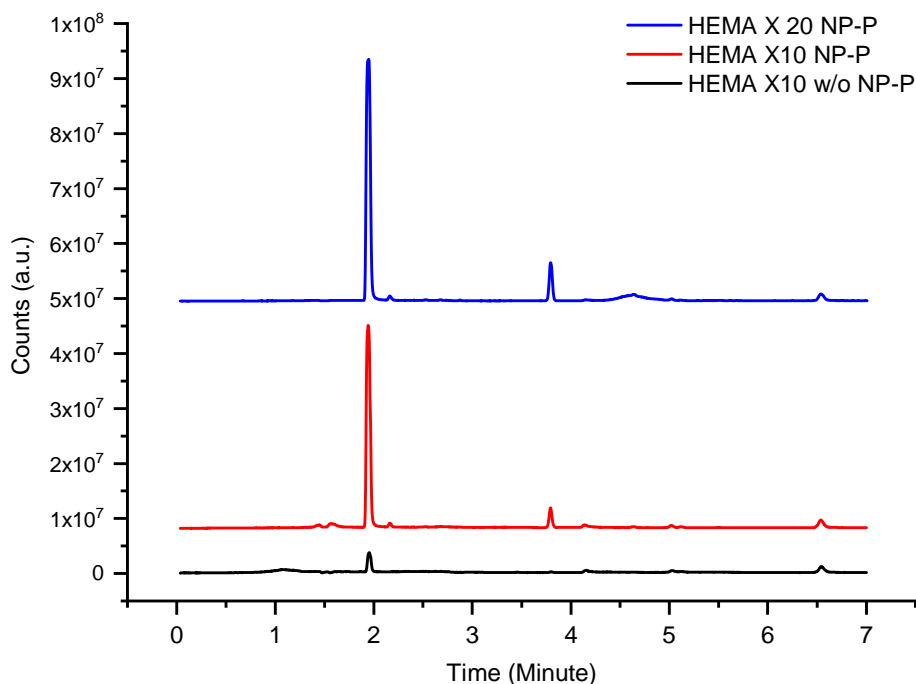


Figure 4-21. Chromatograms of a gas probes at 90 °C in TGA-DSC series of samples HEMA x10 w/o NP-P, HEMA x10 NP-P and HEMA x20 NP-P.

The chromatograms in Figure 4-22 show the released products from the polymerized samples at 163 °C. The polymerised organic sample without inorganic nanoparticles (HEMA x10 w/o NP-P) presents the major peak at 3rd minute, which belongs to HEMA monomers released by the sample. In the case of the nanoparticles containing samples, HEMA x10 NP-P and HEMA x20 NP-P, the isopropanol peak at 2nd minute is still present and increased with the nanoparticles concentration, indicating that more isopropanol was retained (at the particles surface) in the more concentrated nanoparticulate hybrid. More minor large and narrow peaks were observed indicating different by-producte of the HEMA decomposition (e.g. isopropyl methacrylate at 3.8 minute). The peak at 4.1 minute probably belongs to the HEMA decomposition products and that at 4.6 minute belongs to small chains of p-HEMA since its mass spectrum is similat to HEMA but the retention time is longer. At 163 °C the diffusion-controlled propagation process of the polymerization is terminated. The re-initialization process then governs the reaction, during this stage and isopropanol trapped in the polymer chains can slowly scape by diffusion. A complementary source of the released alcohol consists in non-reacted isopropoxy ligands still attached to TiO₂ nanoparticles, which can convert to isopropanol by reacting with traces of water (Bradly, 1958; Corriu, 2009). The last

process does not result in the inorganic particles coarsening since they are separated by the surrounding polymer chains.

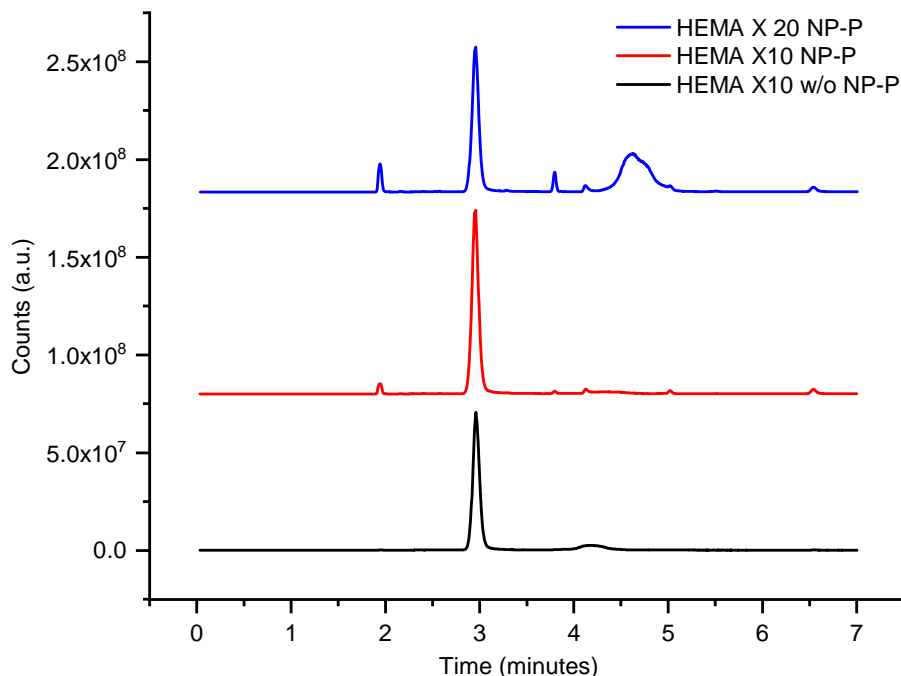


Figure 4-22. Chromatograms of a gas probes at 163 °C in TGA-DSC series of samples HEMA x10 w/o NP-P, HEMA x10 NP-P and HEMA x20 NP-P.

In chromatograms of Figure 4-23 taken at 235°C, the isopropanol peak of sample HEMA x10 w/o NP-P was no more observed. Their decomposition of the polymer was evidenced by the appearance of a large peak between 4 and 6 minutes. We also observed a very small isopropanol peak at 2nd minute and dominant HEMA peak at 3rd minute. The released HEMA may be due to the not complete organic polymerization; the quantity of non-reacting HEMA monomers increases with an increase of nanoparticles concentration and can amount for ~10 % in HEMA x10 NP-P sample with 1.5 mol/l Ti (Gorbovyi et al., 2011). In the same time, the decomposition peak is appreciably suppressed in the hybrid samples HEMA x10 NP-P and HEMA x20 NP-P, which indicates stabilization of the hybrid structure against thermal decomposition by the inorganic component.

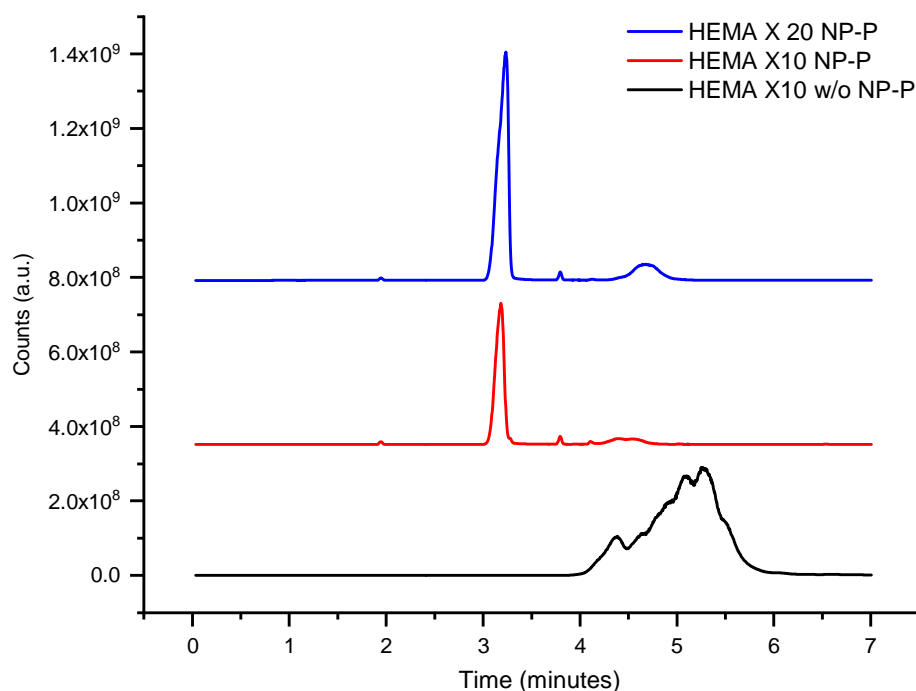


Figure 4-23. Chromatograms of a gas probes at 235 °C in TGA-DSC series of samples HEMA x10 w/o NP-P, HEMA x10 NP-P and HEMA x20 NP-P.

The chromatogram peaks area of isopropanol (left) and HEMA (right) are presented in Figure 4-24. The hybrid samples release isopropanol (left) similarly to that of the hybrid solutions with the same inorganic content (Figure 4-16). The organic polymer without nanoparticles (black) behaved differently from that of the solvent (considered previously) during the polymerization, since it reaches the lowest concentration at 163 °C and remains low at higher temperatures. This behaviour is quite expected, since isopropanol evaporates principally before polymerization and its small fraction trapped in the polymer can be only released via slow diffusion in solid. HEMA x10 NP-P showed the similar behaviour but showing larger quantities of the released alcohol. In contrast, HEMA x20 NP-P with twice higher concentration of the inorganic component showed a steady decrease of even larger quantities of the released isopropanol until 235 °C, most probably because of a higher content of non-polymerized organics (Gorbovyi et al. 2011) shifting the polymerization completion to higher temperatures.

The curves of the released HEMA in Figure 4-24 (right part) show that no HEMA comes out from the sample without nanoparticles, at low temperatures below the polymerisation onset. HEMA only showed up after the polymerization significantly advanced above 100 °C, reaching a maximum at 163 °C. This could be attributed to the evaporation of

the residual non-polymerized monomers contained in the sample. The point taken at 235 °C (hollow black square) cannot be taken as a measure of the true HEMA concentration, since the organics decomposition occurs at this temperature and separation of peaks of many decomposition products became poor in the chromatographic column.

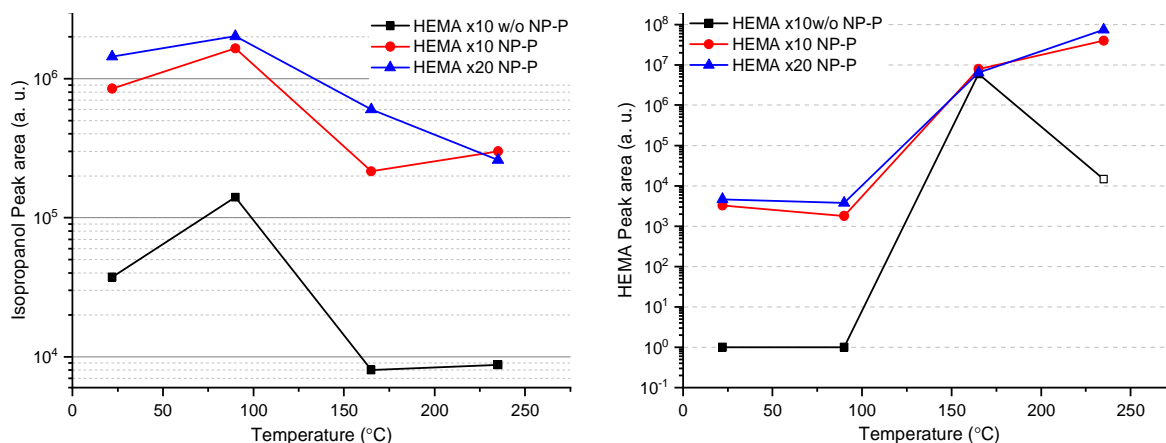


Figure 4-24. GS-MS peak areas of isopropanol ($t=2$ min) and HEMA ($t=3$ min) of HEMA x10 w/o NP-P, HEMA x10 NP-P and HEMA x20 NP-P samples at different temperatures

In presence of nanoparticles, the appearance of released HEMA at low temperatures could be (at least partially) due to a mixed isopropanol-HEMA evaporation. Above onset of the organic polymerization, HEMA concentration increases with temperature. This may signify that there remained more non-reacted HEMA in the hybrid samples, which diffused in its structure and evaporated. This process is responsible for the mass loss and the exothermic polymerization peak widening observed in TGA-DSC experiments. According to the model of radical polymerization kinetics described by Achilias (2007 and 2017), the polymerization reaction follows three main stages. The first one consists in the initiation where the reaction rate depends on the reactants concentration. The second one consists in the polymer chains propagation and is governed by the diffusion of the monomer molecules and macro radicals in the solution. The third one consists in the diffusion-controlled termination of the reactions. This mechanism can explain the difference between different samples by the diffusion propagation barrier imposed by the nanoparticles. Since the nanoparticles slow down the polymer chains propagation, the polymerization efficiency reduced in the hybrid solutions, leaving unreacted monomer free to be evaporated. The relation between the polymerization DSC peaks and the polymerization degree is well explained for 2-hydroxyethyl methacrylate

in nanocomposite materials by Achilias (2017) making evident that even in non-isothermal conditions a widening of the exothermic polymerization peak is directly linked to the reduced polymerization efficiency.

4.3 Conclusions

In this section, we studied preparation of the hybrid solutions and, in particular, the composition changes in course of the solvent distillation and solvent exchange stages. The temperature of the samples varies from room to 235 °C covering the polymerization range. From analysis of the experimental data, we can conclude that:

- The TGA-DSC coupled to GC-MS measurements confirmed solvent purification of MEHQ inhibitor in the distillation process. In contrast, traces of water and MMA monomer precursors MMA remain in HEMA after the distillation.
- The necessary time for the isopropanol-HEMA solvent exchange at constant temperature and primary vacuum conditions does not significantly depend on solvent concentration and presence of nanoparticles. The optimal conditions were obtained via TG-DSC coupled to GC-MS and FTIR measurements.
- The isopropanol was found in gas probes in a wide temperature range above 115 °C, which clearly exceeds the boiling temperature, suggesting the azeotropic HEMA-isopropanol mixture. The TGA-DSC studies of different HEMA-Isopropanol mixtures could be important to conduct in order to determine homogenous or heterogenous nature of the azeotrope.
- The TGA-DSC coupled to GC-MS and FTIR measurements evidenced the decomposition products of HEMA together with HEMA evaporation at relatively low temperature in gas probes, which suggest that HEMA decomposition onset in presence of nanoparticles is lower than that reported in literature.
- The major decomposition products of 1:1 HEMA-isopropanol solvent were 2-methyl propionic acid and 2-hydroxy ethyl acetate; furthermore, methyl methacrylate was observed as the decomposition product and synthesis impurity.
- The analysis TiO₂-HEMA colloids by TGA-DSC coupled to GC-MS showed an important presence of isopropanol in a broad temperature range up to 235 °C. The isopropanol release was increased with an increase of the nanoparticles concentration. This finding clearly evidences the retention of solvents molecules on the nanoparticle surface, which

may have consequences on the material electronic properties and, in particular, on the charge separation efficiency and charge storage capacity, key factors determining functional response for photonic applications (laser microstructuring, waveguides). The quantitative study of isopropanol content in the hybrid solutions at different temperatures could be further inspected by the direct injection in a properly calibrated GC-MS, which is important for the evaluation of its influence on structural and functional properties. Complementary, NMR studies of the hybrid solutions at different temperatures will provide information about molecular interactions and bonds forming between TiO₂ nanoparticle and HEMA molecule.

- The release of the decomposition products was studied with an increase of the medium temperature. The process was found strongly affected by the presence of TiO₂ nanoparticles, which was tentatively explained by their catalytic action. In particular, the quantity of 2-hydroxy ethyl acetate in gas probes significantly increased in the colloids. The kinetic study of the released products in presence of nanoparticles could help to further understanding of the reaction mechanism.
- The consideration of the hybrid polymerisation showed a strong modification of the released gas probes content, which was explained by their trapping in the polymer chains and exit via a slow diffusion process characteristic of solids. The polymerisation onset temperature (compared with HEMA solvent) was decreased by 6 °C in HEMA x10 NP and by 12 °C in HEMA x20 NP. The polymerization exothermic peak increased its FWHF indicated reduction of the monomers conversion efficiency.

Chapter 5 : TiO₂ hybrids with mixed HEMA-EMA inorganic component

The nanoparticulate HEMA-TiO₂ hybrids possess a strong photochromic response due to an effective separation and storage of photoinduced charges in form of polaronic Ti³⁺ centres (Kuznetsov et al., 2009; Gorbovyi et al., 2011). A high concentration of the inorganic component and a strong modification of the material refraction due to the light-induced Ti⁴⁺→Ti³⁺ conversion by $\Delta n = -2.4 \times 10^{-23} \text{ cm}^3 / \text{per Ti}^{3+} \text{ center}$ (Uklein et al., 2013) make these materials valuable candidates for fabrication of flexible micro-optical elements and applications in optoelectronics (Evlyukhin et al., 2018). The structuring of the hybrids can be performed by the two-photon laser photo-polymerization method, which is now widely applied for the rapid manufacturing of 3D microstructures with resolutions below 100 nm [Farsari and Chichkov, 2009; Zhou et al., 2015]. This method consists in a tight focusing of the laser beam into a liquid monomer solution with an addition of a photoinitiator to trigger polymerization reactions at the focal point following a two-photon absorption. The 3D structures are achieved by moving the focal point within the solution. The materials used can be purely organic, typically monomers with vinyl groups, or consist on a hybrid with included inorganic network chemically bonded to organic backbones.

The HEMA-TiO₂ hybrids are difficult to maintain as non-aggregated colloid because of their extreme sensitivity to water. As a result, an occasional contact with the environmental humidity accelerates precipitation of TiO₂ nanoparticles, making rather sophisticated laser processing of these media. For this reason, more stable colloids having a better tolerance to humidity by conserving a good photonic response are of high interest. A considerable extension of lifetime of a hermetically closed colloid beyond a week (for easy material delivery) and stability in a humid atmosphere during laser processing (during ~1 hour) are required for an easy handling in the structuring process.

To achieve these desirable properties, copolymerization of HEMA with hydrophobic monomers could be a solution of the above problem. In this chapter, liquid solutions of HEMA with a similar but hydrophobic molecule ethyl methacrylate (EMA) will be studied. The sample preparation for the experiments presented herein was as follows:

1. 1 ml of HEMA + 5 ml of NP solution followed by solvent exchange to a volume of 1 ml (HEMA x5 NP)
2. 0.5 ml of HEMA + 0.5 ml of EMA + 5 ml of NP solution followed by solvent exchange to a volume of 1 ml (HEMA-EMA x5 NP)

3. 1 ml of HEMA + 10 ml of NP solution followed by solvent exchange to a volume of 1 ml (HEMA x10 NP)
4. 0.5 ml of HEMA + 0.5 ml of EMA + 10 ml of NP solution followed by solvent exchange to a volume of 1 ml (HEMA-EMA x10 NP)
5. 1 ml of HEMA + 20 ml of NP solution followed by solvent exchange to a volume of 1 ml (HEMA x20 NP)
6. 0.5 ml of HEMA + 0.5 ml of EMA + 20 ml of NP solution followed by solvent exchange to a volume of 1 ml (HEMA-EMA x20 NP)
7. For polymerization experiments 0.1 mol % of AIBN was added to the previously mentioned samples, the name assigned to these new samples adds P at the end: e.g. HEMA x5 NP-P, HEMA-EMA x5 NP-P and so on.

A series of experiments were performed to determine the colloid stability by the controlled addition of water until reaching the gelation point. For the polymerization study, TGA-DSC experiments were performed in LSPM at Paris 13 and in ITODYS at Paris 7, in order to confirm the results.

5.1 Colloid stability

The stability of the HEMA and HEMA-EMA colloids was studied by performing two different tests. In the first one, the colloid stability was evaluated by leaving the samples in a globe box in closed recipients for a long period and the gelation/precipitation time was measured. In the second test, a dropwise addition of 1 μ l water was applied on 0.5 ml of different HEMA-EMA hybrid solutions, followed by 1 min wait time after each addition, until the gelation or precipitation of samples and the total amount of the added water was recorded; the solutions were maintained manually agitated during the preparation. In these last experiments, factors determining the colloids stability were formation of macroscopic chains (gelation) or microscopic agglomerates (precipitation) of inorganic TiO₂ nanoparticles.

Figure 5-1 shows the stabilization time of the colloid containing different amounts of TiO₂ nanoparticles: x5, x10, x20 and x30 (x1 = 0.15 mol/l Ti). As we can see, the stability of HEMA-EMA colloids significantly increased compared with their HEMA counterparts: by a factor of three for x5, twice for x10 and four times for x20. Moreover, the most concentrated

colloid x30, was completely unstable in HEMA solvent while conserved the stability of seven days in HEMA-EMA mixture.

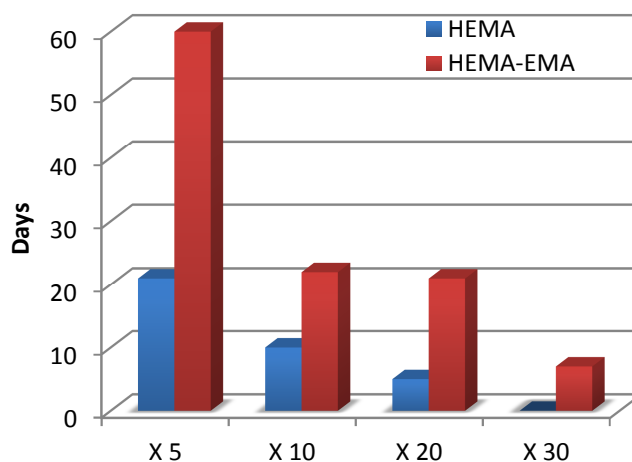


Figure 5-1. Stability time of the nanoparticulate TiO_2 colloids x5, x10, x20 and x30 ($x1=0.15$ mol/l Ti) in HEMA and HEMA-EMA solvents.

Figure 5-2 shows the critical quantity of added water to HEMA-EMA hybrid solutions, which provokes the lost of the colloid stability. In particularly, the precipitation point was taken when the solutions became opaque because of the appearance of submicronic-size agglomerates of nanoparticles. After an addition of more water, some hybrid solutions formed cream-like liquids, while others formed a gummy-like soft gel. In contrast to x5, x10 and x20 hybrids, the hybrid solution x30 (4.5 mol/l Ti) formed a translucent hard gel. We notice that in HEMA-EMA colloids, a cloudy solution was formed after some water addition, which however turned again translucent after the agitation and more water were required to add to reach the point when large agglomerated particles were formed indicating the precipitation process. After this point, the colloid turns into a white gel if more water was added.

These experiments led us to the conclusion that EMA addition to HEMA increases the nanoparticulate colloid lifetime and stability against the nanoparticles condensation in contact with the atmospheric humidity and/or in presence of traces of liquid water. The increase stability of the co-polymeric hybrids can be explained by the enhanced hydrophobicity of the organic component containing EMA. In contrast, an addition of EMA does not change the nanoparticles stability, which convert from hydrophilic to hydrophobic after the grafting -OEMA ligands on the particle surface. In these conditions, a partial substitution of the the

hydrophilic HEMA environment by hydrophobic EMA one maintains the colloid by prohibiting bulk water diffusion.

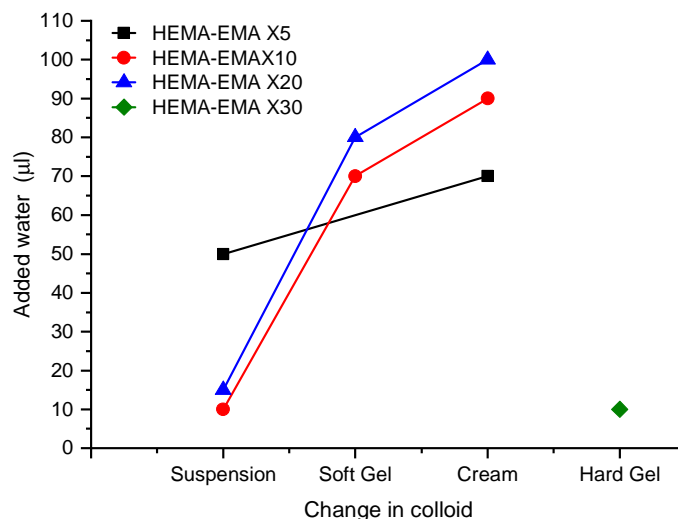


Figure 5-2. Colloid behaviour after water addition.

The obtained results confirm that these hybrid solutions can be used in standard laboratory room conditions without the need to control the humidity and/or using sample processing in a confined environment such as a glove box or under dry air flow. The new materials permit an easy scalability towards industrial applications.

However, the only colloid stability improvement could be meaningless unless polymerization and optical properties were not checked to be maintained after the EMA addition. Consequently, in the next section we will study the organic polymerization of copolymer HEMA-EMA colloids and compare with that of simple HEMA colloids.

5.1.1 Polymerization

The polymerization of HEMA-EMA hybrids and the NP influence on this process was studied by the TGA-DSC method. The HEMA-EMA samples were prepared as indicated in the beginning of Chapter V, and 1 mol % of AIBN initiator was added to the hybrid solutions as a source of radical to trig the process. The TGA-DSC series were run under air atmosphere with a heating ramp of 4 °C/min from ambient temperature to 800 °C.

Figure 5-3 shows the TGA-DSC thermograms for eight samples: HEMA and HEMA-EMA without nanoparticles, HEMA and HEMA-EMA with nanoparticles of x5 concentration

($x_1 = 0.15 \text{ mol/l}$), HEMA and HEMA-EMA with nanoparticles concentration x_{10} and HEMA and HEMA-EMA with nanoparticles concentration x_{20} .

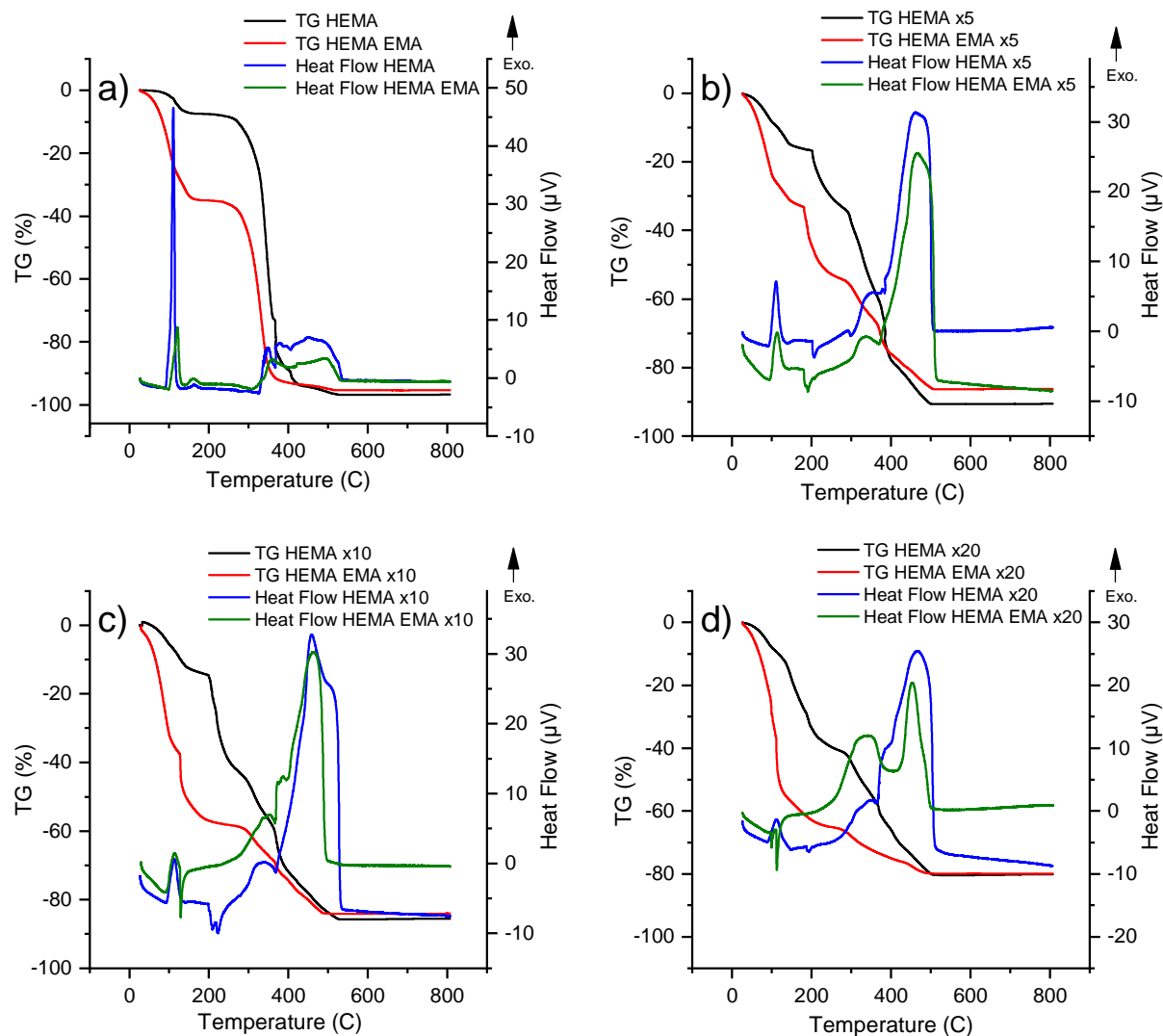


Figure 5-3. TGA-DSC experiments of organic (a) and organic-inorganic hybrid (b-d) HEMA and HEMA-EMA solutions.

The heat flow curves in Figure 5-3a) show the same number of exothermic peaks in both organic solutions: HEMA (blue line) and HEMA-EMA (green line). The first with onset $103.5 \text{ }^\circ\text{C}$ and offset $116.9 \text{ }^\circ\text{C}$ temperatures and released heat $52.9 \text{ } \mu\text{V s mg}^{-1}$ was observed in HEMA, while HEMA-EMA showed somewhat lower onset $108.3 \text{ }^\circ\text{C}$ an offset $127.1 \text{ }^\circ\text{C}$ temperatures and released heat $32.0 \text{ } \mu\text{V s mg}^{-1}$. This feature apparently belongs to the polymerization process. The second exothermic peak appeared with onset $155.5 \text{ }^\circ\text{C}$ and offset $185.0 \text{ }^\circ\text{C}$ temperatures and released heat of $1.97 \text{ } \mu\text{V s mg}^{-1}$ in HEMA and onset $150.0 \text{ }^\circ\text{C}$ and

offset 171.7 °C temperatures and released heat $5.17 \mu\text{V s mg}^{-1}$, which according to Ramirez-Jimenez *et al.* (2012) may belong to the copolymer glass transition. Then, the third exothermic phenomenon appeared in both samples starting with ~ 276 °C and terminating at ~ 530 °C, which can be assigned to the decomposition/combustion of HEMA and HEMA-EMA.

The mass loss in Figure 5-3a) in HEMA (black line) is of 7.4 % between 53.5 °C and 155 °C can be due to the residual water and HEMA evaporation. The second mass loss 84.4% appears in HEMA at 216.7 °C and ends at 420.3 °C, and third and the last mass loss of 3.85 % appears between 428 and 541.8 °C. These two last mass losses that constitute 88.2 % are due to the decomposition/combustion process. The total mass loss in this sample ~ 95.2 % resulted in the crucible black powder most probably composed of carbon and metal organic particles. HEMA-EMA (red line) showed the similar behavior to HEMA; however, the larger initial mass loss of 34.8 % was measured in this case. Since the polymerization process was shifted to higher temperatures, the monomers evaporation was considered as most probable explanation of this observation. One can therefore conclude that the final composition of the mixed organic sample after polymerization was changed and the mass loss could be attributed to EMA losses because of its higher volatility compared with HEMA. Taking into account the initial composition HEMA:EMA=1:1 and mass loss 7.4 % of HEMA component presenting 50% of the solution, the remaining mass loss of 31.1 % of the total one 34.8 % may belong to EMA. An estimation of the final composition of the organic component results in HEMA-EMA=1.35:1 in the polymerized sample. After polymerization, a second mass loss of 62.1 % between 276 and 533.5 °C corresponds to the decomposition/combustion of HEMA and EMA. From this first experiment we can conclude that polymerization is affected by an addition of EMA, resulting in a lower heat released during the process. This signifies that the evaporation compensates the heat release and/or that the monomer conversion is lower.

After addition of nanoparticles, the heat flow and mass loss change significantly. The polymerization peak of HEMA x5 (blue line in Figure 5-3b) was inhibited, with onset 96.44 °C and offset 121.84 °C temperatures and released heat $26.38 \mu\text{V s mg}^{-1}$. The second endothermic peak with onset 199.56 °C and offset 253.47 °C temperatures and an absorbed heat $12.15 \mu\text{V s mg}^{-1}$ can be attributed to an evaporation process. We have not identified the released species, which may be a product of the decomposition or even water released in the beginning of combustion. The large decomposition/combustion peak begins at 382.85 °C end

terminates at 523.62 °C. The main features of HEMA-EMA x5 behavior are similarly HEMA x5. Firstly, the polymerization peak appears with onset 98.89 °C and offset 126.96 °C temperatures and released heat 18.76 $\mu\text{V s mg}^{-1}$. However, the presence of EMA shifts the polymerization of HEMA x5 to higher temperatures by 2.45 °C. The released heat is also affected being smaller by 7.62 $\mu\text{V s mg}^{-1}$ indicating probably a lower polymerization degree. The second endothermic peak corresponds to onset 188.38 °C and offset 200.53 °C temperatures and absorbed heat 9.14 $\mu\text{V s mg}^{-1}$. This peak in comparison with HEMA x5 shifts to lower temperatures by 19.2 °C and has a lower absorbed heat 3.01 $\mu\text{V s mg}^{-1}$, indicating that the evaporation is weaker. Finally, the strong exothermic peak appearing at 421.1 °C and terminating at 510.9 °C corresponds to the decomposition/combustion of the organic components.

The TG signal of HEMA x5 sample (black line in Figure 5-3b) presents several mass loss domains. The first between 36 and 175 °C occurs at the same time as the polymerization and accounts for the mass loss of 16.1 %. The second mass loss appears at 200.6 °C and terminates at 209.8 °C accounting for 18.5 % of the initial mass; it can be attributed to the remaining water and isopropanol desorption (Wang et al., 2018), since it matches the endothermic peak appearing of the heat flow. The mass loss of 27.0 % in the range between 293.2 °C and 373.4 °C corresponds to the decomposition process, since it correlates with the third exothermic peak of the heat flow. This is followed by the mass loss of 29.3 % between 384.0 °C and 600.0 °C, which corresponds to the strongest exothermic peak of decomposition/combustion of the organic component. The remaining material in the crucible is most probably consists of TiO₂ and carbon. The mass loss of HEMA-EMA x5 is similar to HEMA x5 but showed more pronounced steps. It includes 32.2 % between 33.5 °C and 159.98 °C, corresponding to the polymerization stage; 23.1 % between 180.5 °C and 292.2 °C, corresponding to the desorption; 19.9 % between 236 °C and 393.92 °C and completing by 11.0 % between 401 °C and 612.5 °C, which is attributed to the organics decomposition/combustion.

The heat flow curve of HEMA x10 sample in Figure 5-3c) (blue line) show three main peaks, which corroborate the previous analysis of x5 samples. The exothermic polymerization peak appears with onset 95.6 °C and offset 126.4 °C temperatures and released heat 18.1 $\mu\text{V s mg}^{-1}$. The endothermic peak due to the desorption of residual water and isopropanol appears between 202.4 °C and 239.4 °C with absorbed heat 16.2 $\mu\text{V s mg}^{-1}$, confirming our analysis of Chapter 4.2. The third exothermic peak with onset 418.5 °C and

offset 529.9 °C temperatures corresponds to the decomposition/combustion of the organics. The HEMA-EMA x10 sample confirmed this behaviour. However, exothermic polymerization peak appearing at 95.7 °C overlapped with endothermic desorption peak, which makes difficult to determine the offset and released heat. The position of the endothermic process was estimated between 127.4 °C and 134.7 °C. The decomposition/combustion exothermic peak begins at 361 °C and terminates at 491.2 °C.

The TG analysis of HEMA x10 in Figure 5-3c), black line) showed four main domains of the mass loss: 13.8 % mass loss between 35 °C and 179.18 °C corresponds to the polymerization, 27.8 % between 181 °C and 265.28 °C corresponds to the desorption and 32.38 % between 270 °C and 417 °C and completing with 11.7 % terminated at 570.6 °C corresponds to decomposition/combustion of the organic component; the total mass loss therefore amounts for 85.7 %. Similar to HEMA-EMA x5, HEMA-EMA x10 sample exhibited pronounced mass loss steps, by keeping the same tendency as HEMA x10. For example, the polymerization stage accomplishes with a stronger mass loss of 37.3 % terminated at 125 °C. The mass loss of 21.6 % terminated at 278.2 °C, which corresponds to the endothermic peak, apparently belongs to desorption; this mass step is similar to that in HEMA x10, indicating the departure of remaining solvents. The last mass loss of 25.3 % starts at 280 °C and terminates at 539 °C, which belongs to the thermal decomposition/combustion of the organic components; the total mass loss of this sample is 84.1 %.

The heat flow and TG curves of samples containing NP in concentration x20 (3.0 mol/l Ti) are shown in Figure 5-3d). In agreement with previous results, heat flow of HEMA x20 showed the polymerization peak between 94.2 °C and 128.0 °C with released heat 21.465 $\mu\text{V s mg}^{-1}$, the desorption peak appears between 187.1 °C and 199.0 °C with an absorbed heat of 1.87 $\mu\text{V s mg}^{-1}$ and the strongest decomposition/combustion peak appears between 366.7 °C and 507.9 °C. In contrast, the exothermic peak of polymerization was not observed in HEMA-EMA x20; instead, it appears that the endothermic peak of species desorption was shifted to lower temperatures, completely overlapping with the polymerization peak and splitting into two apparent endothermic peaks with the first onset at 97.3 °C. After this first phenomenon, we observed the decomposition/combustion also divided in two peaks with the first between 285.7 °C and 375.3 °C and the second between 429.8 °C and 496.3 °C.

Regarding TG response, HEMA x20 (black line in Figure 5-3d) shows a similar behavior to the previous samples with mass losses 12.8 % between 35 °C and 134 °C, 28.8 % between 140 °C and 283 °C and 38.8 % between 300 °C and 538.5 °C, resulting in the total mass loss of 80.4 %. HEMA-EMA x20 showed principal mass loss steps of 57.2 % between 35 °C and 150 °C, 8.0 % between 160 °C and 258 °C and 10.0 % between 280 °C and 404.7 °C, completing with 4.6 % until 548 °C, resulting in the total mass loss of 79.9 %, which is similar to that of HEMA x20.

The above measurements show that all hybrid samples based on pure HEMA monomer show desorption peak around 200 °C, independently on the nanoparticles concentration. The area of this peak decreases with an increase of the inorganic content in the material. According to the results of Chapter 4.2 based on GC-MS and FTIR analyses, this desorption can be attributed to water, isopropanol and non-reacted HEMA. Also in agreement with the results of Chapter 4.2, the released heat of polymerization decreases with the increase of the nanoparticles concentration, which peak widens and shifts to higher temperatures. This can be due to smaller polymerization efficiency, as explained by Achilias (2007 and 2017) and also noticed by Gorbovyi et al. (2011) in pHEMA-TiO₂ hybrids. The heat-flow polymerisation peak of HEMA-EMA mixture is smaller than that of pure HEMA, which can be explained by additional monomer losses because of the higher process temperature (see Figure 4-23a) and higher volatility of the co-monomer EMA. The particularity of hybrid samples based on a mixture HEMA-EMA (in comparison with those based on HEMA) concerns the endothermic desorption peak, which first appeared at about 200 °C (x5 ≡ 0.75 mol/l Ti) and progressively shifted with an increase of the nanoparticles concentration to lower temperatures ~97 °C (x20 ≡ 3 mol/l Ti). As a result of this process, the polymerisation and desorption coexist in HEMA-EMA x20 hybrid. The difference between hybrid samples based on HEMA and HEMA-EMA organics consists in a stronger mass loss of the last in the range of moderate temperatures below T~300 °C, at which the material completes polymerization and heat does not yet damage the polymer structure. This stronger mass loss could be due to the evaporation of more volatile EMA monomers. However, as has been shown in Chapter 4.2, this evaporation cannot be attributed uniquely to EMA since the presence of isopropanol in the released gases has been evidenced by GC-MS measurements in this range of temperatures. The complex process occurring in HEMA-EMA hybrids cannot be fully understood in this limited series of experiments. Liquid chromatography and gas chromatography could be used to exactly determine the quantities of HEMA, EMA and

isopropanol in the colloids at the polymerization stage in order to confirm the effectiveness of the solvent exchange in the hybrid samples. In addition, a better insight on HEMA and HEMA-EMA interactions could be obtained with other techniques such as Magnetic Nuclear Resonance of solids to determine the final configuration of the chemical bonds in the polymer, which will show the location of the Ti-O, OH, C-O and C=O bonds in the polymer chain.

5.1.2 TEM micrography

In this section, Transmission Electron Microscopy (TEM) of the hybrid samples was applied to understand the nature of the elementary building block constituting the inorganic component, on which depend the internal contact area with the organics and the components coupling. These data may be important for elucidation of the material functional properties and optimization of the photochromic response, useful for the photonic applications. The hybrid samples were prepared according to a standard procedure described in the previous chapters of this manuscript. The polymerization of 5 ml volume hybrid solution was performed under vacuum after degasification in a sealed glass vial at temperature of 90 °C for one night.

Figure 5-4a shows TEM image of HEMA x5 sample. As EDX spectrum in Figure 4-29b evidences, dark areas with a weak contrast belong to TiO₂ nanoparticles, which are homogeneously distributed over the scanned area. These nanoparticles clearly have a size below 5 nm, which is characteristic of the nanoparticles in beginning of the preparation process (Gorbovyi et al., 2011).

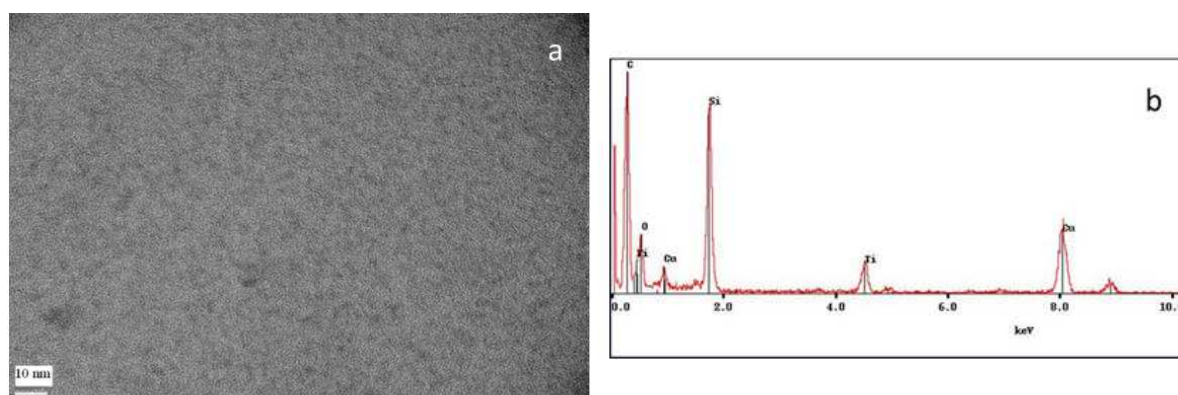


Figure 5-4. TEM image (a) and EDX spectrum (b) of HEMA x5 sample; scale 10 nm in (a).

More clearly, the nanoparticles size was evidenced in TEM images of HEMA-EMA x5 hybrid in Figure 5-5 (a-c) at three scales of 20 nm, 5 nm and 2 nm. The large area image (a) evidences highly homogeneous distribution of the inorganic nanoparticles over the organic component. In complement, the high-resolution images (b) and (c) show the mean particles size of $2R=3.0$ nm with a very small polydispersity. This finding seems surprising since the size of the inorganic particles generated by the chemical reactor and injected into the organic monomer solution is $2R=5.2$ nm (Gorbovyi et al., 2011). The understanding of this observation provide recent article by Cheng et al. (2017), which gave a clear idea about the nucleation process and elementary titanium oxo-alkoxy nucleus. This work defined the nucleus as most stable unit against solvent perturbations and measured its radius $R=1.6$ nm by using the DLS method. In contrast, the size of bigger units can vary depending on the environmental conditions (e.g. nature of solvent). Consequently, the diagram of the titanium oxo-alkoxy species stability reported by Azouani et al. (2007) allowed interpreting the 5.0-nm nanoparticles issued of the micromixing reactor as assembling of several such nuclei. Based on these results, we can conclude that the 5.0-nm TiO_2 particles, which keep their size after the solvent exchange stage (Gorbovyi et al., 2011), undergo partial fragmentation upon polymerization process: they split into the smallest fundamental units– nucleus. This important observation nicely supports the results of Cheng et al. (2017), validating the fundamental building block of Titania solids. It would be important to notice that this size corresponds to the stability domain of the bulk solid structure, which defines the material electronic structure and functional properties (Monticone et al., 2000; Satoh et al., 2008).

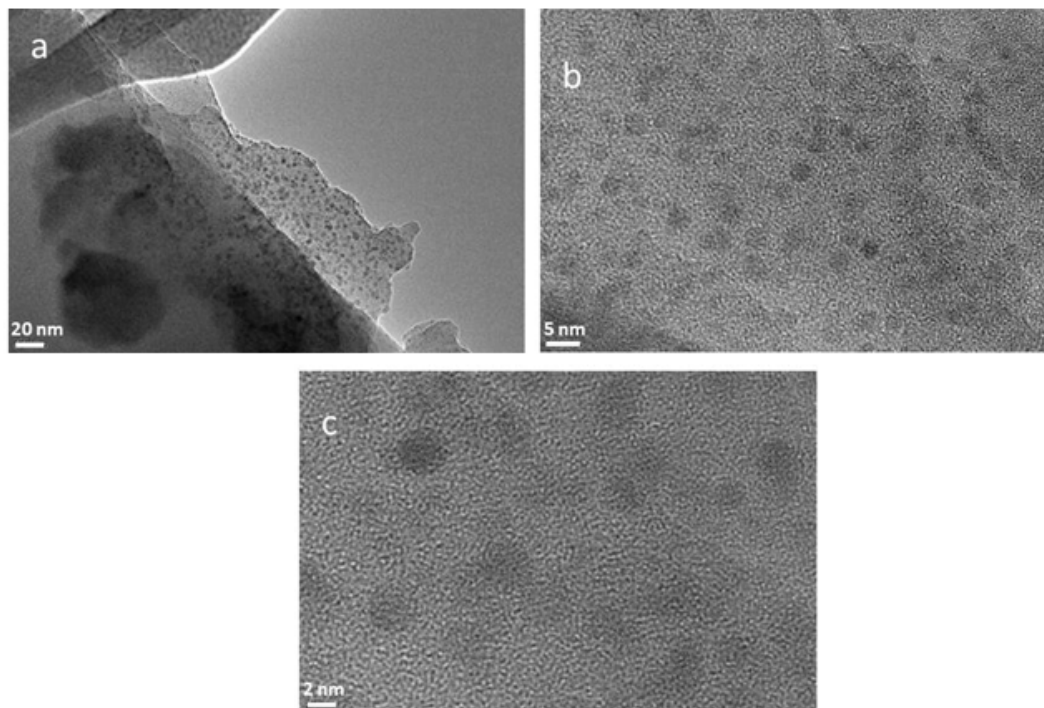


Figure 5-5. TEM images of HEMA-EMA x5 sample taken with different magnification.

The preparation procedure inhibits the nanoparticles aggregation. In agreement with a model of the nanoparticles aggregation (Rivalline et al., 2005), this signifies an undercritical number density of hydroxyls on the particles surface. A rough estimation of the surface hydroxyls in our preparation conditions can be obtained from the diagram (R, H) of titanium oxo-alkoxy species stability (Azouani et al., 2007). In fact, nucleus is formed at the critical hydrolysis ratio $H^*=1.45$ and accumulates surface hydroxyls with an increase of the water amount until $H=1.75$; than nuclei begin to stick together forming larger nanoparticles until $H=2.0$. Taking into account the nanoparticles fragmentation back to nuclei and preparation conditions with $H=2.0$, one can estimate that about $CTi(H-H^*)$ hydroxyls may remain at the particle surface after the polymerization stage. This is a huge number of hydroxyls, amounting for example in case of x10 hybrids for ~ 0.8 mol/l. Since hydroxyls are tightly bound to the nanoparticles surface, stronger than iso-propoxy ligands, they should remain in sufficient quantities even after the organic polymerization stage.

The inorganic component composed the hybrids belong to the so-called oxo-alkoxy phase, which species are characterized by well organized non-crystalline structure and possess an inorganic titanium oxide core and surface propoxy and hydroxy groups (see Roses et al., 2006). In this sense, x-ray diffraction measurements, which reflect a long-range order, would

provide structureless patterns. However, FFT analysis (Figure 5-6. Fourier transform image of HEMA-EMA x5 sample. The interplane distance depicted by dashed line is 2.72 Å. Figure 5-6) of TEM pictures of the hybrid materials revealed distinct maxima accounting for crystalline planes with lattices distances in the range between 1.75 and 3.41 Å, which correspond to crystalline anatase TiO₂. This finding shows a structural fragility of the nanoparticles (nucleus), which exhibit the phase transformation under exposition to the e-beam of TEM gun.

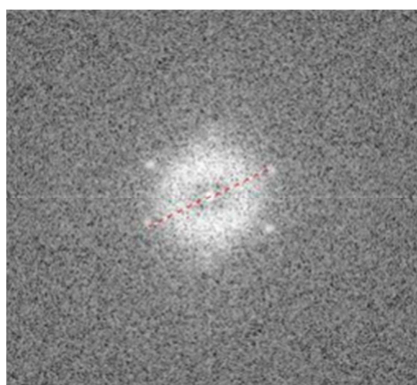


Figure 5-6. Fourier transform image of HEMA-EMA x5 sample. The interplane distance depicted by dashed line is 2.72 Å.

5.2 Conclusions

In this chapter, we applied the copolymer approach to the organic-inorganic hybrid synthesis in order to reinforce the material tolerance to environmental contaminations, leading to a poor morphology control of the inorganic component. We showed that the lifetime of the colloid increased with the addition of EMA due to its hydrophobic nature. In particular, x10 and x20 nanoparticulate colloids in EMA-contained solvents were preserved in humid environment about 3 weeks instead of several days in pure HEMA. This increase stability permitted hybrids manipulation in experimental rooms without any protection at atmospheric conditions, which is an important advantage for applicability in microstructuring technology.

Upon polymerization, both HEMA and HEMA-EMA were largely affected by the presence of the inorganic nanoparticles, which seems to reduce the monomer conversion efficiency. The nanoparticles also promote evaporation of non-polymerised organics: e.g. more volatile EMA with an increase of temperature. The future GC-MS studies may provide a fine inspection of the released species and lead to the optimization of the co-polymerization process.

The obtained HEMA and HEMA-EMA polymers look rather similar in respect of their optical transparency (required applications in photonics). However, pHEMA-EMA copolymer possessed more cracks than pure pHEMA. To improve the structural quality of the copolymer, a more detailed study of the copolymerization process will be required with a variation of EMA content, initiator nature and concentration and polymerization temperature. For example, different photoinitiators could be employed instead of AIBN (which last released N_2 , capable producing structural microcracks).

The recorded TEM micrographs evidenced unprecedentedly homogenous distribution of the smallest TiO_2 nanoparticles of the size 3.0 nm, which have been previously observed in the sol-gel synthesis at low hydrolysis ratio (Cheng et al., 2017). This new observation confirms their assignment to nucleus – the smallest structural block of TiO_2 solids. It appeared during the organic polymerization as a result of the fragmentation of larger TiO_2 units (nanoparticles), in which they are connected by relatively weak bonds. This finding is important advancement in the colloid chemistry for understanding of sol-gel mechanisms of the solid formation.

Chapter 6 : Two-photon polymerization of hybrid solutions

6.1 Introduction

The direct laser writing (DLW) technique allows the fabrication of three-dimensional structures with sub-micro resolution (Rill et al., 2008; Deubel et al., 2004.). At present, 3D printing technology has been received increasing attention and applied in the fields, including large-scale industrial prototyping, production of the tissue scaffolds, biomimetic microvascular systems, manufacture of bespoke electronic and pneumatic devices (Murphy et al., 2014). The 3D printing begins with a 3D model of the object, which is then digitized and sliced into model layers by using a dedicated software. The 3D printing system then prints 2D layers into a 3D array by adding each new layer on top of the prior layer. These layers are combined to form the final product.

One of this technique, nonlinear optical nano-stereolithography based on the two photon polymerization (2PP) of photosensitive materials, has been researched extensively by several groups (Sun et al., 2014 ; Ovsianikov et al., 2008 ; Sun et al., 2006 ; Maruo et al., 1997). The two-photon absorption is defined as the simultaneous absorption of two photons of identical or different frequencies in order to excite a molecule from one state (usually the ground state) to an energetically higher-lying state. The energy difference between these states is equal to the sum of the energies of the two photons. The two photon absorption is a second-order process and as such, its strength depends on the square of the light intensity, which permits its preferential spatial localization in the focal point of a lens. Also ultrafast lasers (femtosecond) of the near-IR spectral range are preferentially used in the 2PP process. When the beam of such laser is tightly focused into a photosensitive material, the radical polymerization process can be initiated in a small focal volume ($\sim 0.001 \mu\text{m}^3$) due to the two-photon absorption of the initiator molecules.

The fabrication of 3D photonic crystals by two-photon polymerization has been researched extensively by several groups with a high resolution not only of the microscopic spatial scale but also at the nanoscale (Wu et al., 2006). So far, femtosecond laser-induced 2PP microfabrication has been widely applied in the fields of micro/nanophotonics (Sun et al., 1999), micro-electromechanical systems (MEMS) (Sun et al., 2008), microfluidics (Wu et al., 2008), biomedical implants and microdevices (Tayalia et al. 2008; Zhang et al., 2013). Any typical and useful microstructures such as photonic crystals (Ovsianikov et al., 2008), mechanical devices and 3D hydrogels (Ovsianikov et al., 2010) have been fabricated by 2PP

microfabrication. Practically, 3D hydrogels have achieved growing research interest due to their promising biomedical applications in tissue engineering and drug delivery (Torgersen et al., 2013 ; Peppas et al., 2006).

In general, a material suitable for structuring with the DLW technique includes at least two components: (i) a monomer, or a mixture of monomers/oligomers, which will provide the final polymer and (ii) a photoinitiator, which will absorb the laser light and provide the active species that will cause the polymerization. So far, several monomer/oligomer and photoinitiator combinations have been used for this purpose. These are mostly negative photoresists such as hydrogels, acrylate materials (LaFratta et al., 2007), the epoxy-based photoresist SU-8 (Sun et al., 1999), and, more recently, hybrid materials (Farsari et al., 2009). The sol-gel organic-inorganic hybrid technology provides a very powerful tool for the development of photosensitive materials. The sol-gel materials benefit from straightforward preparation, modification, and processing. In combination with their high optical quality, post processing chemical and electrochemical inertness, good mechanical and chemical stability, they have found several applications in photonic devices such as photonic crystals and waveguides (Farsari et al., 2009 ; Zheng et al., 2019). The sol-gel materials provide the possibility of the incorporation of various functional groups by using a guest host or a side-chain main-chain strategy. One example is the incorporation of a nonlinear optical chromophore to produce an electro-optically active sol gel. Planar devices made of such materials have been extensively studied (Zhang et al., 2005). Similar sol gel systems have been used for 3D lithography (Ovsianikov et al., 2008) previous to this work.

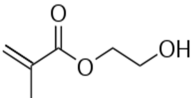
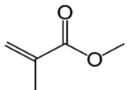
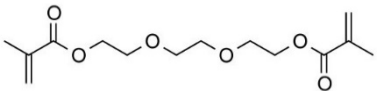
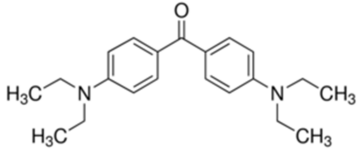
The objective of this chapter is to validate 3D structures in the prepared hybrid materials by applying the DLW (2PP) technique. The experiments have been realised in collaboration within PHC Procope project N° 37656ND (2017-2018). In course of these experiments, the laser microstructuring of HEMA and EMA monomer solutions with and without addition of cross-linker (TEGDMA) was studied. Furthermore, the microstructuring of copolymer mixtures EMA-TEGMA and HEMA-TEGMA with TiO₂ nanoparticles was investigated. At the end of this Chapter, the development stage of the microstructures fabrication will be explained following by the materials characterization.

6.2 Experiment

6.2.1 Materials

The chemicals used for the hybrids preparation are presented in Table 6-1. HEMA (97% purity, Aldrich) was preliminarily distilled in order to eliminate impurities and traces of hydroquinone (hQ), which is an inhibitor of spontaneous polymerization of the monomer. The sol particles were generated in isopropanol solutions with TTIP at concentration $C_{Ti}=0.15$ mol/l and hydrolysis ratio $H=2.0$. The solution was mixed with different the monomers quantity, after the monomer purification by distillation and the products passed the degassing stage at primary vacuum with liquid nitrogen trap and carefully stocked in a close flask.

Table 6-1. Chemicals used in experiments.

Name	Function	Structure
2-Hydroxyethyl methacrylate(HEMA)* 98% CAS Number 868-77-9	Monomer	
Ethyl methacrylate (EMA) 99% CAS Number: 97-63-2	Monomer	
Triethylene glycol demethacrylate (TEGDMA) 95% CAS Number: 109-16-0	cross-linker	
4,4'-bis(dimethylamino) benzophenone CAS Number: 90-94-8	Photo-initiator	

6.2.2 Two photo adsorption direct laser writing

In the present work, Ti:sapphire laser (Chameleon, Coherent) delivering pulses of 140 fs duration with the repetition rate of 80 MHz at wavelength of 780 nm was used. A x100 microscope objective lens (Zeiss, Plan Apochromat, NA 1.4) was used to focus the laser beam into the volume of the photosensitive material. The experimental setup and procedure has been described in details elsewhere (Serbin et al., 2004).

The experimental procedure for fabricating a 3D structure is schematically presented in Figure 6-1. (I) The laser beam is tightly focused into the volume of the material. (II) Either the focused beam or the sample move following a computer-generated pattern. (III) After the

laser writing of the structure, the sample is immersed into an appropriate developer. (IV) The freestanding structure is revealed.

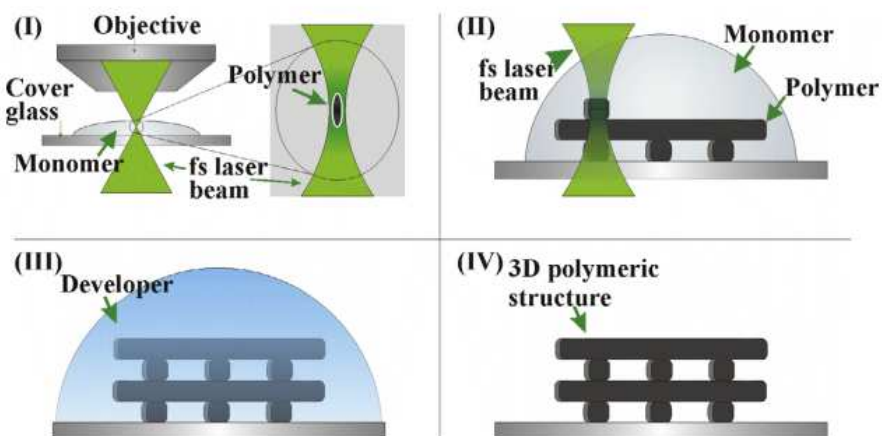


Figure 6-1. Experimental procedure: (I) beam focusing (II) laser writing (III) development (IV) completed structure.

6.3 Results

6.3.1 Monomer with and without a cross-linker

This part of the work concerns the monomer component with and without a cross-linker (TEGDMA). For all the samples, 4'-bis (dimethylamino) benzophenone is used as photoinitiator. The samples tested and the results are summarized in Table 6-2.

Table 6-2. Summary of investigated monomer samples with and without a cross-linker

Number	HEMA	EMA	TEGDMA	Photoinitiator
1	1mL			0.01g
2		1mL		0.01g
3			1mL	0.01g
4		1mL	0.1mL	0.01g
5		1mL	0.2mL	0.01g
6	1mL		0.1mL	0.01g
7	1mL		0.2mL	0.01g
8	0.5mL	0.5mL	0.1mL	0.01g

No polymer was observed in pure monomer samples 1 (HEMA) and 2 (EMA), by the microscope after DLW (2PP) processing. In contrast, a cylinder shown in Figure 6-2 was

observed in pure TEGDMA monomer (sample 3) after the processing. This structure was, however, not stable and disappeared in few seconds.

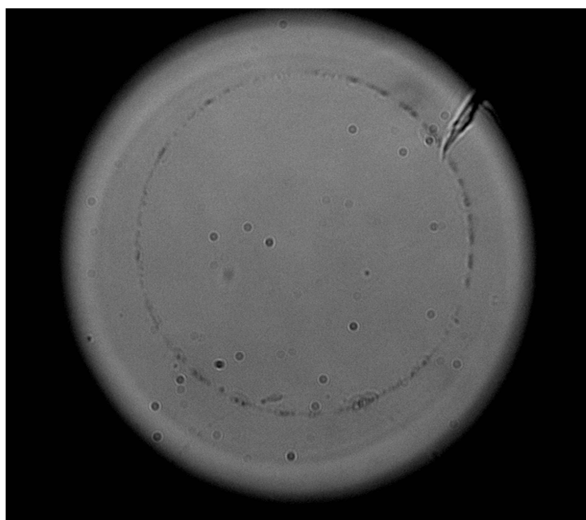


Figure 6-2. Structure obtained in TEGDMA solution (sample 3) after DLW (2PP) processing.

For the monomer mixtures, a solid cylinder depicted in Figure 6-3 could be fabricated in samples 4 and 5 (EMA + TEGDMA), however, this result was not safely reproducible. In contrast, no structures were observed in samples 6 - 8.

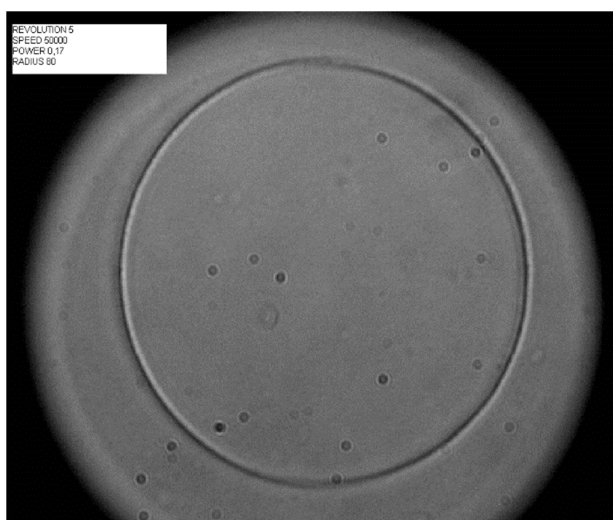


Figure 6-3. Structure obtained in EMA + TEGDMA solutions (samples 4 and 5) after DLW (2PP) processing.

In order to understand the low monomer conversion efficiency and guide future development of the materials, we analysed the photopolymerization mechanisms. In fact, the radical-mediated photopolymerization reaction consist of photoinitiation, chains propagation and chains termination reactions as depicted in Figure 6-4:

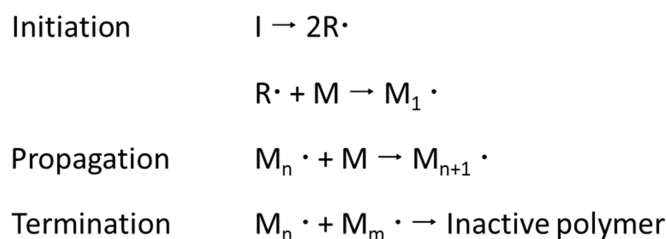


Figure 6-4. Major steps of the photopolymerization process (*I* = Photoinitiator; *R*= Reactive species; *M*= monomer).

Initiation

In our case, 4,4'-Bis(N,N-diethylamino) benzophenone (DEABP) was introduced as a photo-reactant which is a benzophenone derivative and a hydrogen abstraction-type free radical-generating photoinitiator. Figure 6-5 shows the UV-visible absorption spectra of HEMA solutions containing 0% and 1% of DEABP. The last material shows a strong absorption centered at $\lambda \approx 365$ nm. From these spectra, it is clear that the predominant absorption in the considered spectral range can be ascribed to multiphoton transitions in DEABP.

At a given location of the solution, the initiation rate, R_i is described by (Bowman et al., 2008):

$$R_i = 2f\phi\epsilon[I]I_0$$

where both the light intensity, I_0 , and initiator concentration $[I]$ may depend on spatial position within the solution, and ϵ , ϕ and f stay respectively for the initiator molar absorptivity, quantum yield and efficiency. In particular, it is well recognized that the initiator efficiency changes along the reaction time with primary radicals less readily escaping the solvent cage and tending to recombine into nonreactive products. Despite of this effect, the

initiation reaction is generally the most resolved one being not appreciably affected by mass and heat transfer limitations imposed by the crosslinking photopolymerization processes. By consequence, we consider that the photoinitiation was not the main cause of poor photopolymerization effectiveness.

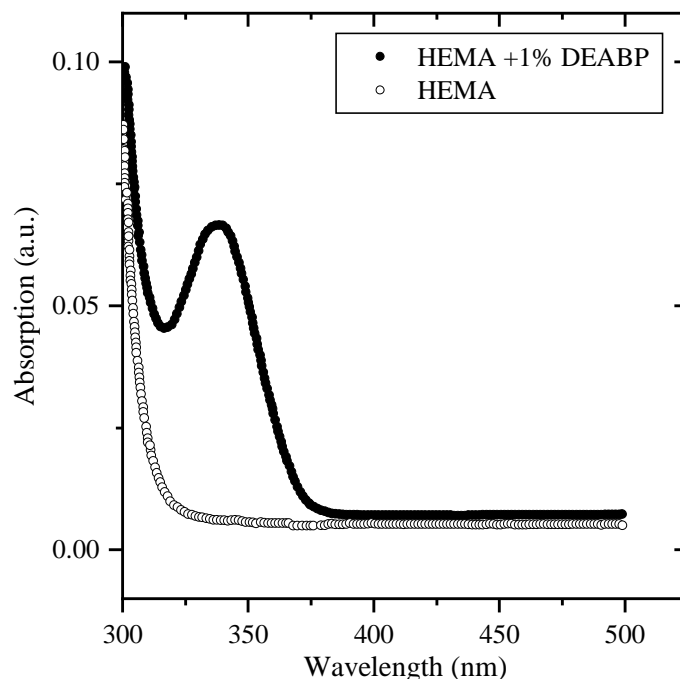


Figure 6-5. Absorption spectra of pure HEMA and HEMA with 1% DEABP.

Chains propagation

The polymer chains propagation generally involves radical species growth by the radical addition to C=C double bond, generating a new radical at the end of the polymer chain. This bimolecular reaction between the radical and the double bond is generally assumed to be chain-length independent, though there were clear indications that the oligomer/polymer chain length below 10 - 50 does have a significant effect on the degrees of polymerization. In overall, the propagation reaction rate is generally written as:

$$R_p = k_p [M][M_n \cdot]$$

where k_p represents the propagation rate constant, $[M]$ represents the double bond concentration, and $[M_n \cdot]$ represents the total propagating radical concentration. The viscosity

of HEMA is 6.1 cP at 25°C and it is less viscous compared to the resins used (Wang et al., 2007). At a given location with light irradiation, the radical diffusion decreases the value of $[M_n^\bullet]$. Consequently, oligomers formation in our experiments was promoted by the viscosity, even in our most successful processing (Figure 6-3). An increase of the solution viscosity has been proposed to enhance the monomer conversion and promote the polymerization process (Wang et al., 2007). In agreement, by using high-pressure-ramp-induced process, high purity organic materials of pHEMA have been realized (Evlyukhin et al., 2015). Besides, using hybrid materials with an increased bulk viscosity due to the presence of the inorganic component could be another solution (Evlyukhin et al., 2018). This will be described in the following section.

6.3.2 Hybrid materials

In order to obtain hybrid samples, the TiO₂ nanoparticles of the equivalent concentration x10 (1.5 mol/l) were added to different monomer solutions as depicted in Table 6-3. In all samples, 4 4'-bis(dimethylamino) benzophenone is used as photoinitiator. The liquid mixtures were dropped onto the borosilicate glass plates and kept in dark during 12 hours. This procedure was applied to induce association of nanoparticles in gel structures. The appearance of gel increases bulk viscosity of the medium, which slowed down the diffusion of polymerized species and reinforces the produced structures.

Table 6-3. Summary of structured hybrid materials.

Number	HEMA ml	EMA ml	TiO ₂ mol/l	TEGDMA ml	Photoinitiator g
1	1	-	1.5	-	0.01
2	-	1	1.5	-	0.01
3	-		1.5	1	0.01
4	-	1	1.5	0.1	0.01
5	-	1	1.5	0.2	0.01
6	1	-	1.5	0.1	0.01
7	1	-	1.5	0.2	0.01
8	0.5	0.5	3.0	0.1	0.01

We noticed that gels were conveniently formed in samples 1, 2, 7. Samples 4 and 5 of HEMA-EMA form gels inside the bottles almost immediately after addition of the photo-

initiator dissolved in isopropanol. In contrast, fast condensation was observed in samples 3 and 6 prohibiting gel formation. Finally, the gelation of nanoparticles competed with precipitation in sample 8, forming gel with the white appearance. For all these samples, solid structures of 'woodpile' type were observed in situ before the development stage (Figure 6-6).

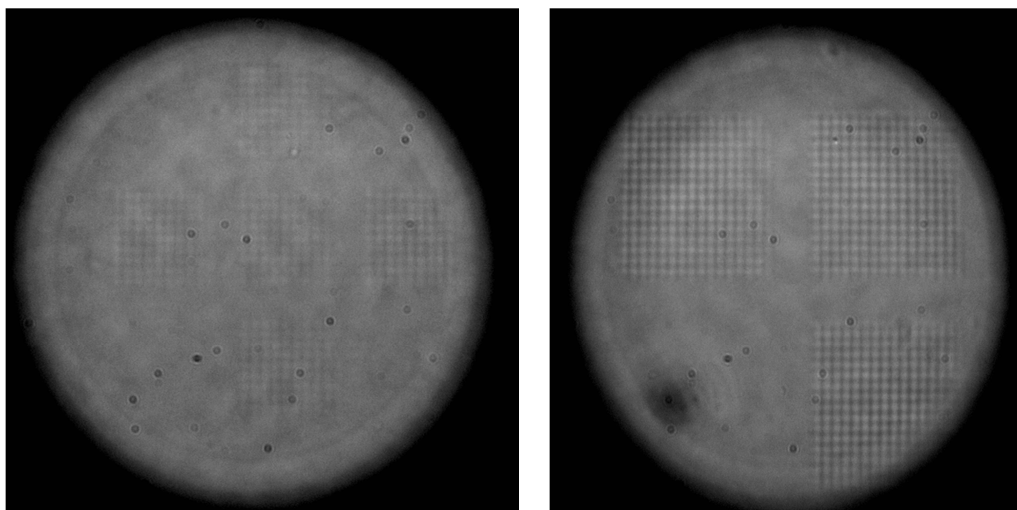


Figure 6-6. View of 2PP laser structuring in sample 1.

6.3.3 Development and characterization

Oleic acid and acetyl acetone are known to be able effectively dissolving monomers without destroying the polymer structure. The development process by using the above chemicals was controlled in-situ by optic microscope. Three samples HEMA X5, X10, X20 were developed in oleic acid during 3 days. This development was not perfect. In fact, in HEMA X20 the structure was removed from the plate being not completely purified from non-polymerised material and in HEMA x5 and x10, the structure remained on the plate being very fragile (soft). Moreover, acids are known to dissolve inorganics, thus converting organic-iniorganic to pure organic material. In contrast, the development process with acetyl acetone can be achieved in 3 hours by preserving the inorganic component.

The developed structures were visualised with optical microscope and SEM. An example of SEM images of structures in sample 4 is shown in Figure 6-7. The dark agglomerate are 'burning parts' due to the local overheating induced by absorbed laser photons. The white line of a length 60 μm is a part of the presumed woodpile structure

recorded by laser. The complete stable 3D woodpile structure was not observed. Figure 6-8 shows a side view of a part of the segmented polymerized line. Its thickness 3 μm was smaller than the vertical z-spacing between recorded lines of 5 μm , which explains why the complete woodpile structure was not obtained.

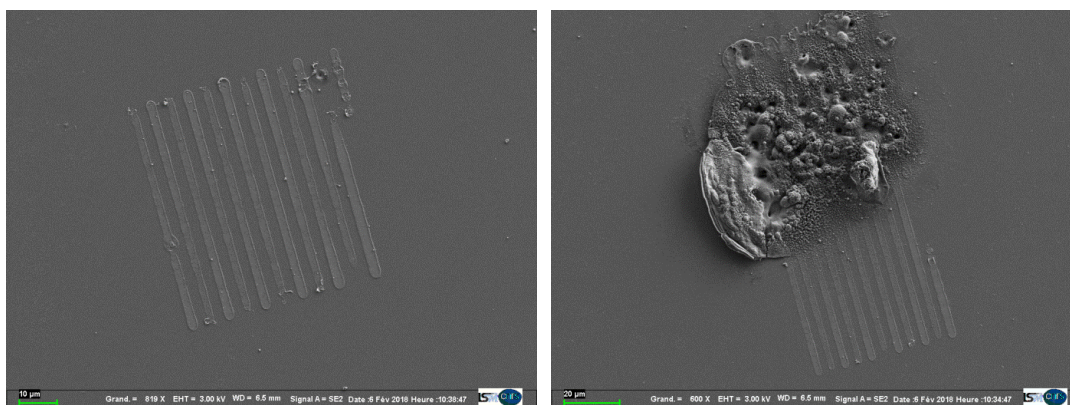


Figure 6-7. SEM image of segmented woodpile obtained in sample 4 (top view).



Figure 6-8. SEM image of segmented line in Fig 6-7 (side view 45°)

6.4 Conclusions

In this chapter, the availability of the obtained nanoparticulate organic-inorganic hybrid materials was investigated by applying DLW (2PP) processing. Different monomers (HEMA and EMA) with and without cross-linker (TEGDMA) were analysed following by the mixtures EMA-TEGMA and HEMA-TEGMA with TiO_2 nanoparticles. The laser structuring was not successful in pure monomer organics, which was explained a low solution viscosity

leading to the structures detachment by the convective fluid movement during the laser processing. In contrast, the structuring was observed in situ in the hybrid solutions containing TiO_2 nanoparticles of a concentration $\times 5$ and larger. Although solid 3D woodpile structures could not be developed in these preliminary experiments, the feasibility of 2PP laser structuring was demonstrated in the nanoparticulate hybrids. Acetyl acetone appered to be most suitable chemical for the development process, which preserves the material composition.

General conclusions

This work is a continuation of previous studies devoted to the elaboration of the nanoparticulate TiO₂-based organic-inorganic hybrid materials. In course of this work, the elaboration process was inspired from a concept of Kameneva et al. (2005) and Gorbovyi (2012) and technical/methodological improvements were introduced. This concerns AIBN purification by recrystallization: thanks to it, the behavior of the initiator was more stable eliminating uncertainties related to aging and deterioration of the reagent and thus contributing to improvement of its reactivity. Furthermore, an importance of HEMA purification by distillation was proved, which led to a better reproductivity of polymerization, especially in the field of high pressure-induced processing of polymers (see Evlyukhin et al., 2015). Another important point concerned the degassing of samples, a process step performed before polymerization, which led to an increase in transparency of big samples and reduced the appearance of bubbles inside polymers. Finally, a somewhat minor, but an important point was the deeper investigation of the solvent exchange stage of the material elaboration, which can affect reproductibility of the material properties.

We experimentally analysed the material composition during this stage performed at different temperatures, and the results were presented in Chapter 4 of this manuscript. In this study, probes of the organic and hybrid solutions were taken at regular time intervals during the solvent exchange and injected in a dedicated TGA-DSC / GC-MS / FTIR coupled installation. The variation on isopropanol and monomer concentrations provided us the better understanding of the compositional variation with time and temperature and influence of the inorganic (TiO₂) nanoparticles on the solvent release, decomposition and products. This will also allow us to know the material composition after the polymerization stage which will be almost frozen because of their much slower diffusion and release in the soft matter compared with liquids. Between major results, we obtained that:

- Isopropanol remains in the organic solutions in a wide temperature range above the boiling point, suggesting the azeotropic HEMA-isopropanol mixture.
- Major decomposition products of HEMA-isopropanol solvent are 2-methyl propionic acid and 2-hydroxy ethyl acetate and methyl methacrylate, which last was also revealed as a synthesis impurity.

General conclusions

- The decomposition products of HEMA appear in the hybrids at relatively low temperatures, which suggest a decrease of the decomposition onset in presence of the inorganic nanoparticles. Their release was found strongly affected by the presence of TiO₂ nanoparticles, which was explained by their catalytic effect.
- The inorganic nanoparticles retain surface isopropanol in a broad temperature range up to 235 °C (organics decomposition temperature) in quantities proportional to the nanoparticles concentration. Its presence may significantly affect the material electronic properties and, in particular, on the charge separation efficiency and charge storage capacity, key factors determining functional response for photonic applications (laser microstructuring, waveguides).

The polymerisation stage strongly modified the released products, which was explained by their trapping in the polymer chains and slow exit via diffusion process characteristic of solids.

The further experiments addressing the stage of organic polymerization in Chapter V showed an important presence of isopropanol, which has to be taken into account for understanding of the material composition and functional properties. The presence of the inorganic nanoparticles alters polymerization kinetics shifting the polymerization exothermic peak to lower temperatures and reducing the total released heat of the process, which was correlated with the reduction of the monomer conversion (polymerization efficiency). The nanoparticles may trigger the polymerization process as well as stop it at the surface. More experiments are required to elucidate possible mechanism.

We applied the copolymer approach to the organic-inorganic hybrid synthesis in order to reinforce the material tolerance to environmental contaminations, leading to a poor morphology control of the inorganic component. We showed that the lifetime of the colloid increased with the addition of EMA due to its hydrophobic nature. In particular, x10 and x20 nanoparticulate colloids in EMA-contained solvents were preserved in humid environment about 3 weeks instead of several days in pure HEMA. This increase stability permitted hybrids manipulation in experimental rooms without any protection at atmospheric conditions, which is an important advantage for applicability in microstructuring technology.

The recorded TEM micrographs evidenced unprecedentedly homogenous distribution of the smallest TiO₂ nanoparticles of the size 3.0 nm, which have been previously observed in the sol-gel synthesis at low hydrolysis ratios. This new observation confirms their assignment to nucleus – the smallest structural block of TiO₂ solids. It appeared during the organic polymerization as a result of the fragmentation of larger TiO₂ units (nanoparticles), in which they are connected by relatively weak bonds. This finding is important advancement in the colloid chemistry for understanding of sol-gel mechanisms of the solid formation.

We studied availability of the obtained nanoparticulate organic-inorganic hybrid materials for micromachining via DLW (2PP) processing. Pure HEMA and EMA monomers with and without TEGDMA cross-linker as well as mixtures EMA-TEGMA and HEMA-TEGMA with TiO₂ nanoparticles were analysed. The realization of laser structuring was not successful in pure monomer organics, which was explained a low solution viscosity leading to the structures detachment by the convective fluid movement during the laser processing. In contrast, the structuring was observed in situ in the hybrid solutions containing TiO₂ nanoparticles of a concentration x5 and larger ($C_{Ti} \geq 0.75$ mol/l). Although solid 3D woodpile structures could not be developed in these preliminary experiments, the feasibility of 2PP laser structuring was demonstrated in the nanoparticulate hybrids. Acetyl acetone appeared to be most suitable chemical for the development process, which preserves the material composition.

Perspectives

Our measurements showed that the main part of the significant solvent exchange (mass release) takes place at the same time, which does not depend on the presence and concentration of inorganic nanoparticles. However, this exchange is not complete and the remaining isopropanol may still affect functional properties of the prepared hybrids. Therefore, quantitative measurements of the isopropanol content in the hybrid solutions at different temperatures has to be further performed as well as the study of its influence on the material functional properties.

The kinetic study of the released solvent and decomposition products in presence of nanoparticles could help to further understanding of the reaction mechanism and optimized the elaboration process. A more detailed polymerization kinetic analysis that could give light

General conclusions

to the mechanisms behind the influence of nanoparticles could be achieved by applying the kinetic analysis (see e.g. Achilias *et al.*, 2007) employing TGA-DSC in isothermal conditions. The study of different HEMA-isopropanol mixtures could be important to conduct in order to determine homogenous or heterogenous nature of the azeotrope.

The obtained HEMA and HEMA-EMA polymers look rather similar in respect of their optical transparency (required applications in photonics). However, pHEMA-EMA copolymer possessed more cracks than pure pHEMA. To improve the structural quality of the copolymer, a more detailed study of the copolymerization process will be required with a variation of EMA content, initiator nature and concentration and polymerization temperature.

References

- Alberti, G.; Constantino, U.; Allulli, S. and Tomassinni, N. *Crystalline Zr(R-PO₃)₂ and Zr(R-OPO₃)₂ compounds (R = organic radical): A new class of materials having layered structure of the zirconium phosphate type*, **1978**, J. Inorg. Nucl. Chem., vol. 40, 1113 -1117.
- Achilias, D.S. and Kiparissides C., *On the validity of the steady-state approximations in high conversion diffusion-controlled free-radical copolymerization reactions*, **1994**, Polymer, vol. 8, 1714-1721.
- Achilias, D.S. *A Review of Modeling of Diffusion Controlled Polymerization Reactions*, **2007**, Macromol. Theory Simul., vol. 16, 319-347.
- Achilias, D.S.; Siafaka, P.I. *Polymerization kinetics of poly(2-hydroxyethyl methacrylate) hydrogels and nanocomposite materials*, **2017**, Processes, vol. 5(2), 21.
- Amberg-Schawab,S; Hoffmann, M; Bader,H; Gessler,M; *Inorganic-organic polymers with barrier properties for water vapor, oxygen and flavors*, **1998**, Sol-gel Sci.Technol., vol. 13, 141-146.
- Armagero, W.L.F.; Lin Li Chan, C.; *Purification of laboratory chemicals*, 7th edition, **2012**, Chapter 1, pp. 8-14.
- Azouani, R.; Soloviev, A.; Benmami, M.; Chhor, K.; Bocquet, J.F. and Kanaev A.; *Stability and Growth of Titanium-oxo-alkoxy Ti_xO_y(OiPr)_z Clusters*, **2007**, J. Phys. Chem., vol. 111, 16243-16248.
- Azouani R., Michau A., Hassouni K., Chhor K., Bocquet J.-F., Vignes J.-L., Kanaev A., *Elaboration of pure and doped TiO₂ nanoparticles in sol-gel reactor with turbulent micromixing: application to nanocoatings and photocatalysis*, **2010**, Chemical Engineering Research & Design, 88, 1123-1130.
- Bałdyga, J.; Pohorecki, R., *Turbulent micromixing in chemical reactors - a review*, **1995**, The Chem. Eng. J., vol. 58, 183-195.
- Barge, L.M.; Doloboff, I.J.; White, L.M.; Stucky, G.D.; Russell M.J. and Kanik I. *Characterization of Iron–Phosphate–Silicate Chemical Garden Structures*, **2012**, Langmuir, vol. 28, 3714-3721.

References

- Beck, J.S.; Vartuli, J.C.; Roth, W.J; Leonowicz , M.E.; Kresge, C.T.; Schmitt, K.D.; Chu C.T.W; Olson , D.H.; Sheppard, E.W.; McCullen, S.B.; Higging, J.B.;Schlenker J.L.; *A new family of mesoporous molecular sieves prepared with liquid crystal templates*, **1992**, J. Am. Chem. Soc., vol. 114, 10834-10843.
- Bityurin, N.; Znaidi, L. and Kanaev A. *Laser-induced absorption in titanium oxide based gels*. **2003**, Chem. Phys. Lett., vol. 374, 95-99.
- Blanco-Andujar, C.;Ortega, D.; Pankhurstab, Q.A. and Thanh N.T.K *Elucidating the morphological and structural evolution of iron oxide nanoparticles formed by sodium carbonate in aqueous medium*, **2012**, J. Mater. Chem., vol. 22, 124998-12506.
- Blumstein, A. *Etude des polymerisations en couches adsorbee*, **1961**, I. Bull. Soc. Chim. Fr., vol. 98, 899-906
- Bonderer, L.J.; Stdart, A.R. and Gaukler, L.J. *Bioinspired design and assembly of platelet reinforced polymer films*. **2008**, Science, vol. 319, 1069-1073.
- Bowman, C.N.; Kloxin, C.J. *Toward an enhanced understanding and implementation of photopolymerization reactions*, **2008**, AIChE J., vol. 54, 2775-2795.
- Bozzi A, Yuranova T, Guasaquillo I, Laub D, Kiwi J. *Self-cleaning of modified cotton textiles by TiO₂ at low temperatures under daylight irradiation*. **2005** J. Photochem. Photobiol. A, vol. 174, 156-164.
- Bradley, D.C. *A Structural Theory for Metal Alkoxide Polymers*. **1958** Nature, vol 182, 1211-1214.
- Brinker, C.J. and Scherer, G.W. *Sol-gel Science: The Physics and Chemistry of Sol-gel Processing*, **1990**, Academic Press Inc.
- Chen, J.; Liu, M.; Zhang, L.; Zhang, J. and Jin, L. *Application of Nano TiO₂ towards Polluted Water Treatment Combined with Electro-Photochemical*, **2003**, Method. Water Res., vol. 37, 3815-3820.
- Cheng, K.; Chhor, K. and Kanaev, A. *Solvent effect on nucleation-growth of titanium-oxo-alkoxy nanoparticles*, **2017**, Chem. Phys. Lett., vol. 672, 119-123.
- Chiu, W.M.; Zhang, Y.S.; Tsai, P.A.; Wu, J.H.; *Chatacterization of antireflective coatings on poly(methyl methacrylate) subtrate by different process parameters*, **2013**, J. Appl. Polym. Sci., vol. 129, 2411-2417.

- Choi Y.J., Seeley Z., Bandyopadhyay A., Bose S., Akbar S.A., *Aluminum-doped TiO₂ nano powders for gas sensors*, **2007**, Sens. and Actuators B: Chem., vol. 124, 111-117.
- Chou, T.P.; Chandrasekaran, C. and Cao, G.Z. *Sol-gel derived hybrid coatings for corrosion protection*, **2003**, J. Sol-gel Sci. Technol., vol. 26, 321-327.
- Choujaa, H.; Johnson, A.L.; Kociok-Köhn, G. and Molloy K.C. *Synthesis of heterobimetallic tungsten acetylacetonate/alkoxide complexes and their application as molecular precursors to metal tungstates*, **2013**, Polyhedron, vol. 59, 85-90.
- Corriu, R. and Anh N.T. *Molecular Chemistry of Sol-Gel Derived Nanomaterials*, **2009**, John Wiley & Sons, Ltd.
- Danks, A.E., Hall, S.R. and Schnepf, Z. *The evolution of 'sol-gel' chemistry as a technique for materials synthesis*, **2016**, Mat Horiz., vol 3, 91-112.
- Daude, N.; Gout, C. and Jouanin C. *Electronic band structure of titanium dioxide*, **1977**, Physical review B, vol. 15, 3229-3235.
- De Souza Machado, R. *Sintese e caracterizacao de microesferas porosas de Poli(Estireno-co-divinilbenzeno-co-metacrilato de glicida)* **2008**, Universidade Federal do Rio Grande do Sul.
- Deubel, M.; von Freymann, G.; Wegener, M.; Pereira, S.; Busch, K.; Soukoulis, C.M. *Direct laser writing of three-dimensional photonic-crystal templates for telecommunications*, **2004**, Nat. Mater., vol. 3, 444-447.
- Ebewel, R. "*Polymer Science and technology*", **2000**, CRC press, Boca Raton New York.
- Evlyukhin, E.; Muser, L.; Traore, M.; Perruchot, Ch.; Zerr, A.; Kanaev, A. "A new route for high-purity organic materials: high-pressure-ramp-induced ultrafast polymerization of 2-(hydroxyethyl) methacrylate", Sci. Reports, vol. 5 (2015) 18244.
- Evlyukhin, E.; Muser, L.; Diaz Gomez, A.P.; Traore, M.; Brinza, O.; Zerr, A. and Kanaev A. *Synthesis of organic-inorganic hybrids via high-pressure-ramp process: Effect of inorganic nanoparticles loading on structural and photochromic properties*, **2018**, Nanoscale, vol. 10, 22293-22301.
- Farsari, M.; Chichkov, B.N. *Two-photon fabrication*, **2009**, Nature Photonics, vol. 3, 450-452.

References

- Gieseking, J.E., *The mechanism of cation exchange in the montmorillonite-beidellite-nontronite type of clay minerals*, **1939**, Soil Sci., vol. 47, 1-13.
- Gomez-Romero, P and Lira-Cantu, M. *Hybrid organic-inorganic electrodes: the molecular material formed between polypyrrolle and the phosphomolybdate anion*. **1997**, Adv, Mater., vol. 9, 144-147.
- Gómez-Romero P. *Hybrid Organic–Inorganic Materials—In Search of Synergic Activity*, **2001**, Adv. Mat., vol 13-3, 163-174.
- González-Henríquez, C.M.; Pizarro, G.C.; Sarabia-Vallejos, M.A.; Terraza C.A. and López-Cabaña, Z.E. *In situ-preparation and characterization of silver-HEMA/PEGDA hydrogel matrix nanocomposites: Silver inclusion studies into hydrogel matrix*, **2014**, Arabian J. Chem., In Press Corrected proof.
- Gorbovyi, P.; Uklein, A.; Tieng, S.; Brinza, O.; Traore, M.; Chhor, K.; Museur L., Kanaev A. *Novel nanostructured pHEMA–TiO₂ hybrid materials with efficient light-induced charge separation*, **2011**, Nanoscale, vol. 3(4), 1807-1812.
- Gorbovyi, P. *Elaboration des matereiaux photosensibles organiques-inorganiques pour des applications en photonique*, **2012**, PhD Thesis, University Paris 13, France.
- Guglielmi, M. and Carturan, G. *Precursors for sol gel precursors*, **1988**, J. Non Cryst Sol., vol. 100, 16-30.
- Hagenmuller, P.; Portier, J.; Barbe, B, and Bouclier, P.; Z.Anorg. Allg. Chem., **1967**, vol. 355, 209-218.
- Hajji, P.;David, L.;Gerard, J.F.; Pascault J.P. and Vigier, G. *Synthesis, structure, and morphology of polymer–silica hybrid nanocomposites based on hydroxyethyl methacrylate*, **1999**, Polymer physics, vol. 37, 3172-3187.
- Hrelescu,C.; Stehr,J.; Ringler, M.; Sperling,R.A.; Parak,W.J.; Klar,T.A. and Feldmann J. *DNA melting in gold nanostove clusters*, **2010**, J. Phys. Chem., vol 114, 7401-7411.
- Iller, K.R., *Method of esterefyng the surface of a Silica substrate having a reactive Silanol and a product thereof*, **1953**, US Patent Office, Patented Oct. 27, 1953.
- Innocenzi, P.; Lebeau, B.; *Organic-inorganic hybrid materials for non linear optics*, **2005**, J. Mater. Chem., vol. 15, 3821-3831.

- Jittiarporn,P.;Badilescu, S.;Al Sawafta, M.N.;Sikong,L. and Truong, V.V. *Electrochromic properties of sol–gel prepared hybrid transition metal oxides – A short review*, **2017** Journal of Science: Advanced Materials and Devices, vol. 2, 286-300.
- Judeinstein, P., Sanchez, C.J. *Investigation of New Ion-Conducting ORMOLYTES: Structure and Properties*, **1996**, Mater. Chem., vol 6, 711-715.
- Kalfa, O.M.; Yalcinkaya, O.; Türker, A.R. *Synthesis of Nano B₂O₃/TiO₂ composite material as a new solid phase extractor and its application to preconcentration and separation of cadmium*, **2009**, J. Hazard. Mater., vol. 166, 455-461.
- Kameneva, O.; Kuznestov, A.I.; Smirnova, L. A.; Rozes, L.; Sanchez, C.; Alexandrov,A; Bityurin, N; Chhor,K. and Kanaev, A.; *New photoactive hybrid organic–inorganic materials based on titanium-oxo-PHEMA nanocomposites exhibiting mixed valence properties*, **2005**, J. Mater Chem., vol. 15, 3380-3383.
- Kameneva O., Kuznetsov A., Rozes L., Sanchez C., Bityurin N., Kanaev A.,*Extinction measurements of light-induced Ti³⁺ centers in titanium oxide gels and gel-based organic-inorganic hybrid materials”*, **2006**, Chem. Phys. Letts., vol. 429, 523-527.
- Kanatzidis,M.G.; Tonge,L.M.; Marks,T.J.;Marcy, H.O., and Kannewurf, C.R., *In situ intercalative polymerization of pyrrole in FeOCl: a new class of layered, conducting polymer-inorganic hybrid materials*, **1987**, J. Amer. Chem. Soc., vol. 109, 3797-3799.
- Kickelbick , G, *In introduction to hybrid material*, **2007**; Wiley-VCH, pp. 1-48.
- Kickelbick , G, *Hybrid materials- Past, Present and Future*, **2014**, Hybrid Material, vol 1, 39-51.
- Kuo,CN; Chen, HF; Lin JN; Wan, BZ; *Nano-gold supported on TiO₂ coated glass-fiber for removing toxic CO gas from air*, **2007**, Catal Today, vol. 122, 270-276.
- Kuznetsov,A.I.; Kameneva,O.; Bityurin, N.; Rozes,L.; Sanchez,C. and Kanaev, A.; *Laser-induced photopatterning of organic–inorganic TiO₂-based hybrid materials with tunable interfacial electron transfer*, **2009**, Phys. Chem. Chem. Phys., vol. 11, 1248-1257.
- LaFratta, C.N. ; Fourkas, J.T. ; Baldacchini, T. ; Farrer, R.A. *Multiphoton Fabrication*, **2007**, Angew. Chemie Int. Ed., vol. 46, 6238–6258.

References

- Levy, D.; *Photocromic sol-gel materials*, **1997**, Chem, Mater Vol-9: 2666-2670.
- Li,Q;Mahendra,S.; Lyon,D.Y.; Brunet, L.; Liga,M.V.; Li,D. and Alvarez,P.J.; *Antimicrobial Nanomaterials for Water Disinfection and Microbial Control: Potential Applications and Implications*, **2008**, Wat. Res., vol. 42-18, 4591-4602.
- Liu Y.; Wang C.; Wei Y.; Zhu L.; Li D.; Jiang J.S.; Markovic N.M.; Stamenkovic V.R., Sun S. *Surfactant-induced postsynthetic modulation of Pd nanoparticle crystallinity*, **2011**, Nano Lett., vol. 11, 1614-1617.
- Livage, J.;Henry,M.and Sanchez, C. *Sol-gel chemistry of transition metal oxides*, **1988**, Progress in Solid State Chemistry, vol. 18, 259-341.
- Mabilleau,G; Cincu, C; Basle,M.F and Chappard, D.; *Polymerization of 2 (hydroxyethyl)methacrylate by two different initiator/accelerator systems: a Raman spectroscopic monitoring*, **2008**, J. Raman Spectrosc, vol. 39, 767-771.
- MacEwan D.M.C, *Identification of the montmorillonite group of minerals by X-rays*. **1944**, Nature, vol. 154, 577-578
- Macwan, D.P.; Dave, P.N. and Chaturvedi S. *A review on nano-TiO₂ sol-gel type syntheses and its applications*, **2011**, J Mater Sci, vol. 46, 3669-3686.
- Maruo, S.; Nakamura, O.; Kawata, S. *Three-dimensional microfabrication with two-photon-absorbed photopolymerization*, 1997, Opt. Lett., vol. 22, 132.
- Meen, T.H.; Water, W.; Chen, W.R.; Chao, S.M.; Ji, L.W.; Huang C.J. *Application of TiO₂ nano-particles on the electrode of dye-sensitized solar cells*, **2009**, J. Phys. Chem. Solids, vol. 70, 472-476.
- Michelsen, V.B.; Moe, G.; Skalevik, R.; Jense, E. and Lygre,H. *Quantification of organic eluates from polymerized resin-based dental restorative materials by use of GC/MS*, **2007**, J. Chromatogr. B, vol. 850, 83-91.
- Michelsen, V.B.; Moe, G.; Strøm, M.B; Jense, E. and Lygre H. *Quantitative analysis of TEGDMA and HEMA eluted into saliva from two dental composites by use of GC/MS and tailor-made internal standards*, **2008**, Dental Materials, vol 24, 724-731.
- Miyata, S. and Kimura, T. *Synthesis of new hydrotalcite-like compounds and their physicochemical properties*. **1973**, Chem. Lett. 843-848.

- Moad, G. and Solomon, D.H. “*The chemistry of radical polymerization*”, **2006**, 2nd fully revised edition, Elsevier, The Netherlands.
- Mohapatra, R.; Swain, A.K.; Mohapatra, R.; Rana, P.K. and Sahoo, P.K. *Poly(2-Hydroxy Ethyl Methacrylate-co-Acrylic Acid) as Novel Biodegradable Macroporous Hydrogel*, **2005**, *Polymers & Polymer Composites*, vol. 13, 807-814.
- Montheard, J.P.; Chatzopoulos, M. and Chappard, D. *2-Hydroxyethyl Methacrylate (HEMA): Chemical Properties and Applications in Biomedical Fields*. **1992**, *J. Macromol. Sci., Part C*, vol. 32, 1-34.
- Monticone, S.; Tufeu, R.; Kanaev, A.V.; Scolan E. and Sanchez C. *Quantum size effect in TiO₂ nanoparticles : does it exist?*, **2000**, *Appl. Surf. Sci.*, vol. 162-163, 565-570.
- Moran, P.D.; Bowmaker, G.A.; Cooney, R.P.; Finnie, K.S.; Bartlett, J.R. and Woolfrey, J.L.; *Vibrational Spectra and Molecular Association of Titanium Tetraisopropoxide*, **1998**, *Inorg. Chem*, vol. 37(11), 2741-2748.
- Muneer M. Ba-Abbad, Abdul Amir H. Kadhum, Abu Bakar Mohamad, Mohd S. Takriff, Kamaruzzaman Sopian. *Synthesis and Catalytic Activity of TiO₂ Nanoparticles for Photochemical Oxidation of Concentrated Chlorophenols under Direct Solar Radiation*, **2012**, *Int. J. Electrochem. Sci.*, vol 7, 4871-4888.
- Murphy, S.V.; Atala, A. *3D bioprinting of tissues and organs*, **2014**, *Nat. Biotechnol.*, vol. 32, 773–785.
- Musetha, P. L.; Revaprasadu, N.; Kolawole, G. A.; Pullabhotla, Rajasekhar V S R; Ramasamy, K. and O'Brien, P. *Homoleptic single molecular precursors for the deposition of platinum and palladium chalcogenide thin films*. **2010**, *Thin Solid Films*, vol. 519, 197-202.
- Nakamoto, K., **2009**, *Infrared and Raman Spectra of Inorganic and Coordination Compounds Part A*, Wiley.
- Novak B.M. "Living" titanium(IV) catalyzed coordination polymerizations of isocyanates, **1991**, *J. Amer. Chem. Soc.*, vol. 113, 5065-5066.
- Ochs M.; Carregal-Romero S.; Rejman J.; Braeckmans K.; De Smedt S.C. and Parak W.J. *Light-addressable capsules as caged compound matrix for controlled triggering of cytosolic reactions*. **2013**, *Angew. Chem. Int. Ed. Engl.*, vol. 52, 695-699.

References

- Odian, G. *Principles of polymerization*, **2004**, Fourth edition, Wiley interscience.
- Ovsianikov, A.; Viertl, J.; Chichkov, B.; Oubaha, M.; MacCraith, B.; Sakellari, I.; Giakoumaki, A.; Gray, D.; Vamvakaki, M.; Farsari, M.; Fotakis, C. *Ultra-Low Shrinkage Hybrid Photosensitive Material for Two-Photon Polymerization Microfabrication*, **2008**, ACS Nano, vol. 2, 2257–2262.
- Ovsianikov, A.; Gruene, M.; Pflaum, M.; Koch, L.; Maiorana, F.; Wilhelmi, M.; Haverich, A.; Chichkov, B. *Laser printing of cells into 3D scaffolds*, **2010**, Biofabrication., vol. 2, 014104.
- Pazik, R.; Tekoriute, R.; Hakansson, S.; Wiglusz, R.; Strek, W.; Siesenbaeva, G.A.; Gun'ko, Y.K. and Kessler, V.G, *Precursor and solvent effects in the non-hydrolytic synthesis of complex oxide nanoparticles for bio-imaging applications by ether elimination (Bradley) reaction*, **2009**, Chem. Eur. J., vol. 15, 6820-6826.
- Peppas, N.A.; Hilt, J.Z.; Khademhosseini, A.; Langer, R. *Hydrogels in Biology and Medicine: From Molecular Principles to Bionanotechnology*, **2006**, Adv. Mater., vol. 18, 1345–1360.
- Phattepur, H.; Siddaiah, G.B. and Ganganagappa N. *Synthesis and Characterisation of Mesoporous TiO₂ Nanoparticles by Novel Surfactant Assisted Sol-gel Method for the Degradation of Organic Compounds*, **2019**, Periodica Polytechnica Chemical Engineering, vol. 63, 85-95.
- Pierre, A.C., *Introduction to Sol-Gel Processing*, **1998**, Kluwer Academic Publishers.
- Pol, S.V.; Pol, V.G.; Kessler, V. G.; Seisenbaeva, G.A.; Sung, M.; Asaid, S. and Gedanken A. *The Effect of a Magnetic Field on a RAPET (Reaction under Autogenic Pressure at Elevated Temperature) of MoO(OMe)₄: Fabrication of MoO₂ Nanoparticles Coated with Carbon or Separated MoO₂ and Carbon Particles*, **2004**, J. Phys. Chem. B, vol. 108, 6322-6327.
- Pucci, A.; Willinger, M.G.; Liu, F.; Zeng, X.; Rebutini, V.; Clavel, G.; Bai, X.; Ungar, G. and Pinna N. *One-step synthesis and self-assembly of metal oxide nanoparticles into 3D superlattices*. **2012**, ACS Nano, vol 6, 4382-4391.
- Purcar, V.; Stamatina, I.; Cinteza, O.; Petcu, C.; Raditoiu, V.; Ghiurea, M.; Miclaus, T.; Andronie, A.; *Fabrication of hydrophobic and antireflective coatings based on hybrid silica films by sol-gel process*, **2012**, Surf. Coat. Technol., vol. 206, 4449-4454

- Holman, R. *UV&EB Curing Formulation for Printing Inks Coatings & Paints*, Selective Industrial Training Associates Limited, London, **1984**.
- Radhakrishnan S, Siju CR, Mahanta D, Patil S, Madras G *Conducting polyaniline–nano-TiO₂ composites for smart corrosion resistant coatings*, **2009**, *Electrochim Acta*, vol. 54, 1249-1254
- Ramirez-Jimenez, A.; Alvarez-Lorenzo, C.; Concheiro, A. and Bucio, E. *Radiation-grafting of 2-hydroxyethyl methacrylate and oligo (ethylene glycol) methyl ether methacrylate onto polypropylene films by one step method*, **2012**, *Radiation Physics and Chemistry*, vol. 81, 27-32.
- Rill, M.S.; Plet, C.; Thiel, M.; Staude, I.; von Freymann, G.; Linden, S.; Wegener, M. *Photonic metamaterials by direct laser writing and silver chemical vapour deposition*, **2008**, *Nat. Mater.*, vol. 7, 543–546.
- Ritch, J.S.; Chivers, T.; Ahmad, K.; Afzaal, M. and O'Brien, P. *Synthesis, Structures, and Multinuclear NMR Spectra of Tin(II) and Lead(II) Complexes of Tellurium-Containing Imidodiphosphinate Ligands: Preparation of Two Morphologies of Phase-Pure PbTe from a Single-Source Precursor*, **2010**, *Inorg. Chem.*, vol 49, 1198-1205.
- Rivallin, M.; Benmami, M.; Kanaev, A. and Gaunand, A. *Sol-gel reactor with rapid micromixing: modelling and measurements of titanium oxide nanoparticles growth*, **2005**, *Chem. Eng. Res. Design*, vol. 83, 67-74.
- Rivera Gil, P.; Hühn, D.; del Mercato, L.L.; Sasse, D. and Parak, W.J. *Nanopharmacy: Inorganic nanoscale devices as vectors and active compounds*. **2010**, *Pharmacol. Res.*, vol. 62, 115-125.
- Rozes, L.; Steunou, N.; Fornasieri, G. and Sanchez, C. *Titanium-oxo clusters, versatile nanobuilding blocks for the design of advanced hybrid materials (Review)*, **2006**, *Monatshefte für Chemie*, vol. 137, 501-528.
- Ruiz-Hitzky, E. and Rojo, J.M., *Intracrystalline grafting on layer silicic acids*, **1980**, *Nature*, vol 287, 28-30.
- Ruiz-Hitzky, E. and Aranda, P., *Polymer-salt intercalation complexes in layer silicates*, **1990**, *Adv. Mat.*, vol 2, 545-547.
- Ruiz-Hitzky, E.; Letaïef, S. and Prévot V. *Novel organic–inorganic mesophases: self-templating synthesis and intratubular swelling*, **2002**, *Adv. Mater.*, vol 14, 439-443.
- Russel, G.T., *The kinetics of free-radical polymerization; Fundamental aspects*.

References

- 2002**, Aust. J. Chem., vol. 55, 399-414.
- Sallar, S., *Etudes électrochimiques des cinétiques de polycondensation sol-gel et de la fractalité des xérogels*, in *Laboratoire de Photophysique Photochimie Supramoléculaires et Macromoléculaires*, **2004** ENS-Cachan/CNRS/UMR 8531, Ecole Normale Supérieure de Cachan.
- Sanchez C. and Ribot, F. *Design of hybrid organic-inorganic materials synthesized via sol-gel chemistry*, **1994**, New J. Chem., vol. 18(10), 1007-1047
- Sanchez C., Julian B., Belleville P., Popall M., *Applications of hybrid organic-inorganic nanocomposites*, **2005**, J. Mater. Chem., vol. 15, 3559.
- Satoh, N.; Nakashima, T.; Kamikura K. and Yamamoto K., *Quantum size effect in TiO₂ nanoparticles prepared by finely controlled metal assembly on dendrimer templates*, **2008**, Nature Nanotech., vol. 3, 106-111.
- Schwarzer, H.-C. and Peukert, W., *Combined Experimental/Numerical Study on the Precipitation of Nanoparticles*. **2004** AIChE J. vol 50, 3234-3247.
- Seisenbaeva, G.A; and Kessler, V.A., *Precursor directed synthesis – “molecular” mechanisms in the Soft Chemistry approaches and their use for template-free synthesis of metal, metal oxide and metal chalcogenide nanoparticles and nanostructures*, **2014**, Nanoscale, vol 6-12, 6229-6244.
- Serbin, J.; Ovsianikov, A.; Chichkov, B. *Fabrication of woodpile structures by two-photon polymerization and investigation of their optical properties*, **2004**, Opt. Express, vol. 12, 5221.
- Shea, K.J.;Loy,D.A. and Webster, O. *Arylsilsesquioxane gels and related materials. New hybrids of organic and inorganic networks*, **1992**, J.Am. Chem. Soc. Vol 114, 6700-6710.
- Smakula, A.; Kalnajs,J. and Redman, M.J. *Optical Materials and Their Preparation*, **1964**, Appl. Opt. vol 3-3, 323-328.
- Soloviev, A.; Jensen H.; Sjøgaard E.G.and Kanaev A.V, *Aggregation kinetics of sol-gel process based on titanium tetraisopropoxide*, **2003**, J. Mater. Sci. vol 38-15, 3315-3318
- Song, M.;Pan,C.; Chen,C.; Li,J.; Wang,X. and Gu, Z, *The application of new nanocomposites: Enhancement effect of polylactide nanofibers/nano-TiO₂ blends on biorecognition of anticancer drug daunorubicin*, **2008**, Appl Surf Sci, vol 255-5, 610-612.

- Stevens, M.P. *Polymer Chemistry, an introduction*, **1999**, Third edition, Oxford university press.
- Su W.F. *Radical Chain Polymerization. In: Principles of Polymer Design and Synthesis*. **2013** Lecture Notes in Chemistry, vol 82. Springer, Berlin, Heidelberg.
- Sun, H.-B.; Kawakami, T.; Xu, Y.; Ye, J.-Y.; Matuso, S.; Misawa, H.; Miwa, M.; Kaneko, R. *Real three-dimensional microstructures fabricated by photopolymerization of resins through two-photon absorption*, **2000**, Opt. Lett., vol. 25, 1110.
- Sun, H.-B.; Kawata, S. *Two-Photon Photopolymerization and 3D Lithographic Microfabrication*, **2006**, in: Springer, Berlin, Heidelberg, pp. 169–273.
- Sun, H.-B.; Matsuo, S.; Misawa, H. *Three-dimensional photonic crystal structures achieved with two-photon-absorption photopolymerization of resin*, **1999**, Appl. Phys. Lett., vol. 74, 786–788.
- Sun, Z.-B.; Dong, X.-Z.; Chen, W.-Q.; Nakanishi, S.; Duan, X.-M.; Kawata, S. *Multicolor Polymer Nanocomposites: In Situ Synthesis and Fabrication of 3D Microstructures*, **2008**, Adv. Mater., vol. 20, 914–919.
- Tayalia, P.; Mendonca, C.R.; Baldacchini, T.; Mooney, D.J.; Mazur, E. *3D Cell-Migration Studies using Two-Photon Engineered Polymer Scaffolds*, **2008**, Adv. Mater., vol. 20, 4494–4498.
- Theng, B.K.G, *The Chemistry of Clay-Organic Reactions*, **1975**, Halsted Press, Division of John Wiley and Sons, Inc., New York and Adam Hilger Ltd.
- Tishchenko, V. *Effect of amalgamated aluminium on alcohol. Aluminium alkoxides, their properties and reactions*. **1899**, Journal of the Russian Physico-Chemical Society, vol 31, 694-770.
- Torgersen, J.; Qin, X.-H.; Li, Z.; Ovsianikov, A.; Liska, R.; Stampfl, J. *Hydrogels for Two-Photon Polymerization: A Toolbox for Mimicking the Extracellular Matrix*, **2013**, Adv. Funct. Mater., vol. 23, 4542–4554.
- Trabelsi, S.; Janke, A.; Hässler, R.; Zafeiropoulos, N.E.; Fornasier, G.; Bocchini, S.; Rozes, L.; Stamm, M.; Gérard, J.-F. and Sanchez C. *Novel organo functional titanium oxo cluster based hybrid materials with enhanced thermomechanical and thermal properties* **2005**, Macromolecules vol. 38, 6068-6078.
- Tishchenko, V.E. J. Russ. Phys.-Chem. Soc., **1899**, 31, 694.

References

- Uklein A.; Gorbovyi, P.; Traore, M.; Museur L. and Kanaev A. *Photo-induced refraction of pHEMA-TiO₂ nanoparticulate hybrids*, **2013**, Opt. Mater. Express, vol. 3, 533-545.
- Vargun E. *Living radical polymerization of hydroxyethyl methacrylate and its block copolymerization with poly(dimethyl siloxane) macroazoinitiator*, The Graduate School Of Natural And Applied Sciences of Middle East Technical University, PhD Thesis, **2009**.
<https://etd.lib.metu.edu.tr/upload/3/12610605/index.pdf>
- Veith, M.; *Molecular precursors for (nano) materials — a one step strategy*, **2002**, J. Chem. Soc., Dalton Trans. 12, 2405-2412.
- Wang, J.; Suna, W.; Zhang, Z.; Jianga, Z.; Wang, X.; Xu, R.; Li, R. and Zhang, X. *Preparation of Fe-doped mixed crystal TiO₂ catalyst and investigation of its sonocatalytic activity during degradation of azo fuchsine under ultrasonic irradiation* **2008**, Journal of Colloid and Interface Science, vol 320, 202-209.
- Wang, J.J.; Wang Y.Q.; Cao, F.F.; Guo, Y.G.; Wan, L.J.; *Synthesis of monodispersed wurtzite structure CuInSe₂ nanocrystals and their application in high-performance organic-inorganic photodetectors*, **2010**, J.Am.Chem.Soc. Vol-132:12218-12221.
- Wang, L. and Fox, R.O., *Comparison of Micromixing Models for CFD Simulation of Nanoparticle Formation*, **2004**, AIChE J. vol 50, 2217-2232.
- Wang, Y.; Pai, J.-H.; Lai, H.-H.; Sims, C.E.; Bachman, M.; Li, G.P.; Allbritton, N.L. *Surface graft polymerization of SU-8 for bio-MEMS applications*, **2007**, J. Micromechanics Microengineering, vol. 17, 1371–1380.
- Wu, S.; Serbin, J.; Gu, M. *Two-photon polymerisation for three-dimensional micro-fabrication*, **2006**, J. Photochem. Photobiol. A, vol. 181, 1–11.
- Wu, D.; Chen, Q.-D.; Niu, L.-G.; Wang, J.-N.; Wang, J.; Wang, R.; Xia, H.; Sun, H.-B. *Femtosecond laser rapid prototyping of nanoshells and suspending components towards microfluidic devices*, **2009**, Lab Chip., vol. 9, 2391.
- Wypych, G. *Handbook of Polymers*. **2011**, ChemTec Publishing, Ontario, Canada.
- Yamanaka S. *Synthesis and characterization of the organic derivatives of zirconium phosphate*, **1976**, Inorg. Chem, vol. 15, 2811-2817.
- Yang, W.E; Hsu M.L; Lin, M.C; Chen,Z.H.; Chen L.K.; Huang, H.H; *Nano/submicron scale TiO₂ network on titanium surface for denta implant*

- application*, **2009**, J. Alloys Comp., 479-642
- Yariv, S and Cross H *Organo –clay complexes and interactions* **2002**, Geoderma, vol. 109, 161-164
- Young, R. J. *Introduction to Polymers*, **1987** Chapman & Hall, ISBN 0-412-22170-5
- Yu, H., Zhang, K. and Rossi C. *Theoretical study on photocatalytic oxidation of VOCs using nano-TiO₂ photocatalyst*. **2007** Journal of Photochemistry and Photobiology A: Chemistry, 188, 65-73.
- Zandi-Zand, R.; Ersjad-Langroudi, A.; Rahimi, A.; *Silica based organic-inorganic hybrid nanocomposite coatings for corrosion protection*, **2005**, Prog. Org. Coat., vol 53, 286-291.
- Zhang Z1, Yuan Y, Fang Y, Liang L, Ding H, Jin L. *Preparation of photocatalytic nano-ZnO/TiO₂ film and application for determination of chemical oxygen demand*, **2007**, Talanta, vol 73-3, 523-528.
- Zhang, H.; Fallahi, M.; *Electro-optic waveline based on hybrid sol-gel doped with organic chromophore*, **2005**, Opt. Commun., vol. 248, 415-418.

Index of figures

Figure 1-1. Acid Catalysis Mechanism	20
Figure 1-2. Base Catalysis Mechanism.	21
Figure 1-3. General representation of the Hydrolysis reaction	28
Figure 1-4. Particle size distributions for different injection rate correspondent to $Re=2 \cdot 10^3$ (a), $3 \cdot 10^3$ (b), $6 \cdot 10^3$ (c) and $8 \cdot 10^3$ (d). Solid curves are Gaussian fits of experimental data.	32
Figure 1-5. Schema of hybrid materials elaboration proposed by Kameneva et al. (2006).	42
Figure 1-6. Schematic representation of HEMA polymerization.	43
Figure 1-7. pHEMA-TiO ₂ hybrids obtained by Kameneva et al. (2006).	43
Figure 1-8. Characteristic ACF of oxo-TiO ₂ nanoparticles after preparation in the sol-gel reactor ($[Ti] = 0.15$ M, $H = 2$, $T = 20$ °C, 2-propanol solution) (a) and after surface exchange with HEMA ($[Ti] = 1.5$ M) (b). Taken from Gorbovyi et al. (2011)	46
Figure 1-9. Laser-induced absorption of different pHEMA-TiO ₂ hybrids (labels #0, #1, #2 and #3 designate hybrids based on Ti ₁₆ -cluster isolated condensed species, linear gel chains at the gelation point and branched gel chains after aging) and of wet alcogel. Taken from Gorbovyi, 2012.	47
Figure 1-10. Schema of relevant photoinduced processes in TiO ₂ hybrids. Taken from Gorbovyi, 2012.	48
Figure 2-1. The principal schema of the sol-gel reactor.	54
Figure 2-2. Schematic representation of the T-mixer, used in the sol-gel reactor: (a) side view; (b) top view..	55
Figure 2-3. Broadening of the spectrum, caused by Doppler Effect.	56
Figure 2-4. Electron effects present in SEM.	57
Figure 2-5. The principles of Rayleigh diffusion, Stokes diffusion and anti-Stokes diffusion.	59
Figure 2-6. Right: DSC measuring principle, U is the potential difference in μ V between the two crucibles. Left: TGA-DSC sample holder used in the experiments of Chapter IV, the thermocouples are RTD type of Platinum/Platinum Rhodium, the sample plates are in Pt and the DSC rods in Pt-Rh.	60
Figure 2-7. Coupled TGA-DSC/GC-MS/FTIR system as used at ChimieParistech	62
Figure 2-8. Thermogram of TGA-DSC coupled with FTIR experiment of a 1:1 mixture of Isopropanol and HEMA in a temperature program of 30 to 250 °C at 4 °C min ⁻¹ .	63
Figure 2-9. Above: Gramm-Schmidt representation, below: FTIR spectra of the maximum point of the first peak identified as isopropanol. TGA-DSC coupled with FTIR	

Index of Figures

experiment of a 1:1 mixture of Isopropanol and HEMA in a temperature program of 30 to 250 °C at 4 °C min ⁻¹ .	64
Figure 2-10. Total Ion Current (TIC) of a 1:1 Isopropanol – HEMA sample with initiator heated from 20 to 110 °C at a speed of 5 °C min ⁻¹ . In black: TIC of the experiment, in red: TIC of Ion 60, in blue: TIC of Ion 69.	66
Figure 3-1. Schematic of the distillation setup.	76
Figure 4-1. TGA-DSC of HEMA x10 w/o NP and HEMA x20 w/o NP samples (T = 30 °C, P = 62 mBar).	89
Figure 4-2. TGA-DSC of HEMA x10 NP and HEMA x20 NP (T = 30 °C, P = 62 mBar).	90
Figure 4-3. TGA-DSC curves of solvent isopropanol:HEMA=1:1. The sample temperature increase is shown by black line. The injections points for GC-MS analysis are labeled with numbers in a circle.	93
Figure 4-4. 3D representation of FTIR spectra aquired during TGA-DSC series of 1:1 isopropanol:HEMA solvent.	95
Figure 4-5. FTIR spectra of 1:1 isopropanol:HEMA solvent obtained at the GC-MS injection times (in red) and spectra of reference products: 1) 0.8 minute, 2) 24 minute, 3) 43 minute.	96
Figure 4-6. Chromatograms of 1:1 isopropanol-HEMA solvent during TG-DSC series at selected injections points.	97
Figure 4-7. Relevant products of chromatograms in Figure 4-6.	98
Figure 4-8. Mass spectra aquired for each by-product of the samples during the experiment.	98
Figure 4-9. TGA-DSC curves of HEMA x10 w/o NP, HEMA x10 NP and HEMA x20 NP.	101
Figure 4-10. First derivative of mass loss curves (see Figure 4-9) of tree samples HEMA x10 w/o NP, HEMA x10 NP and HEMA x20 NP.	102
Figure 4-11. Chromatogram of gas probes at 34 °C in TGA-DSC series of samples HEMA x10 w/o NP, HEMA x10 NP and HEMA x20 NP.	103
Figure 4-12. Schematic representation of HEMA fragmentation by pyrolysis analyzed by GC-MS taken from Vargün (2009).	104
Figure 4-13. Chromatograms of a gas probes at 90 °C in TGA-DSC series of samples HEMA x10 w/o NP, HEMA x10 NP and HEMA x20 NP.	104
Figure 4-14. Chromatograms of a gas probes at 162 °C in TGA-DSC series of samples HEMA x10 w/o NP, HEMA x10 NP and HEMA x20 NP.	106
Figure 4-15. Chromatograms of gas probes at 235 °C in TGA-DSC series of samples HEMA x10 w/o NP, HEMA x10 NP and HEMA x20 NP.	106
Figure 4-16. GS peak areas of isopropanol (2 nd minute) and HEMA (3 rd minute) of HEMA x10 w/o NP, HEMA x10 NP and HEMA x20 NP samples at different temperatures.	107

Figure 4-17. Peak area at 3.8, 4.15 and 5.1 minutes of HEMA x10 w/o NP, HEMA x10 NP and HEMA x20 NP samples at different temperatures.	108
Figure 4-19. TGA-DSC curves of HEMA x10 w/o NP-P (a), HEMA x10 NP-P (b), HEMA x20 NP-P (c) and TiO ₂ powder (d). Measurements were performed at 4 °C min ⁻¹ under air atmosphere.	112
Figure 4-20. Gram-Schmidt representation of polymerization of three hybrid solutions during TGA-DSC series. The most significant released species are indicated.	113
Figure 4-21. Chromatograms of a gas probes at 22 °C in TGA-DSC series of samples HEMA x10 w/o NP-P, HEMA x10 NP-P and HEMA x20 NP-P.	115
Figure 4-22. Chromatograms of a gas probes at 90 °C in TGA-DSC series of samples HEMA x10 w/o NP-P, HEMA x10 NP-P and HEMA x20 NP-P.	116
Figure 4-23. Chromatograms of a gas probes at 163 °C in TGA-DSC series of samples HEMA x10 w/o NP-P, HEMA x10 NP-P and HEMA x20 NP-P.	117
Figure 4-24. Chromatograms of a gas probes at 235 °C in TGA-DSC series of samples HEMA x10 w/o NP-P, HEMA x10 NP-P and HEMA x20 NP-P.	118
Figure 4-25. GS-MS peak areas of isopropanol (t=2 min) and HEMA (t=3 min) of HEMA x10 w/o NP-P, HEMA x10 NP-P and HEMA x20 NP-P samples at different temperatures	119
Figure 5-1. Stability time of the nanoparticulate TiO ₂ colloids x5, x10, x20 and x30 (x1=0.15 mol/l Ti) in HEMA and HEMA-EMA solvents.	125
Figure 5-2. Collod behaviour after water addition.	126
Figure 5-3. TGA-DSC experiments of organic (a) and organic-inorganic hybrid (b-d) HEMA and HEMA-EMA solutions.	127
Figure 5-4. TEM image (a) and EDX spectrum (b) of HEMA x5 sample; scale 10 nm in (a).	132
Figure 5-5. TEM images of HEMA-EMA x5 sample taken with different magnification.	134
Figure 5-6. Fourier transform image of HEMA-EMA x5 sample. The interplane distance depicted by dashed line is 2.72 Å.	135
Figure 6-1. Experimental procedure: (I) beam focusing (II) laser writing (III) development (IV) completed structure.	142
Figure 6-2. Structure obtained in TEGDMA solution (sample 3) after DLW (2PP) processing.	143
Figure 6-3. Structure obtained in EMA + TEGDMA solutions (samples 4 and 5) after DLW (2PP) processing.	143
Figure 6-4. Major steps of the photopolymerization process (I = Photoinitiator; R= Reactive species; M= monomer).	144
Figure 6-5. Absorption spectra of pore HEMA and HEMA with 1% DEABP.	145
Figure 6-6. Example of a woodpile structuring obtained in sample 1.	147

Index of Figures

Figure 6-7. SEM image of segmented woodpile obtained in sample 4 (top view).	148
Figure 6-8. SEM image of segmented line in Fig 6-7 (side view 45°)	148

Index of tables

Table 1-1. Evolution of Hybrid synthesis since early XX century up to our days.	18
Table 1-2. Half-life of the mos common initiators in respect to temperature.	38
Table 1-3. Comercial photoinitiators and their initiating wavelenght (Holman, 1984)	39
Table 1-4. Photonic sensitivity of different hybrid samples. Taken from Gorbovyi, 2012.	48
Table 3-1. Parameters used in the synthesis of TiO ₂ nanoparticles	78
Table 3-2. Concentrations of HEMA and TiO ₂ for each sample prepared.	80
Table 3-3. Concentration of HEMA-EMA and TiO ₂ for each sample preapred.	80
Table 3-4. Concentration of HEMA-TEGDMA and TiO ₂ for each sample preapred	80
Table 4-1: Calculated mass % of Isopropanol on tested samples from their volumetric proportions	88
Table 4-2. Experimental mass loss, calculated mass loss and their difference expressed as residual isopropanol masss for samples with and without nanoparticles.	90
Table 4-3. Parameters used in TGA-DSC experiments	91
Table 4-4. Parameters used in GC-MS experiments	92
Table 4-5. Time and temperature of injections in GC-MS experiments	93
Table 4-6. Onset temperature and released heat of radical polymerization of selected hybrid solutions and HEMA solvent (measurements presented in Figure 4-19).	111
Table 4-7. Mass loss of nanoparticulate hybrids, HEMA solvent and TiO ₂ powder.	113
Table 6-1. Chemicals used in experiments.	141
Table 6-2. Summary of investigated monomer samples with and without a cross-linker	142
Table 6-3. Summary of structured hybrid materials.	146

Publications

Appeared:

- Evlyukhin, E.; Museur, L., Diaz-Gomez-Trevino, A.P.; Traore, M.; Brinza, O.; Zerr, A. and Kanaev, A. *Synthesis of organic-inorganic hybrids via a high-pressure-ramp process: the effect of inorganic nanoparticle loading on structural and photochromic properties*, **2018**, *Nanoscale*, vol. 10, pp. 22293-22301.
- Gorbovyi, P.; Diaz-Gomez-Trevino, A.P.; Traore, M.; Museur, L.; Rozes, L.; Ribot, F., Sanchez, C.; Kuznetsov, A.I.; Chichkov, B.N. and Kanaev, A. *Alkoxysilane effect in hybrid material : A comparison of pHEMA-TiO₂ and pMAPTMS-TiO₂ nanoparticulate hybrids*, **2019**, *Material research Bulletin*, vol. 114, pp. 130-137.
- Tieng, S.; Brinza, O.; Labidi, S.; Diaz-Gomez Trevino, A.P.; Kanaev, A. and Chhor, K. *A major non-volatile intermediate product of photo-catalytic decomposition of ethylene on Fe(III)-TiO₂*, **2019**, *Catalysis*, vol. 374, pp. 328-334.

In preparation:

- Diaz Gomez, A.P.; Traore, M. and Kanaev, A. *Improved stability of nanoparticulate pEMA-pHEMA-TiO₂ hybrids*, **2019**.
- Diaz Gomez, A.P.; Traore, M. and Kanaev, A. *Solvent exchange in nanoparticulate TiO₂-based organic-inorganic hybrids*, **2019**.

Résumé:

Des matériaux hybrides organiques/inorganiques formés de nanoparticules de TiO_2 et d'un polymère ont été synthétisés. Une copolymérisation de monomères hydrophobes (EMA) et hydrophiles (HEMA) a permis d'améliorer la stabilité des solutions hybrides en présence d'humidité, notamment sous atmosphère ambiante, tout en préservant, pendant au moins une semaine, la morphologie des nanoparticules jusqu'à des concentrations en titane de 3 mol/l. Les modifications de la composition des hybrides ont été investiguées pendant les étapes d'échange du solvant et de polymérisation. Il a été montré que les nanoparticules retiennent sur leur surface des molécules du solvant (2-propanol) même à haute température au-dessus du point d'ébullition (et jusqu'au point de décomposition). Les produits de décomposition les plus importants du HEMA ont été identifiés : 2-méthyl propionique acid, 2-hydroxy ethyl acetate et méthyl methacrylate. Ce dernier a été également observé comme une impureté de la synthèse. Les quantités des produits libérés sont proportionnelles à la concentration des nanoparticules. Des analyses MET ont mis en évidence une distribution très homogène des nanoparticules d'une taille de 3,0 nm préalablement attribuée au noyau servant de brique élémentaire dans la formation des solides de TiO_2 . Ces résultats doivent être pris en compte lors des études de propriétés électroniques et fonctionnelles des matériaux afin d'envisager leurs champs d'application. Nous avons évalué ces matériaux hybrides inorganiques-organiques pour le micro-usinage laser par un procédé d'écriture direct par laser à deux photons.

Mots clés : Hybrides organiques-inorganiques, nanoparticules de TiO_2 , copolymère, échange de solvant, polymérisation organique.

Abstract:

TiO_2 -based nanoparticulate organic-inorganic hybrid materials with the organic component consisting of co-polymers were prepared. A successful association of hydrophobic and hydrophilic organics makes the hybrid solutions stable against atmospheric moisture and preserved single nanoparticle morphology at high inorganics concentrations up to 3 mol/l Ti over a week. The compositional modifications of the hybrids were investigated at the solvent exchange and polymerization stages of preparation. It was shown that the inorganic nanoparticles retain solvent molecules at the surface even at high temperatures above boiling point (up to the organics decomposition temperature). The nanoparticles also catalyze the organics decomposition shifting this process to lower temperatures. The major products of HEMA-isopropanol decomposition were assigned to 2-methyl propionic acid and 2-hydroxy ethyl acetate and methyl methacrylate, which last was also observed as the synthesis impurity. The quantities of the released species were proportional to the nanoparticles concentration. The TEM measurements evidenced unprecedentedly homogenous distribution of the smallest nanoparticles of the size 3.0 nm previously assigned to nucleus, which serves as elementary building block of TiO_2 solids. These findings have to be taken into consideration by investigating electronic properties of the materials and determining their application fields. We evaluated availability of the obtained nanoparticulate organic-inorganic hybrid materials for micromachining via DLW (2PP) processing.

Keywords : Organic-inorganic hybrids, TiO_2 nanoparticles, co-polymer, solvent exchange, organic polymerisation.